Technische Universität München

TUM School of Life Sciences

Spatiotemporal structure of rheotactic behavior in larval zebrafish

Amir Asgharsharghi Bonab

Vollständiger Abdruck der von der TUM School of Life Sciences der Technischen Universität München zur Erlangung des akademischen Grades eines

Doktors der Naturwissenschaften

genehmigten Dissertation.

Vorsitzender: Prof. Dr. Ilona Grunwald Kadow

Prüfer der Dissertation:

1. Prof. Dr. Harald Luksch
2. Prof. Dr. Thomas Misgeld

Die Dissertation wurde am 14.04.2021 bei der Technischen Universität München eingereicht und durch die TUM School of Life Sciences am 07.07.2021 angenommen.

Abstract

For aquatic animals that can be displaced by currents, visual signals are the most salient sensory cues to evaluate self-motion relative to an external reference frame. Yet, in the absence of visual information fish can orient to the direction of water currents, an innate behavior called rheotaxis.

In this study, I used behavioral data from controlled environmental conditions to reveal insights of mechanosensory control of rheotaxis in larval zebrafish. My data suggest that larval zebrafish perform rheotaxis by exploiting inhomogeneities in the flow, the most salient of which is radial differences in flow velocity. However, the radial velocity gradients are insufficient to identify flow direction because the lateral line in the zebrafish larva is a linear sensor-array that is lateral-symmetric and whose axis of sensitivity is bidirectional. Such an array provides intrinsically ambiguous information because it cannot discriminate flow in anterior-posterior from the posterior-anterior direction relative to the anteroposterior body axis of the fish.

This study proposes that to solve this front-rear ambiguity, zebrafish larvae extract hydromechanical information from the laminar flow, which in principle is rotational around submerged objects, including fishes, due to boundary conditions. This rotation results in water

flowing in opposite directions at either side of the animal. The lateral line system is able to use this information to solve the front-rear ambiguity if it can perform recurrent comparisons of rotational flow.

My data reveal that during rheotaxis larval zebrafish use iterative patterns of small-amplitude yaw movements and discrete swim bouts, during which they capture snapshots of mechanical cues across the horizontal plane, suggesting a simple mechanism for lateral line mediated rheotaxis. These data indicate that rheotaxis occurs by vectorial fractionation of mechanical signals, sensory updating by recurrent yaw rotations, and integration of bilateral sensory information.

Zusammenfassung

Bei wasserlebenden Tieren, die durch Strömungen abgetrieben werden können, sind visuelle Signale die wichtigsten sensorischen Hinweise um die Eigenbewegung in Bezug auf einen externen Referenzrahmen bewerten zu können. Fehlen jedoch visuelle Informationen, können sich Fische an der Richtung der Wasserströmung orientieren. Dieses angeborene Verhalten wird das als Rheotaxis bezeichnet.

In der vorliegenden Studie wurden Daten zum Verhalten von Zebrafischlarven unter kontrollierten Umgebungsbedingungen erhoben, um neue Aspekte der mechano-sensorischen Kontrolle der Rheotaxis zu untersuchen. Die Daten legen nahe, dass Zebrafischlarven bestimmte Unregelmäßigkeiten einer Strömung für die Rheotaxis nutzen, im Besonderen die radialen Unterschiede in der Strömungsgeschwindigkeit. Jedoch wurde festgestellt, dass die isolierte Betrachtung der radialen Gradienten der Fließgeschwindigkeit nicht ausreichen, um die Strömungsrichtung vollständig zu bestimmen. Das Seitenlinienorgan der Zebrafischlarve stellt ein lineares Sensorarray dar, das lateral symmetrisch ist und dessen Empfindlichkeitsachse bi-direktional ist. Ein solches Array liefert grundsätzlich mehrdeutige Informationen, da es zwischen einer anterioren und posterioren Ursprungsrichtung relativ zur antero-posterioren Körperachse des Fisches nicht unterscheiden

kann.

Die Ergebnisse dieser Studie legen nahe, dass Zebrafischlarven hydromechanische Informationen aus der laminaren Strömung extrahieren, um die Richtung eindeutig bestimmen zu können. Im Prinzip rotiert die laminare Strömung um Objekte unterhalb der Wasseroberfläche, einschließlich Fische. Diese Rotation führt dazu, dass das Wasser zu beiden Seiten des Tieres in entgegengesetzte Richtungen fließt. Das Seitenlinienorgan kann diese Informationen aus wiederkehrenden Vergleichen des Rotationsflusses verwenden, um die Strömungsrichtung eindeutig zu bestimmen.

Die Daten zeigen, dass Zebrafischlarven zur Rheotaxis iterative Muster von Gierbewegungen mit kleiner Amplitude und diskreten Schwimmmanövern verwenden. Auf diese Weise erfassen sie Momentaufnahmen von mechanischen Reizen über die horizontale Ebene. Dies würde einen einfachen Mechanismus für die seitenlinienvermittelte Rheotaxis darstellen. Diese Ergebnisse zeigen also, dass Rheotaxis durch vektorielle Fraktionierung von mechanischen Signalen bewerkstelligt wird. Sensorische Daten aus wiederkehrenden Gierdrehungen werden ständig aktualisiert und mit bilateralen sensorischen Informationen abgeglichen.

This work is dedicated to my lovely wife and my parents

Acknowledgements

I would like to thank all the people at Helmholtz Zentrum München and Technische Universität München that have supported my doctoral studies. Among all of them I would like to express my greatest appreciation to:

Dr. Hernán López-Schier, my supervisor at Helmholtz Zentrum München, for giving me the opportunity to work in his lab. I am very grateful for his valuable advices and comments on my thesis. His guidance and continuous support helped enormously in difficult moments.

Prof. Dr. Harald Luksch that accepted me as a Ph.D candidate at Wissenschaftszentrum Weihenstephan. I am very grateful for his valuable advices and comments on my thesis, and his kindly support on registration and following the regulations at TUM.

My thesis advisory committee member Prof. Dr. Thomas Misgeld for his advices during my Ph.D and Prof. Dr. Ilona Grunwald Kadow for taking the chair of the thesis evaluation.

The members of López-Schier's and Desborde's lab at Helmholtz Zentrum München for all the scientific exchange, brainstorming and the friendly environment created by all the members. I want to thank Petra Hammerl for her great support in purchasing the optical tools and also her great administrative support.

Dr. Pablo Oteiza for his generous sharing of materials and ideas.

Thomas Gerlach and Alexander Lang at the Helmholtz Zentrum München workshop for their fantastic help in building our experimental behavioral set up.

Dr. Heide Marie Resch and Dr. Peter Föhr for their help in writing the German version of the abstract.

I am deeply grateful to my parents for their love, support and encourage. And my deepest appreciation goes to my wife, Shokoufeh for her love and unconditional support.

Contents

List of Figures

List of Tables

Chapter 1

Introduction

1.1 Overview

Behavior is an output of the central nervous system (CNS) from either internal motivational states or from processing input from the environment. Behavior, therefore, can be a field of study on its own (ethology), or used as a tool to reveal the workings of the CNS. Due to the intrinsic complexity of both the behavior and the nervous system, it is essential to identify approaches, assays and animal species best suitable for the specific problem under investigation (Levin and Cerutti [2009]). In addition, modeling has become a powerful approach in science to represent complex systems in simpler forms. In life sciences, the concept of modeling may involve experimental procedures and animal models. In neuroscience, animal models are chosen to understand or manipulate the nervous system to understand its function. Since neurons are the essential units of all nervous systems, one can choose a model organism that expresses a rich behavioral repertoire and has technical advantages to study behavior. In addition, the

number of the neurons and the physical size of the brain need to be considered. Behavioral analysis and the correlation with neural activity would require sophisticated techniques and advanced tools in an animal with complex nervous system and a large number of neurons. Therefore, a small brain size is beneficial for complex analysis of neuronal activity pattern, finding the connectivity and functionality of brain subsections and correlating these with the behavior. Fishes are increasingly becoming an interesting model to reveal how CNS guides motor responses to sensory stimuli.

1.2 Zebrafish as a model organism

The zebrafish (*Danio rerio*) (Figure 1.1) is a tropical freshwater fish, native to the Indian subcontinent. Their natural habitats are slow moving waters in small rivers and streams, as well as man-made bodies of water including rice paddies (Engeszer et al. [2007]; Parichy [2015]; Holtzman et al. [2016]). Although the zebrafish reaches adulthood at around 3 month of age, it starts to express complex behaviors from 5 day-post-fertilization (dpf). Small brain size together with its transparency makes all neurons accessible for optical imaging. Recently Hildebrand et al. [2017] have reconstructed neuronal circuits of the zebrafish brain with electron microscopy. They further have co-registered these reference atlases with in vivo two-photon fluorescence microscopy. These features make zebrafish an interesting model organism for neuronal and behavioral studies.

In other hand, genetic approaches enable precise editing of the DNA to generate mutants and transgenic lines with mutations in genes of interest (specially with the current technologies like CRISPR (Hwang et al. [2013])). Currently a large number of zebrafish mutants with a wide range of phenotypes are cre-

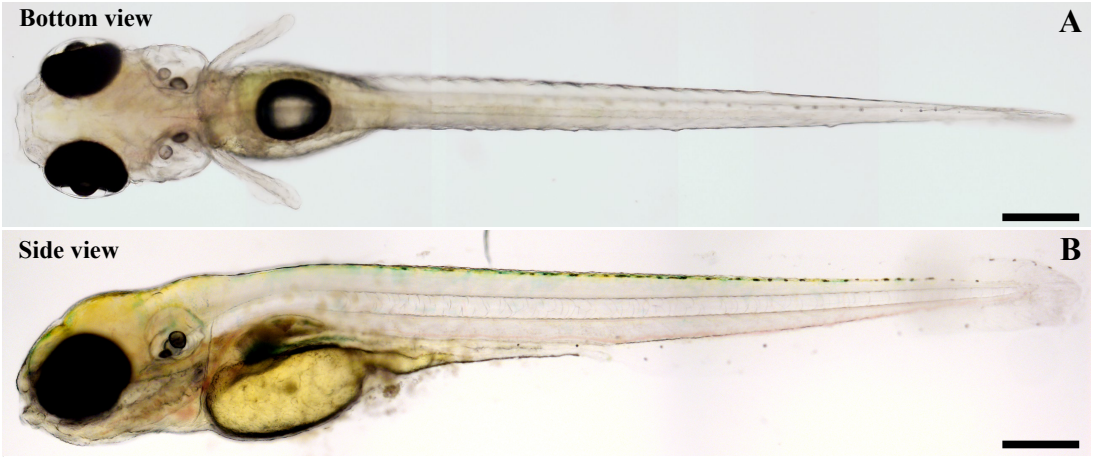

Figure 1.1: *Bright-field image of bottom (A) and side (B) view of zebrafish larvae at 7 dpf, taken with Olympus BX61 microscope with 10x objective and stitched together by using Fiji. Anterior part is to the left, posterior is to the right and dorsal is to the bottom (B). Scale bars are 300 µm in both panels A and B.*

ated in order to target specific cell types and different parts of the brain. With Brainbow technology in zebrafish up to four fluorescent proteins which have different spectrum are mixed randomly and are used to label neurons with about 100 distinguishable colours. The idea is to label each neuron with a distinguishable colour, having one unique colour for each neuron instead of labeling all the neurons with the same fluorescent colour.

Probes for optical recording of neuronal activity include voltage-sensitive dyes and genetically encoded calcium indicators (GCaMP), which can optimally applied to zebrafish thanks to the translucent body and accessibility of the brain (Friedrich et al. [2010]). Also, advances in optical imaging techniques such as two photon microscopy (Denk et al. [1990]; Ahrens et al. [2012]; Renninger and Orger [2013]; Portugues et al. [2014]), light sheet microscopy (Ahrens et al. [2013]), light field microscopy (Broxton et al. [2013]), spatial light modulator microscopy (Quirin et al. [2013]) have brought huge advances in the field of functional imag-

ing of neurons and sensory cells during behavior. Calcium imaging with high resolution microscopy techniques. In addition to imaging, manipulation of the nervous system is necessary in order to understand the function of neural circuits and populations and their relation to the performed behavior. Physiological manipulation can be obtained by classical pharmacological treatment and, recently, by more precise approaches such as laser surgery and genetically encoded effectors that include activators and inhibitors of neuronal activity (Friedrich et al. [2010]).

1.3 Optical sensitivity of zebrafish visual system

Zebrafish have four morphologically different photoreceptors. The peak absorption wavelengths of short single cones, long single cones, double cones and red opsins are 360 nm (ultraviolet (UV) opsins), 415 nm (blue opsins), 480 nm (green opsins) and 570 nm respectively (Meier et al. [2018]). Optokinetic studies of larval zebrafish have found no eye movement responses to 750 nm near infrared light (Hartmann et al. [2018]). On the other hand, Hartmann et al. [2018] conducted experiments with zebrafish larvae under three specific light regimes: near infrared light with a spectral peak at 860 nanometer (nm) and 960 nm, and visible light conditions with a spectrum of 440 nm to 700 nm. Based on their results, larval zebrafish show negative phototaxis towards the visible light source. And interestingly, larval zebrafish also show negative phototactic responses towards near infrared at 860 nm but not to 960 nm. This suggests that near infrared light at 960 nm is not visible for larval zebrafish and can be used in the darkening chamber

for zebrafish behavior experiments.

1.4 The lateral-line mechanosensory system

In addition to the widely conserved sensory systems in vertebrates (visual, acoustic, tactile, gustatory and olfactory) fishes and some amphibians have an additional sensory system called the lateral line. The lateral line is a mechanosensory system that acts as a distance touch sensor.

Steno was the first to describe the lateral line in fishes in 1664 (Parker [1904]). Subsequently, (Hofer [1908]) discovered the function of the lateral line as a mechanosensory system (Mogdans and Bleckmann [2012]). Mechanosensation is an evolutionary ancient and pervasive sensory modality that is at the basis of audition, balance, touch, proprioception and rheoception (Walsh et al. [2015]; Tuthill and Wilson [2016]).

The lateral line plays an important role in mediating behaviors that include predator avoidance (McHenry et al. [2009]), prey detection (Montgomery and Macdonald [1987]; Bleckmann and Bullock [1989]; Janssen et al. [1999]), schooling (Pitcher et al. [1976]), courtship and sexual behavior (Bleckmann [1986]; Satou et al. [1994]), rheotaxis (Arnold [1974]; Montgomery et al. [1997]) and obstacle avoidance (Bleckmann and Zelick [2009]).

The lateral line system comprises a set of discrete mechanosensory organs called neuromasts, which have a receptive field restricted to their immediate surrounding (Van Trump and McHenry [2008]). There are two types of morphologically different neuromasts: superficial neuromasts (which are located on the surface of the fish body) and canal neuromasts (which are within narrow channels inside the body) (Dijkgraaf [1989]). The superficial neuromasts are sensitive to

frequencies lower than 80 Hz (Kroese and Schellart [1992]).

Zebrafish larvae only have superficial neuromasts (Figure 1.2 A and B). The pear-shaped hair cells (Figure 1.2 C) are the mechanoreceptive cells at the core of the neuromast function. Hair cells are surrounded by non-sensory supporting cells (Figure 1.2 D). A mature neuromast contains 15-20 hair cells. During postembryonic growth of zebrafish, the number of lateral line neuromasts increases, canal neuromasts appear and their distribution pattern changes (Ghysen and Dambly-Chaudiere [2007]).

In zebrafish, the lateral-line system is lateral symmetric, including the ascending neuronal pathway (Pujol-Martí et al. [2014]; Hildebrand et al. [2017]). It consists of an anterior branch (Anterior Lateral Line (ALL)) formed by cephalic neuromasts, which have the cell body (ganglion) anterior to the otic capsule and a posterior branch (Posterior Lateral Line (PLL)) whose neuromasts are distributed along the trunk and tail of the fish (Pujol-Martí and López-Schier [2013]) and have the cell body posterior to the otic capsule (Figure 1.4 B and C). Two types of neuromasts, horizontal and vertical neuromasts (Figure 1.3 B), can be found by describing neuromasts regarding their axis of polarity relative to the body axis. The horizontal and vertical neuromasts are responsive to the anterior-posterior and the dorsal-ventral movements respectively. The majority of the posterior neuromasts are sensitive to water currents along to the animals anterior-posterior axis.

Mechanoreception occurs through the hair cells by water movement. Hair bundles, on the apical surface of each hair cell, comprise of a cluster of stereocilia organized in rows of increasing length towards the kinocilium (Figures 1.2 E and 1.3 A). A flexible and jellylike cupula encapsulates the stereocilia and bends upon water movement, causing the opening of the ion channels in apical

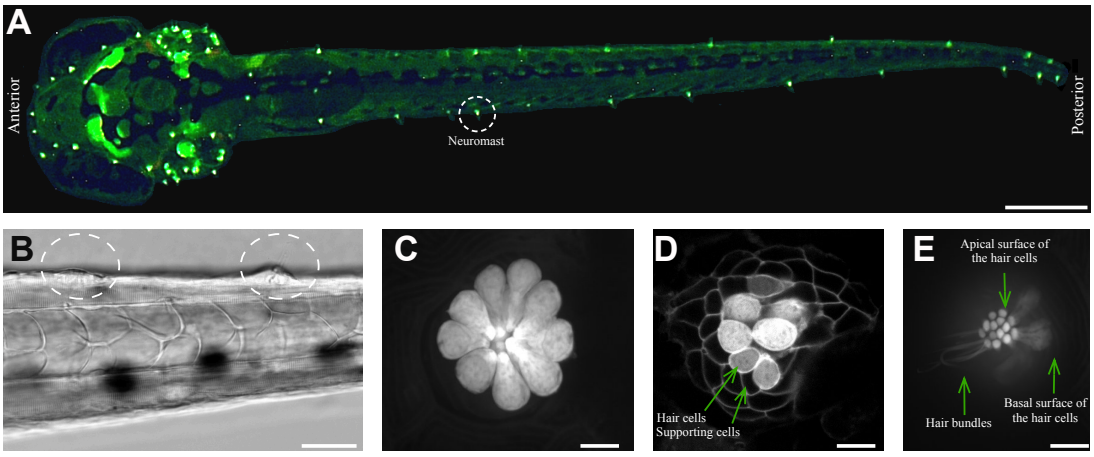

Figure 1.2: *The lateral-line sensory system of zebrafish larva comprises of mechanosensory organs, called neuromasts which are distributed on the tail, head and trunk of the fish, shown in green in panel A for 7 dpf larvae (tg: Brn3c:Gal4;UAS:GFP). These superficial neuromasts are on the skin (B). Pear-shaped hair cells (C) are the sensory cells within the neuromast surrounded by other cells (D). Hair cells have elongated cupula in the surrounding medium (E). Scale bar is 300 µm in panel A, 150 µm in panel B and 5 µm in panels C, D, E.*

mechanosensory bundles. There is a strict synaptogenesis of the lateralis afferent neuron (LAN) with hair cells of identical orientation. Depending of the sign and orientation of the activating stimulus, LANs are named as rostrocaudal (rLANs), caudorostral (cLANs), dorsoventral (dLANs) and ventrodorsal (vLANs) lateralis afferent neurons.

1.5 Lateral-line hair cells

The anatomical orientation of the apical stereocilia defines the hair cell's principal axis of sensitivity to mechanical stimuli (Flock and Wersall [1962]; Hudspeth and Corey [1977]; López-Schier et al. [2004]). This structure morphologically creates polarity within the plane of the neuromast (Figure 1.3 B). Hair cells depolarize when cluster of stereocilia bend in the direction towards the kinocilium, and hyperpolarize when they bend away from the kinocilium. Bundle deflection in a perpendicular direction will not have any effect of mechanoreception and hair-cell responses (Hudspeth [2000]) (Figure 1.3 C).

Each neuromast comprises an equal number of hair cells with opposing polarity, indicating that neuromasts are bidirectionally sensitive along the axis of maximal sensitivity (López-Schier et al. [2004]).

1.6 Lateralis afferent neurons

Lateralis afferent (ascending) neurons (LANs) extend peripheral axons to neuromasts, and central processes that terminate along a column in the ipsilateral hindbrain (Figure 1.4). Generally, four LANs converge onto each neuromast, but

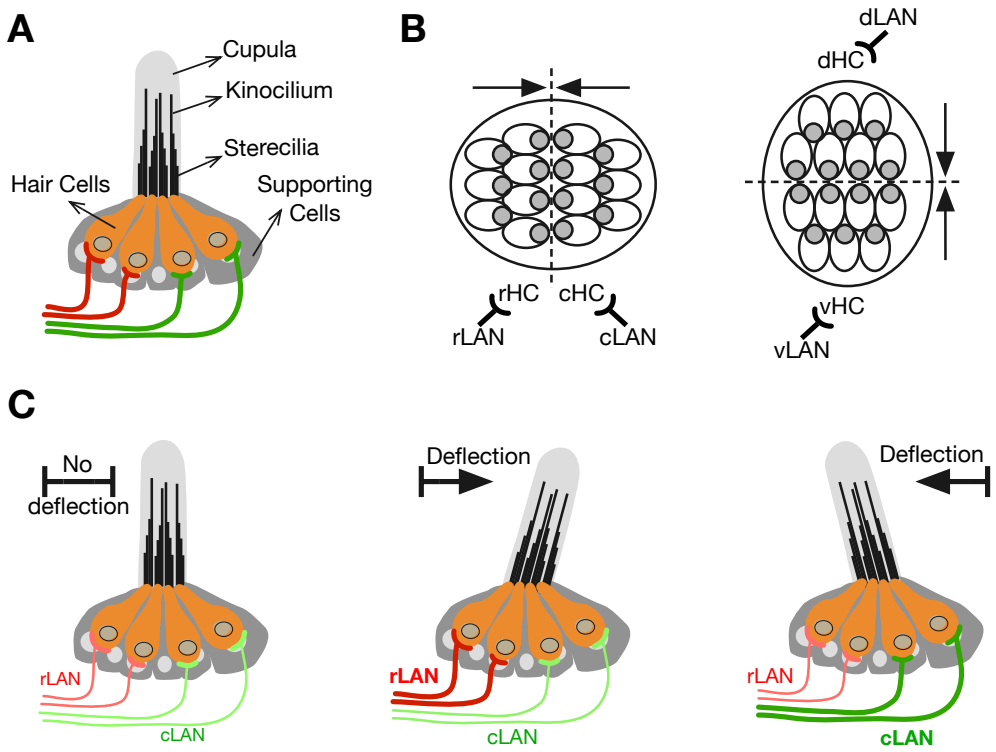

Figure 1.3: *A) Lateral view drawing of a neuromast with hair cells in the middle and wrapped by supporting cells. The stereocilia and kinocilium are encapsulated by the cupula. Afferent neurons (in red and green) synapses with hair cells. B) The top view scheme of a horizontal (left) and a vertical (right) neuromast, highlighting the strict synaptogenesis of each lateralis afferent neuron (LAN) with hair cells of identical orientation. LANs are named rostrocaudal (rLAN), caudorostral (cLAN), dorsoventral (dLAN) and ventrodorsal (vLAN), depending of the sign and orientation of the activating stimulus. C) The lateral view scheme of the activity patterns of the hair cell and LANs upon rostrocaudal and caudorostral mechanical deflection of the neuromast cupula (neuronal-spiking schemes below neuromasts). The excited LAN in each case is shown with the thicker line.*

each LAN exclusively synapses with hair cells of identical orientation (Figure 1.3 B) (Faucherre et al. [2009]; Pujol-Martí et al. [2014]). Therefore, LANs innervating horizontal neuromasts are subdivided into rostrocaudal for those sensitive to water flowing in head-to-tail direction, and caudorostral with the opposite directional tuning (Figure 1.3 B and C).

Approximately 100 LANs on each side of the fish transmit ipsilateral sensory information from the receptors to the hindbrain (Figure 1.4 D) (Pujol-Martí and López-Schier [2013]; Hildebrand et al. [2017]).

Each lateralis ganglion comprises around 60 cell bodies in the one week-old zebrafish larva. This number increases as the fish ages (Metcalfe [1985]; Liao [2010]). Lateralis afferent neurons are the first order neurons since they carry information from sensory hair cells to the brain/CNS (Figure 1.4). Second order neurons make synapses with the central projection of the lateralis neurons to carry information to higher levels in the CNS. Different groups of second order neurons make synapses with central projection of lateralis neurons for various aims. The command neurons Mauthner cell and vestibulospinal neurons are examples of identified second order neurons of the lateral line (Zottoli and Van Horne [1983]; Kimmel et al. [1990]).

1.7 Zebrafish behavior and rheotaxis

Animals perform various orienting behaviors (Fraenkel and Gunn [1961]; Jander [1975]). Orienting behaviors can be short or long range and rely on one sensory system or a contribution of multisensory mechanisms (Coombs and Montgomery [2014]). Orientation behavior induced by water current is called rheotaxis and

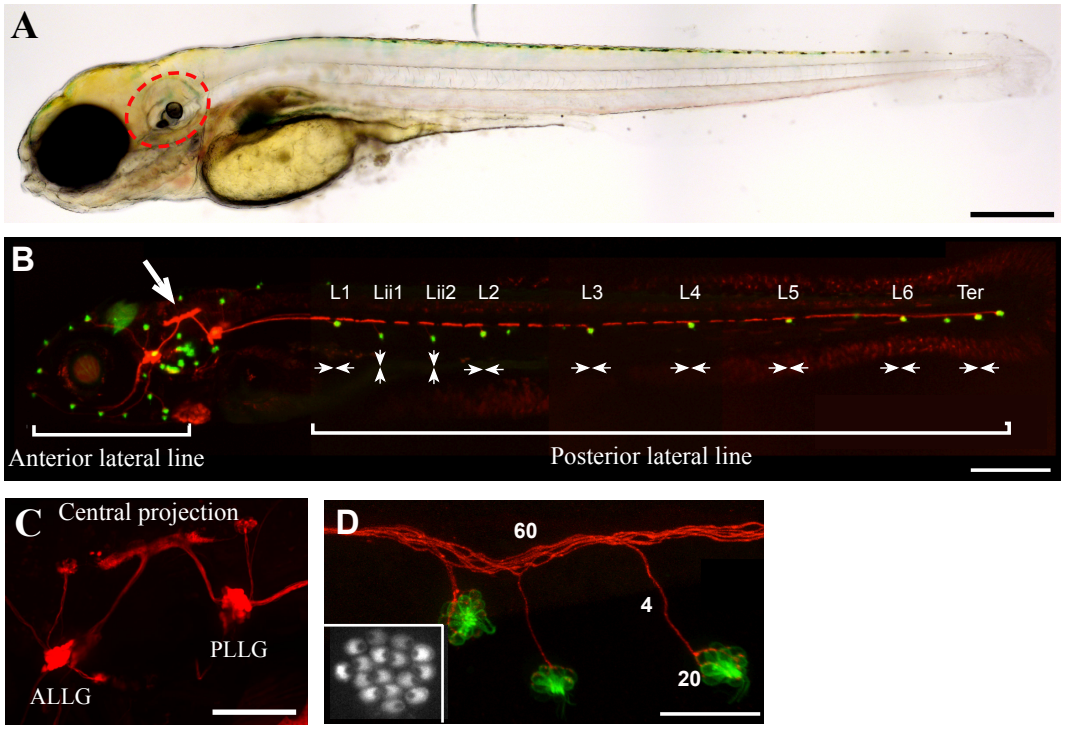

Figure 1.4: *A) Bright-field image of 7 dpf zebrafish larva, anterior to the left, posterior to the right and dorsal to the top. Red line indicates the ear and the central projection. B) A composite maximal projection of a 7 dpf transgenic zebrafish larva expressing mCherry (red) in LANs and GFP (green) in hair cells of neuromasts. Letters and numerals identify each posterior neuromast. The white arrows indicate the neuromast axis of sensitivity to water current (hair cell orientation). C) The maximal projection of posterior and anterior lateral line ganglion with central projection of lateralis afferent neurons, forming a mathematical pi-shape. D) A confocal micrograph magnification of a portion of the posterior lateral line. White numbers indicate the average population size of each component. Inset shows the apical surface of a neuromast, in which phalloidin staining reveals the horseshoe-shaped stereociliary bundle, showing a single axis of planar polarity in neuromasts, with one half of the constituent hair cells oriented opposite to the other half. Scale bars are 300 μm in panels A and B, and 60 μm in panels C and D.*

exists in many fish species (Figure 1.5).

Figure 1.5: *A Salmon fish is performing positive rheotaxis in river. Screen shot from Grizzly Bears Catching Salmon - Nature's Great Events - BBC, http://www.bbc.com/earth/world.*

Rheotaxis is the intention of the species to orient downstream (negative rheotaxis) or upstream (positive rheotaxis) (Lyon [1904]; Arnold [1974]) and is a multisensory behavior where sensory information is extracted from the visual field and also from the relative movement of the water current over the fish body. Nevertheless absence of one sensory modality does not impact the performance of the behavior since other sensory modalities are able to compensate and provide the animal with sufficient sensory information. Studying the physiology of the lateral-line sensory system and rheotaxis can help to understand how sensory information is perceived, transferred and computed by the brain. Even though rheotaxis is multisensory, it can take place when animals rely exclusively on the lateraling line. Oteiza et al. [2017] demonstrated a behavioral algorithm underlying this behavior, but many aspects of this algorithm and their basis remain unsolved.

1.8 Thesis objectives and main results

This study is aimed at understanding the mechanisms that enable fish to extract and process the directional component of water flow to enable rheotaxis.

To this aim, I have used larval zebrafish and have designed and developed a high-resolution behavioral rig. The behavioral assay combines genetic and laser microsurgical manipulation of the lateralis afferent circuit with controlled environmental conditions in the behavioral rig.

I showed that larval zebrafish exploit mechanical inhomogeneities by recurrent yaw rotations across the horizontal plane to determine the direction of water currents. This study revealed that orientation to water current requires bilateral input from the lateral line. Moreover, my experimental data show that rewiring the lateral-line neuronal map does not disrupt rheotaxis, and suggest that directional tuning, as opposed to fine-grained topographic mapping, plays a main role in this orienting behavior.

In summary, this study describes how larval zebrafish performs rheotaxis using vectorial fractionation of mechanical signals, sensory updating by recurrent yaw rotations, and integration of bilateral sensory information.

Chapter 2

Materials and Methods

2.1 Animals and fish husbandry

Zebrafish (*Danio rerio*) were maintained under standard conditions approved by an Ethical Committee, and under protocol Gz.:55.2-1-54-2532-202-2014 approved by the Regierung von Oberbayern, Germany. Briefly zebrafish embryos were collected from natural spawning and kept in fish medium (NaCl 58 mM, KCL 0.7 mM, $MgSO_4$*7H_2O 0.4 mM, $Ca(NO_3)_2$ 0.6 mM, HEPES buffer 5 mM and pH of 7.6) in 14/10 hour light/dark cycle at 28 °C. They were kept in methylene blue (0.6 μM) until they became larvae. Afterwards they were moved to the fish solution and were fed after 7 dpf. For my studies, I used the following transgenic lines:

tg[*Hgn39D*] (Faucherre et al. [2009])

tg[*Brn3c:mEGFP*] (Xiao et al. [2005])

tg[*Myo6b:beta-actin-GFP*] (Kindt et al. [2012])

tg[*hsp70:mCherry-sill1*] (Pujol-Martí et al. [2012])

tg[*Brn3c:Gal4*] (Xiao et al. [2005])

tg[*UAS:GCaMP7a*] (Muto et al. [2013])

2.2 Neurogenin-1 deficient fish

The transcription factor Neurogenin-1 is essential in zebrafish for the generation of the peripheral nervous system (PNS), which includes the sensory neurons of the lateral line (Andermann et al. [2002]). Neurogenin-1 is dispensable for the development of neuromasts (López-Schier and Hudspeth [2005]). To generate Neurogenin-1 deficient larvae, Ngn1-MO (1 nl of 0,5 mM) was injected in Tg[*Brn3c:Gal4;UAS:GCaMP7a*] double-transgenic embryos at one-cell stage. Morpholinos are the molecular tools which are used widely to block translation of a targeted transcript. Morpholino oligonucleotides (MOs) were obtained from Gene Tools (Philomath, OR).

2.3 Rheotaxis behavioral setup

McHenry et al. [2009] have introduced the impulse chamber to study predator escape response of zebrafish larvae. Oteiza et al. [2017] have used the same chamber for rheotaxis studies under controlled environmental conditions. Importantly, this chambers enables the generation of laminar flow, which has a mathematical solution and therefore the statistics of the input can be calculated. I have built a rheotaxis rig based on the same impulse chamber with further modification.

Specifically, the rig consists of a transparent cylindrical Plexiglas tube that is connected to a water reservoir on one of the free ends and to a mobile plunger on the opposite end (Figure 2.1). The relative size of the Plexiglas cylinder (2.4 cm

inner diameter) to zebrafish larvae enables unimpeded movement for the animal.

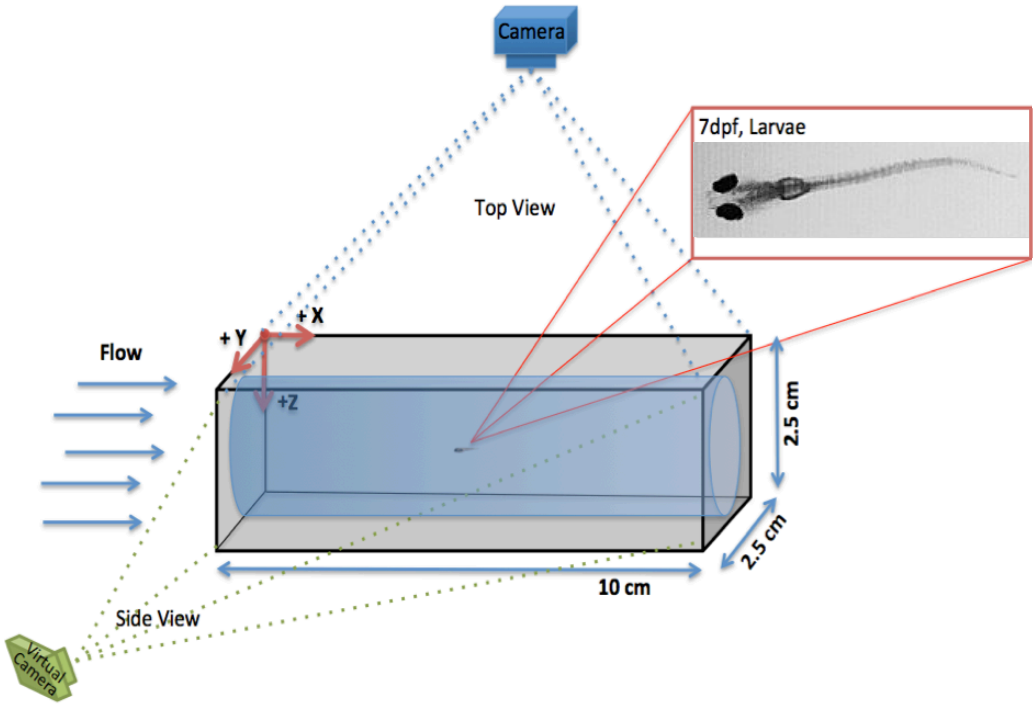

Figure 2.1: *Illustration of the rheotaxis rig. Water current (blue arrows) is created inside a cylindrical Plexiglas (25 mm diameter) that is connected to the water reservoir from one end. Infrared light (940 nm) illuminates the imaging arena. Animal movement is captured by a high speed camera from the top and a mirror enables simultaneous side view allowing 3-dimensional views of the animal. Top left corner is chosen as the center of the Cartesian coordinate system for data quantifications. Inset shows a top view of the fish.*

A fine mesh is placed at either side of the cylindrical Plexiglas to prevent the animal from exiting the imaging area, and also to collimate the water current. An array of infrared (IR) light-emitting diodes (LEDs) emitting at 940 nm were placed below and on one side of the cylindrical Plexiglas to illuminate the imaging arena. It is important to note that, according to literature, the visual system of zebrafish cannot detect IR light (Hartmann et al. [2018]; Meier et al. [2018]).

A camera (NX4 series, Imaging Solution GmbH) with a maximum recording frame rate of 1000 frame-per-second (fps) in full frame (1024 × 1024 pixels) was positioned above the cylindrical Plexiglas ($\sim$ 1.2 meters away) and a mirror was placed on one side of the pipe at 45 degrees, opposite to the LED array.

With this configuration, it is possible to simultaneously capture images from the top and side of the imaging arena. A linear actuator motor (LCA series, SMAC corporation, USA) was connected to the plunger and its back and forth movement created water currents inside the cylindrical Plexiglas. A CAN PCI interface card and digital servo drives (Copley Controls, USA) connected the camera and the motor to the computer running Windows 7.

A camera lens was used in conjunction with the camera to give the necessary magnification and cover the interesting field of view. To increase the spatial resolution of the imaging system, I placed the optical component of a Zeiss stereo microscope (Stemi 2000-C with TV adapter 2/3c, 0.63x) between the camera and the imaging arena. This decreased the field of view to a quarter but considerably improved spatial resolution of images, allowing for a resolution of 10μm.

2.4 Behavioral assay and data acquisition

All experiments were done in IR spectrum of zebrafish larvae (see introduction - optical sensitivity of zebrafish visual system) to eliminate any visual input. The room was quiet and there were no sources of noises nearby. The temperature of the water was maintained continuously at 28°C (standard raising and maintenance temperature for zebrafish) by heating the experimental room with a heater (Fakir 2002 CTF).

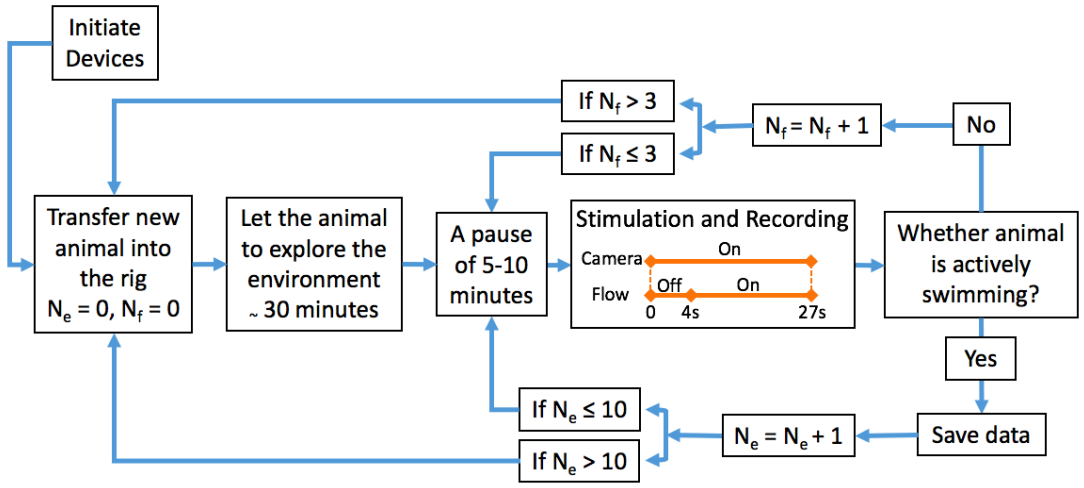

Figure 2.2: *Flowchart of the behavior assay and data acquisition procedure. These sequences of actions were followed in all of the experiments to collect data and save in hardware for further analysis.* N_f *is counting the number of the failure in which fish does not swim actively. After 3 times of failure for the fish under the experiment, I discarded data from this fish and moved to the next fish.* N_e *is counting the number of successful experiments done with any one fish. After 10 experiments, I moved to the next fish. Camera records for 27 seconds while the first 4 seconds flow is off (zero flow) and turns on for the next 23 seconds in the chosen velocity by the user.*

For each experiment, 30 minutes prior to the experiment, one solitary larva was placed inside the rig to allow the animal to adapt to the environment and explore the tube (Figure 2.2). Fish movement was recorded for 27 seconds consisting of 4 seconds prior to flow onset and 23 seconds during flow at a specific velocity. Water flow was generated alternatively in opposing directions by pushing or pulling the plunger inside the tube (see below). Each trial was followed by a pause of 5-10 minutes without water flow to avoid biasing responses to flow.

Flow was started when the fish was near the center of the cylinder. The initial orientation of the fish was not considered and thus assumed random. Animals that did not actively respond to the water currents were discarded ($\sim 2\,\%$). All the settings of the camera such as image properties, lens magnification and lens focus were kept constant in all the experiments to minimize the image processing failures. Height of the water in the reservoir was kept at the required minimum to reduce the gravity effect on water flow inside the tube and was same in all the experiments. Fish swimming pattern inside the tube was recorded by sequences of images through the camera at 200 fps and saved to hardware by the Motion Studio software (Imaging Solution, GmbH) for a posteriori analysis. Matlab (Mathworks Inc.) and Bonsai (Lopes et al. [2015]) were used to analyze these images and extract useful information as will be covered in the next section.

2.5 Image processing and computer vision analysis

Recorded data were fed into Bonsai for extracting the animal's position inside the tube in 3D (horizontal distances from tube periphery, horizontal distance from

tube border and vertical distance from the bottom of the tube) and body rotation relative to axes (pitch and yaw orientation). The computer vision analysis workflow in Bonsai is illustrated in figure 2.3. This program loads a movie file which contains the recorded behavior of the animal by the Bonsai node FileCapture and performs sequences of algorithms for each frame of the movie.

Images were converted to grayscale and were cropped to the Region Of Interest (ROI). Background signal was subtracted from the images, therefore the static part of the scene was removed and the dynamic parts in the scene were kept. Background subtraction node generates foreground images which contains the moving animal in the scene compared to the background. The first frame of the movie was considered as a background image and back ground update set to zero.

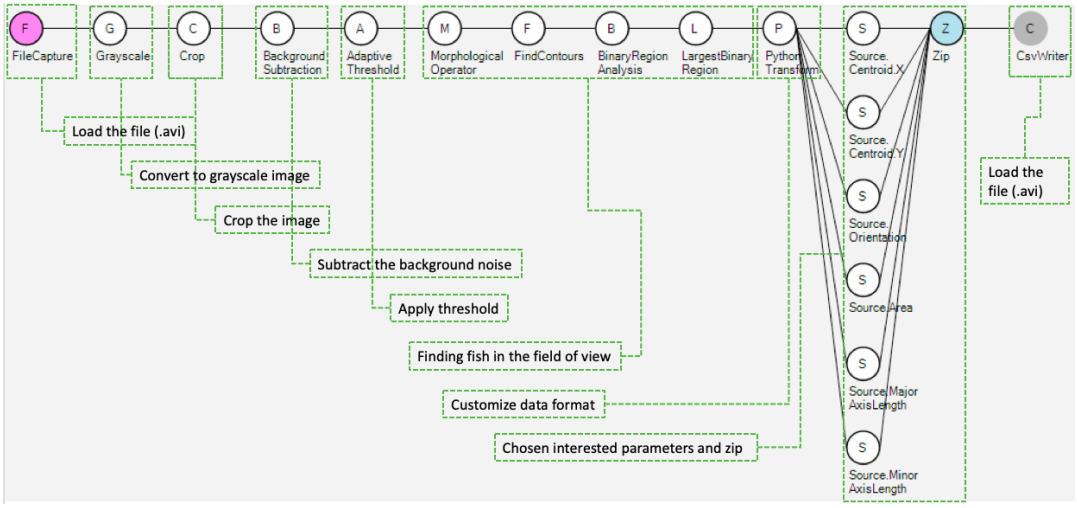

Figure 2.3: *Bonsai workflow to load image sequences and perform computer vision algorithms. Measured parameters are saved as a text file and afterwards were loaded into Matlab for further quantifications. Further details about type of the analysis are provided for each step.*

Thresholding is one of the basic algorithms in image processing to convert an image with continuous distribution to a binary image by assigning a threshold value. There are several thresholding methods such as simple thresholding, adaptive thresholding and Otsu's thresholding. Simple thresholding, as the name suggests, is easy and straightforward. Under this approach, a value is arbitrarily defined by the user. Pixels which have greater values get a new value of 1, those with lower a 0. The threshold value normally is found by trial and error method. More sophisticated methods such as Otsu's method can be used to find the threshold value such as for bimodal images.

Adaptive threshold is the most sophisticated method which assigns a local value for each small region of the image, resulting in better thresholding when light condition vary across the image. The threshold value of each region can be calculated as the mean of neighbourhood area or the weighted sum of neighbourhood values where weights are a Gaussian window. The size of the neighbourhood area can be defined by the user (OpenCV documentation Bradski [2000]).

After subtracting the background and binarization of the image, morphological transformations are used to process the image as morphological shapes. The typical basic binary structuring elements are crosses, squares and ellipses and are used to probe the input image and construct the output image (Soille [1999]). The basic morphological operators are the erosion and the dilation and their combinations can be used for various computer vision tasks. After treating images with the morphological operators, the contours in the image are found and set to the outer counter to ignore the inner counters. Therefore with the contour approach, I have ignored the possible intensity fluctuations in the intensity of the pixels within the animal body shape. Different parameters of this binary image are calculated such as major and minor axes, length and orientation. These data

were saved as text file to be loaded into Matlab for further quantifications.

Figure 2.4 represents a running example of the computer vision workflow on one example of rheotaxis data. The top workflow is for analyzing images from top view camera and the down workflow is for analyzing side view. The output results after performing image processing methods are shown and the final measured parameters of animal orientation and position inside the tube is displayed.

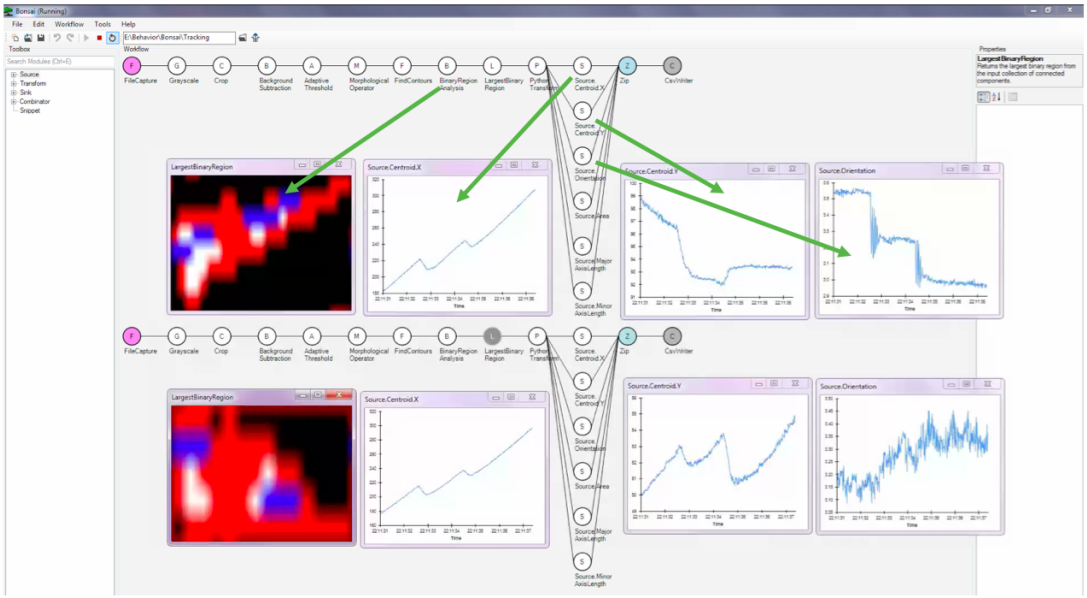

Figure 2.4: *Computer vision workflow example running on rheotaxis data. A movie of zebrafish larvae that is performing rheotaxis was loaded into the program. The output images are shown for some methods being applied in different steps. The final output which includes fish orientation and position in x, y, z for both side and top view is saved.*

Measured parameters (animal position and body orientation) were exported into Matlab custom written script for analysis of rheotactic performance. Depending on the need, various aspects of the measured and quantified parameters are visualized. An example is shown in figure 2.5. In this example a 7 dpf larvae,

imaged at 200 fps (Figure 2.5 B) while 6 mm/s flow is running from left to right inside the tube (black arrows). Transversal and longitudinal view of the animal location inside the tube with its orientation is presented in 2-dimensional (Figure 2.5 A-C) and 3-dimensional (Figure 2.5 D) over the time of experiment which is colour coded in which purple is the starting time point and red is the end of the recording.

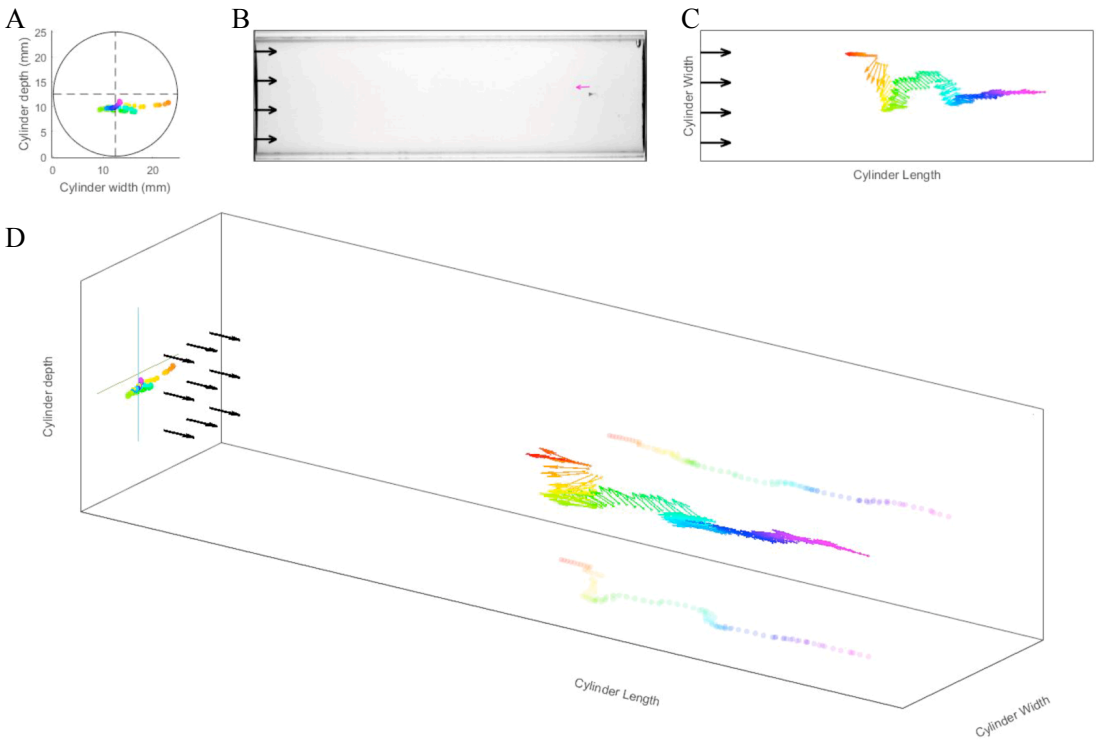

Figure 2.5: *Data acquisition and analysis in Matlab. Bonsai output was saved and later was loaded into Matlab custom written script for further quantifications and visualization. Transversal and longitudinal view of the animal location inside the tube together with its heading was plotted in 2D (A-C) and 3D (D). Black arrows show the flow direction which is from left to the right. Colour represents the time, starts with purple and ends with red.*

2.6 Increasing spatial resolution of the imaging system

In most of the experiments my imaging system covers the whole length of the tube between the nets on either ends as well as the whole width, unless otherwise mentioned. For more detailed studies of animal movement, spatial resolution was increased as a trade-off to the size of the field of view.

To further increase the spatial resolution, I modified the imaging system by placing the Zeiss stereo-microscope (Stemi 2000-C with TV adapter 2/3c, 0.63x) on top of the imaging arena. With this modification, the field of view decreases to a quarter of the size but the improved spatial resolution allows a better resolved observation on details of movement.

2.7 Measuring rheotactic performance in larval zebrafish

Zebrafish larvae exhibit positive rheotaxis. For convenience, the orientation of the larvae perfectly facing incoming flow will be considered as zero (0) angle orientation. Thus, upstream swimming will have a zero degrees orientation, whereas downstream swimming will have 180 angle orientation (negative rheotaxis). Since animal orientation is recorded over a few dozens of seconds, the amount of the angular data is high for comprehensive visualization. I have employed a mathematical cosine function to visualize and quantify the orientation data. Cosine of the orientation (trigonometric function) is a useful mathematical function which makes the range of the index from -1 (negative rheotaxis) to +1 (positive rheo-

taxis) (Figure 2.6).

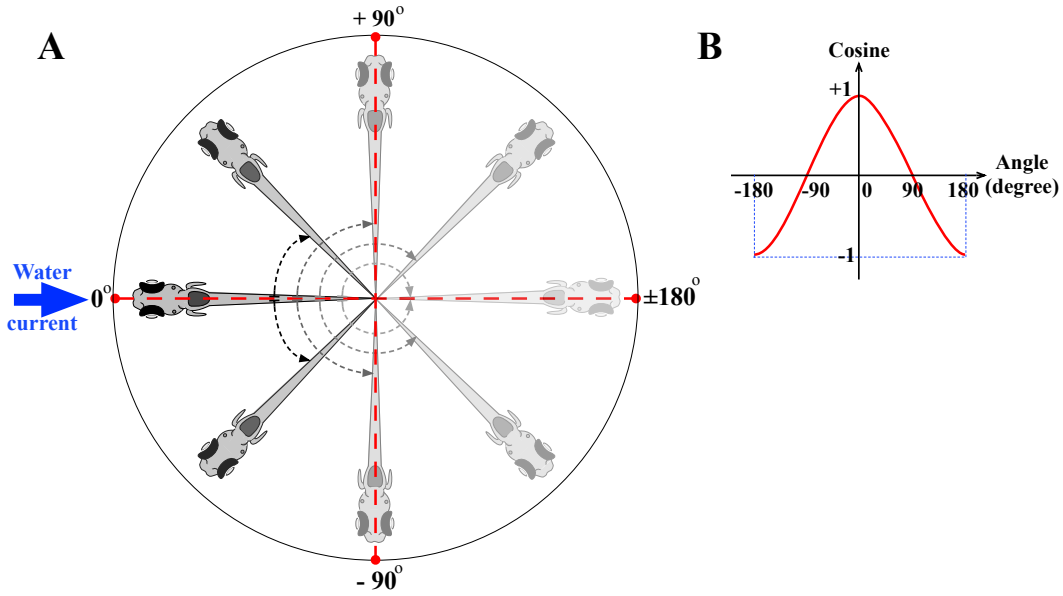

Figure 2.6: *Orientation of the animal is a parameter for rheotaxis measurements. I define the upstream as a zero angle orientation so the larvae in which is facing the flow and performs positive rheotaxis has zero angle and the animal swims in the direction of the flow and performs negative rheotaxis has 180 angle orientation (A). Blue arrow indicate the direction of the water flow which is from left to right. Zebrafish larvae perform positive rheotaxis, orient around the zero degrees (darker fish in panel A) and less orientation in opposite directions (faded fish in panel A). For convenience cosine of the angle is considered as an index for the performance comparison (B).*

2.8 Statistical analysis

All statistical analyses were done with Matlab (MathWorks, Inc.) and the statistics software R (R Core Team [2013]). For the analysis of rheotaxis, Kolmogorov-Smirnov tests and F-tests were employed to check the assumptions for the ANOVA (analyses of variance) used to compare the different conditions. The assumptions of the normal distribution and the homogeneous variance were rejected for some groups, so instead of a one-way analysis of variance I used a Kruskal-Wallis test (also referred to as KruskalWallis one-way analysis of variance by ranks) for the overall comparison of all groups and post-hoc tests according to Dunn for pairwise multiple comparisons.

To compare the occupation profile (3-D profile of the fish location inside the tube) in different conditions and the symmetry of the resulting curves, the pairwise Kolmogorov-Smirnov test was used to test whether two samples are drawn from the same distribution.

2.9 Live microscopy imaging

Microscopy imaging of immobilized animals, was done by first anesthetizing 7-day old larvae with 610 μM solution of the anaesthetic 3-aminobenzoic acid ethyl ester (MS-222). Experimental animals were placed in a glass-bottom Petri dish and covered by 1% low-melting point agarose. Upon solidification of the agarose, MS-222 (610 μM) was added to keep animals anesthetized for the course of the experiment. An inverted Zeiss Axio Observer spinning-disc confocal microscope or an inverted Zeiss laser-scanning confocal microscope was used for imaging. Images were acquired through the microscope software with a 40x air or 63x

water-immersion objective. The z-stacks or a single image of the region of interest (ROI) without binning were captured and saved in the computer running Windows 7 for further analysis. All the fluorescence microscopy images were analyzed with ImageJ software (Schindelin et al. [2015]).

2.10 Laser microsurgery of the lateral-line sensory system

Laser microsurgery was used to eliminate the sensory input from the lateral line to the brain, by severing the central projections or peripheral axons of lateral-line afferent (ascending) neurons, depending on the aim of the experiments, with micro-scale resolution, leaving other nearby neurons and cells intact.

I used the iLas Pulse laser system (Roper Scientific SAS, France) equipped with an ultraviolet laser (355 nm emission) mounted on an inverted microscope Zeiss Axio Observer. Laser pulses were delivered through a 63x water immersion objective. To maximise severing and minimize the optical toxicity and non-targeted damage, the laser power and pulse duration were adjusted empirically based on the experiments. Spatial targeting was calibrated in advance to the experiment. 6 dpf larvae were anesthetized and mounted on a glass-bottom dish in 1 % low-meting point agarose. Multiple laser pulses were applied to the target neurons over a short period until axons were severed.

Distal axon detachment from the neuron was confirmed approximately 1 hour later. Treated larvae were then released from the agarose and kept in fish medium at $28°C$. All the behavioral experiments were done 24 hours after axonal severing to enable recovery of any potential damage to hair cells in neuromasts, which can

arise from handling and agarose mounting. After the behavioral experiments, fishes were imaged with 63x objective to certify the continuous absence of neuronal central projections.

For experiments of re-wiring of neuronal somatotopy, all the peripheral axons of posterior lateral-line neurons were severed using the microsurgery protocol described above, but in 3 dpf fish. The larvae were then kept in fish medium at $28°C$ for 4 days. Then, rheotactic behavior experiments were conducted. Next, fishes were imaged with 63x objective as before to certify the regeneration of peripheral axons.

Chapter 3

Results

3.1 Calcium imaging in zebrafish lateral-line hair cells

The lateral-line system of the fish is directional mechanosensory system which relies on the directional responsive properties of the hair cells. Fish uses the directional sensory information for rheotaxis behavior. This directional mechanosensory functionality of the hair cells can be demonstrated by electrophysiological recording and calcium imaging. I used calcium imaging to show the mechanotransduction functionality of the hair cells in the zebrafish lateral line. Larval zebrafish was mounted carefully in order to prevent damage to the hair cells. A single neuromast was stimulated bi-directionaly by a water jet, and the dynamic response of hair cells was quantified.

The same stimulation protocol was used to stimulate the Neurogenin-1-deficient (ngn1-MO) larval zebrafish, which lacks the peripheral nervous system, including

afferent and efferent neurons of the latter line. I compared the calcium imaging results between the larvae with normal posterior lateral line and the ngn1-deficient larvae. This comparison yielded in the dependency study of the mechanotransduction functionality (as a base of the rheotaxis) to the hair cells innervation by LANs.

3.1.1 Mounting zebrafish larvae for calcium imaging

I optimized an approach to mount the zebrafish larvae for calcium imaging, in which the animal is immobilized only from the head, whereas the trunk and tail are free. In this approach there is no damage to the posterior lateral line, in which the target neuromasts are located. Figure 3.1 shows the steps followed with the explanation of each step.

Briefly, a rod of agarose (Figure 3.1 step 1) is cut in middle, halfway the length of the rod (Figure 3.1 step 2). The 7 dpf larva was placed gently between the two parts of the agarose by opening them up and pushing the fish inside (Figure 3.1 step 3). Orientation of the fish can be modified because the glass capillary can be rotated. At this stage, due to mechanical forces of the two pieces of agarose, the animal is held in place. If needed a small drop of agarose can be placed on top of the fish, to keep it stable (Figure 3.1 step 4).

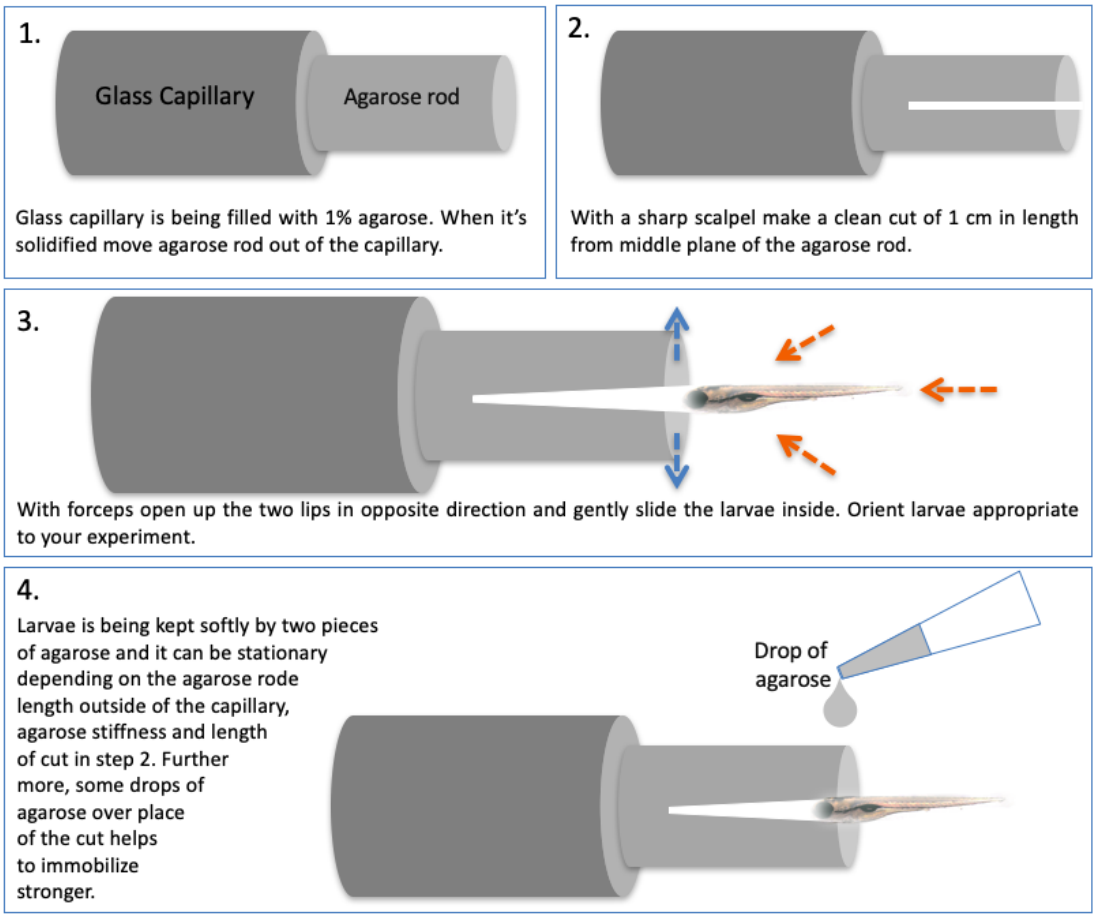

Figure 3.1: *Illustration of the approach to mount 7 dpf zebrafish larvae for calcium imaging in lateral line hair cells. This approach consist of 4 steps as described in the figure.*

To confirm no damage is caused to the fish and the lateral-line neuromasts, I stained the zebrafish larvae with 500 μM solution of DiASP, which generates orange fluorescence upon entering cells. Treated larvae were washed briefly. Crucially, DiASP is taken by hair cells of the lateral line through the mechanical gated channels in intact stereocilia. By incubating *Brn3c:GFP* transgenic line (which marks all the mature hair cells) in DiASP solution, all GFP labeled hair cells will be orange, indicating no damage to existing hair cells. Figure 3.2 A and B show the images of zebrafish larvae after DiASP treatment. In the case of stereocilia damage, no fluorescence would be detected. Upon massive damage, however, DiASP would be unconditionally incorporated by many cells and a very bright non-specific spot orange-fluorescent signal would be seen all over the neuromast. Figure 3.2 confirms that my approach of mounting is not causing damages to the fish and there for I can proceed with calcium imaging.

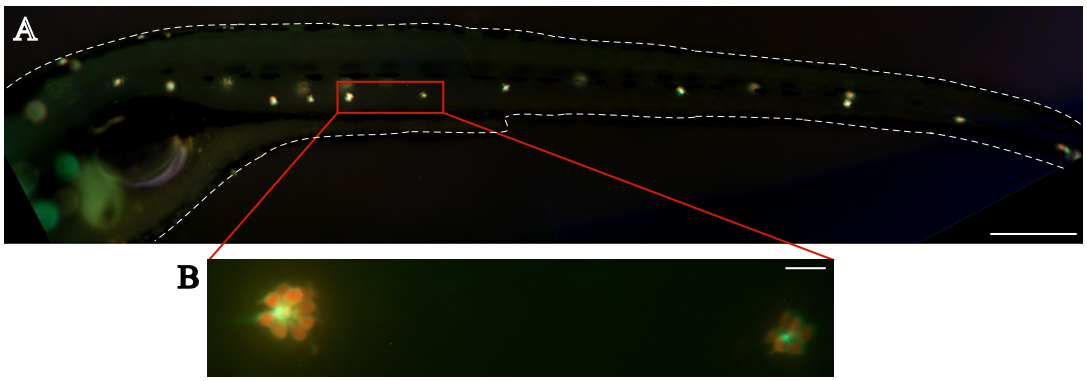

Figure 3.2: *A) DiASP staining and imaging of zebrafish larvae (Brn3d:GFP) at 7 dpf after being mounted with the approach mentioned in the figure 3.1. DiASP passes through the mechanosensory channels of the hair cells if they are functional. In the case of damage caused by mounting or handling larvae, the DiASP will go through easily and a saturated yellow fluorescence will be visible. In my case, DiASP is visible cleanly and only in neuromast (B). Scale bars are 300μm in A and 10μm in B.*

3.1.2 Water-flow stimulation and calcium imaging of posterior lateral line hair cells

I used the general approach of the neuromast hair cells stimulation as described previously (Trapani and Nicolson [2010]) to perform the calcium imaging. A thin pipette with ~ 30 μm tip diameter was pulled from a borosilicate glass capillary and filled with extracellular solution. The pipette was placed approximately one-neuromast-diameter away from the target neuromast (Figure 3.3 A and B). Upon the jet, kinocilia of the neuromast deflect and cause the mechanical opening of ion channels in stereocilia. The effectiveness of the water flow was confirmed by very fast imaging of kinocilia bending as illustrated in figure 3.3 C and D. The water jet was created by using the XenoWorks digital Microinjector (Sutter Instruments, Novato, USA) and calcium fluorescence was imaged in each hair cells during alternating periods of resting (5 seconds) and water-jet stimulation (0.10 seconds).

An Olympus BX61 microscope with a 20x water immersion objective (Olympus, Japan) with numerical aperture of 1.0 was used for imaging. The microscope was equipped with a digital CMOS camera ORCA-Flas4.0 (Hamamatsu Photonics, Japan) and was controlled by the software package in μManager (Edelstein et al. [2010]). Exposure time of ~ 85 ms was used and all images were saved in internal drive for further analysis.

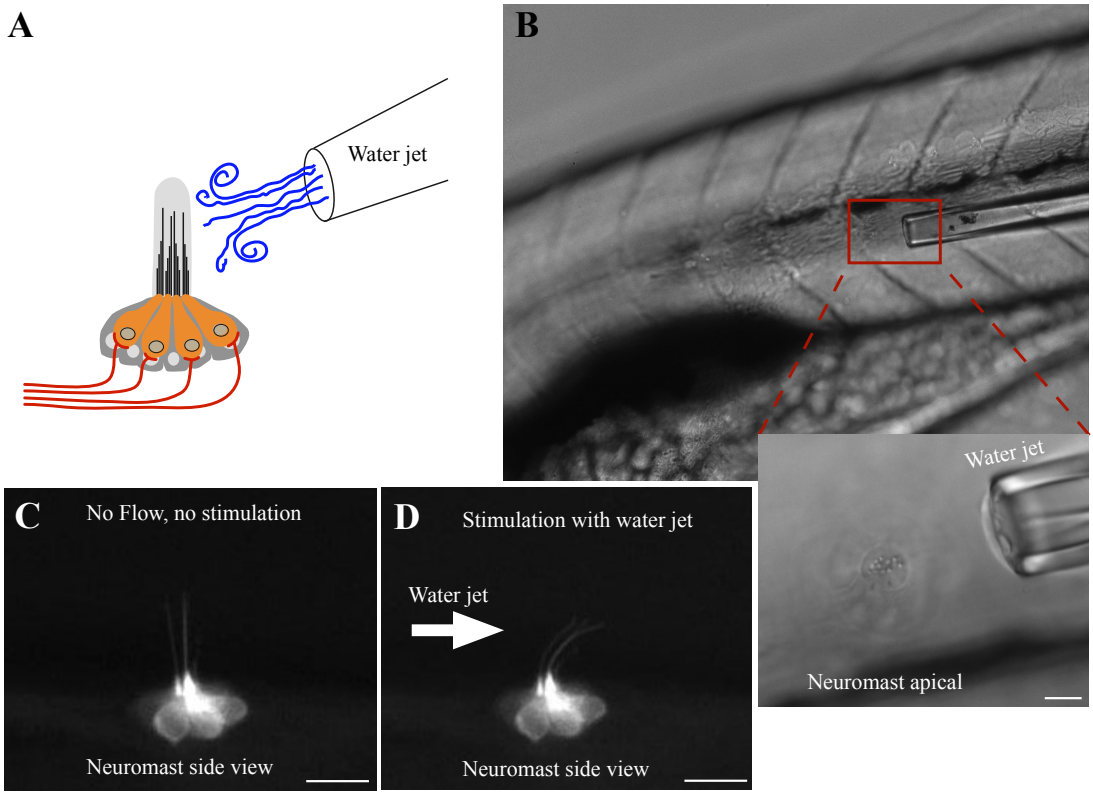

Figure 3.3: *A) Schematic of the hair cells stimulation with the water jet. A pipette with fine opening oriented at small angle of the fish body and connected to a pump to create water flow over the neuromast. Created water flow, displaces the kinocilium and stereocilia to open the mechanical channel. Pipette can blow the water or suck the water in, creating bi-directional stimulation of the hair cells. B) Shows the size and orientation of a example pipette over the trunk of the fish. Inlet shows the zoom in view, in which the neuromast apical and the pipette are in the same depth of field. A neuromast labeled with GFP (Brn3c:GFP) is shown in side view in panels C and D. The kinocilium is visible and used to confirm the effectiveness of the water jet stimulation. Scale bars are 10 µm in B inlet, C and D.*

3.1.3 Data quantification and analysis

All the calcium imaging data were processed using ImageJ and custom written scripts in Matlab. For a chosen calcium imaging recorded images over the length of the experiment, the following procedure was performed: a time window of approximately 4 seconds, including a resting period lasting from 1 to 1.5 seconds which followed by a brief water-jet pulse of duration 0.10 seconds and another resting period lasting from 2.5 to 3 seconds.

I identified each hair cell in the image and drawn a region of interest (ROI) around it. For each ROI the average pixel intensity (fluorescent signal, F in the following equations) over time was measured and at the end, the relative GCaMP7a fluorescence change was calculated by using the formula:

$$\Delta F/F = (F_t - F_t i)/F_t i \tag{3.1}$$

Where F_t is the value of the fluorescent signal measured within the ROI at the current time point and $F_t i$ is the value of the fluorescent signal measured within the same ROI at the time point in which the experiment started.

I considered that hair cells with a $\Delta F/F$ value higher than 0.05 (5 percent of relative fluorescence increase) were responsive to the water jet stimulus, otherwise were discarded. I selected the highest $\Delta F/F$ (Max$\Delta F/F$) shown by these hair cells after water-jet stimulation and calculated the average Max$\Delta F/F$ of hair cells present in neuromasts from wild-type and Ngn1-deficient animals (Figure 3.4). Interestingly, hair cells of Ngn1-deficient zebrafish remain mechanoreceptive and perform mechanotransduction (Figure 3.4).

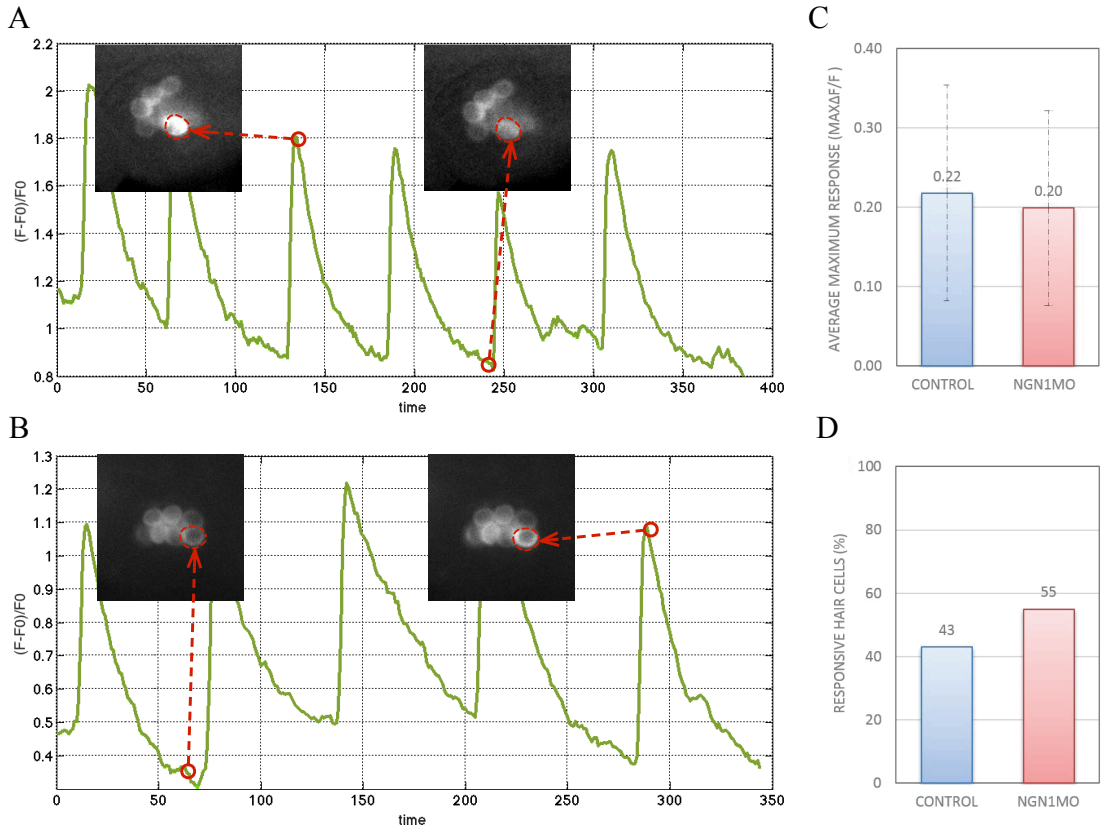

Figure 3.4: *Quantification of calcium imaging in hair cells of wild type (A) and Neurogenin-1 morpholino-injected (B) zebrafish larvae. The calcium-signal changes upon flow stimulation were quantified by calculating the percentage of signal (F) changes from the baseline (F0) divided to the baseline. The value is plotted over the time of the stimulation. The stimulation was created regularly. Example images of high and low calcium levels are shown in panels A and B. Panels C and D represent the quantification of calcium imaging in hair cells from control and Ngn1-deficient larvae upon water-jet stimulation. (C) Average Max$\Delta F/F$ reached after water-jet stimulation in responsive hair cells from control ($n = 6$ hair cells) and Ngn1-deficient animals ($n = 6$ hair cells). Error bars represent the std. (D) Percentage of responsive hair cells to the water-jet stimulation in control ($n = 14$ hair cells) and Ngn1-deficient animals ($n = 11$ hair cells).*

3.2 Design of the behavioral setup with specific hydrodynamics

I set out to establish a quantitative behavioral assay that includes a well-controlled simulation protocol and three-dimensional assessment of behavior. To explore the rheotaxis in zebrafish larvae, I aimed to create laminar water flow because such regime enables the direct correlation between the statistics of the mechanical stimulus and the behavior of the animal.

I constructed a rig that simultaneously enables control of water currents and high-resolution three-dimensional videography of unrestrained zebrafish larvae. The set-up was built with the general approach described in the Material and Method section and is drawn in the figure 3.5 A and B. Of note the rig was inspired by a design of Oteiza et al. [2017] with modifications. The rig consists of a transparent seamless cylindrical pipe made of Plexiglas that is completely filled with water. A linear actuator controls an inner plunger that slides along the pipe to generate flow (see material and methods for more details) (Figure 3.5 A, B). The rig is isolated from larval zebrafish sensitive spectrum (see introduction - optical sensitivity of zebrafish visual system). A homogeneous infrared light (940 nm) illuminates the imaging arena from below and side. This behavioral rig has multiple advantages over the similar setups which are critical for having reliable current stimulus and precise record of swimming pattern. In the following, these improvements are described.

To create a laminar flow, I used an actuator that is precise, stable and reliable to move with predefined constant velocity.

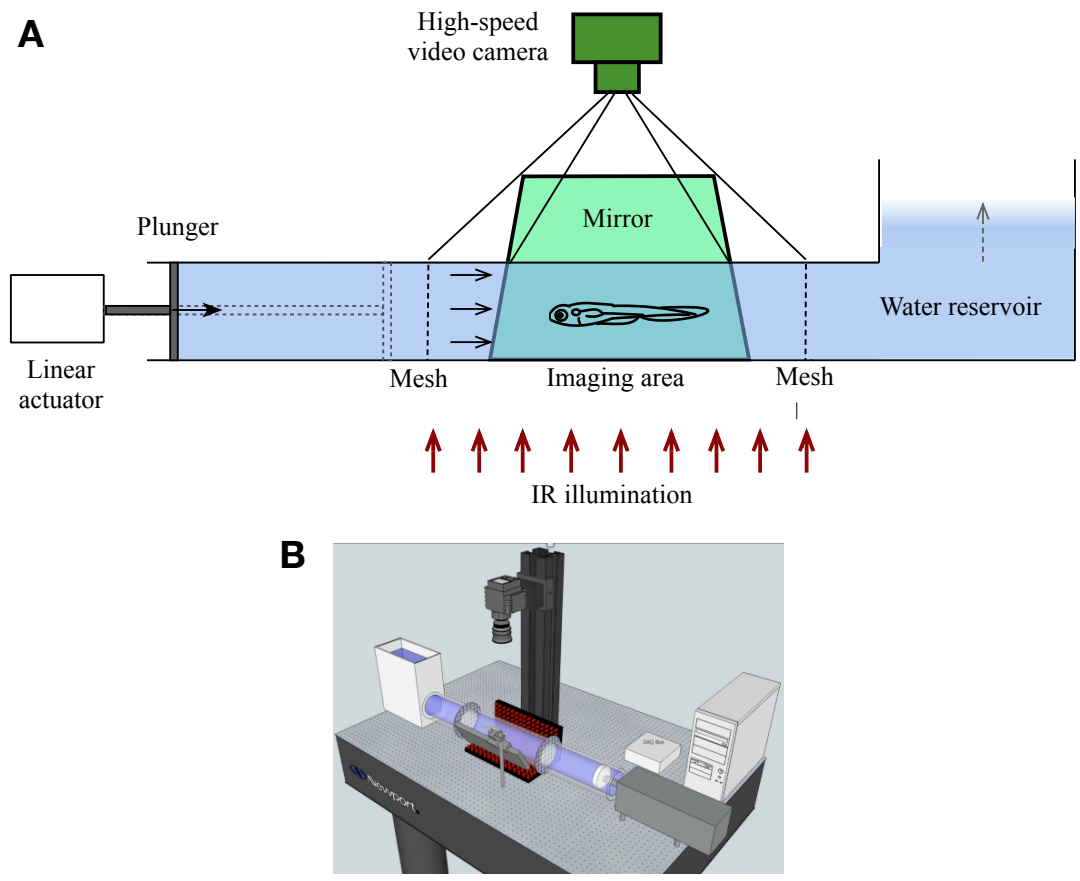

Figure 3.5: *Illustration of designed and constructed rig to probe rheotaxis in zebrafish larvae. A) A linear actuator moves a plunger inside a tube to create water current. Camera is above the rig, capturing the top view and side view (reflection from side mirror) of the chamber. The rig is illuminated only with infrared light. B) The three-dimensional representation of the rig, drawn with Sketchup.*

The pipe has a smooth inner surface, without irregularities, to prevent the formation of turbulence. It was constructed using three pieces that are screwed together (Figure 3.6), avoiding the need of gluing, which might create uneven surfaces. The connections between the individual pieces of pipe are not permanent, facilitating the placing of the fish inside the pipe without the need of a hole in the tube. In this way, the imaging arena is completely transparent without having any optical effects that may affect imaging (Figure 3.6).

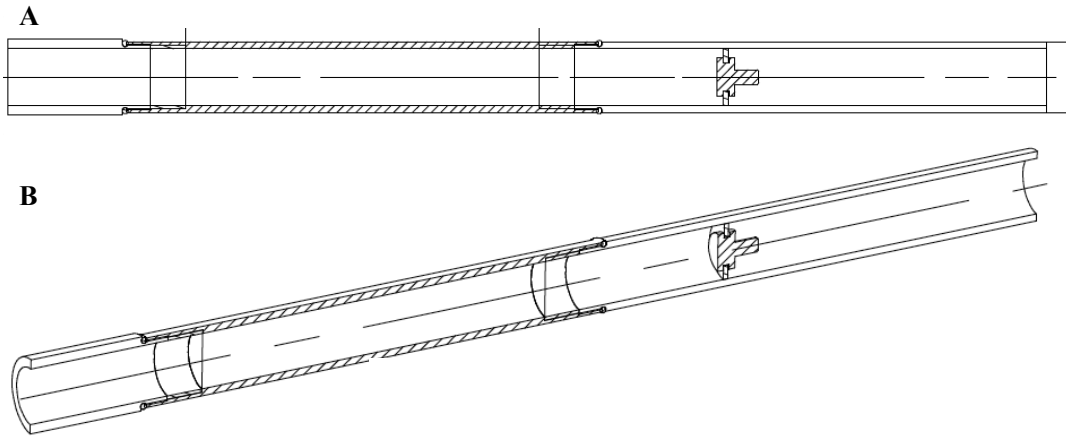

Figure 3.6: *One advantage of this rheotaxis rig is the design of Plexiglas tube in three pieces which can be screwed to each other to be comfortable for fish handling, easy and fast exchange of fish and smooth surface for avoiding the water turbulence. The three pieces are visible in top (A) and tilted view (B). This drawing was created by the central workshop at the Helmholtz Zentrum München*

Water, air and Plexiglas have different refractive indices that cause light refraction when light passes from one to another. Light follows Snell's law when passing media with refractive index of n_i to the medium with the refractive index of n_j as following (Figure 3.7A):

$$n_i \times sin(a_i) \quad = \quad n_j \times sin(a_j) \tag{3.2}$$

Where a_i is the light incident angle and a_j is the outgoing light angle. Note that if the incident angle is zero (perpendicular light) there will be no refraction. However, if the incident angle is larger than zero but smaller than a critical angle, refraction will occur. Incident angles larger than the critical angle will reflect and so called total internal reflection occurs. For water-air interface, the critical angle is around 48 degrees.

Since the refractive index of Plexiglas and water are similar and higher than that of air, their combination with the curvature of the tube will act as a lens, creating an unwanted optical distortion (Figure 3.7 B). This optical distortion may hide the larvae at the edges of the pipe, and elongates it according to its' position inside the pipe.

There are two approaches to compensate such distortion: one is to calculate the magnitude of the distortion based on the position of the larva and to reconstruct the image afterwards as post processing step. This compensation matrix is applied after gathering the data and may not result in as-good-as expected image in every case since the larva will be poorly visible at the edge of the tube, making it impossible to do the reconstruction. An alternative method is to immerse the rig in water. Since water and glass have similar refractive indices and the thickness of the glass at few millimeters is negligible, this will smooth the light refraction and will have better light transmission through the tube, preventing aberrations by suppressing the lensing effect.

To test experimentally the effectiveness of this approach, I printed a sinusoidal curve on a paper (Figure 3.7 C top panel) and placed the tube on top to observe the pattern of the curve (Figure 3.7 C middle panel). The sinusoidal pattern of the curve was disrupted strongly especially at the edge of the pipe which highlights

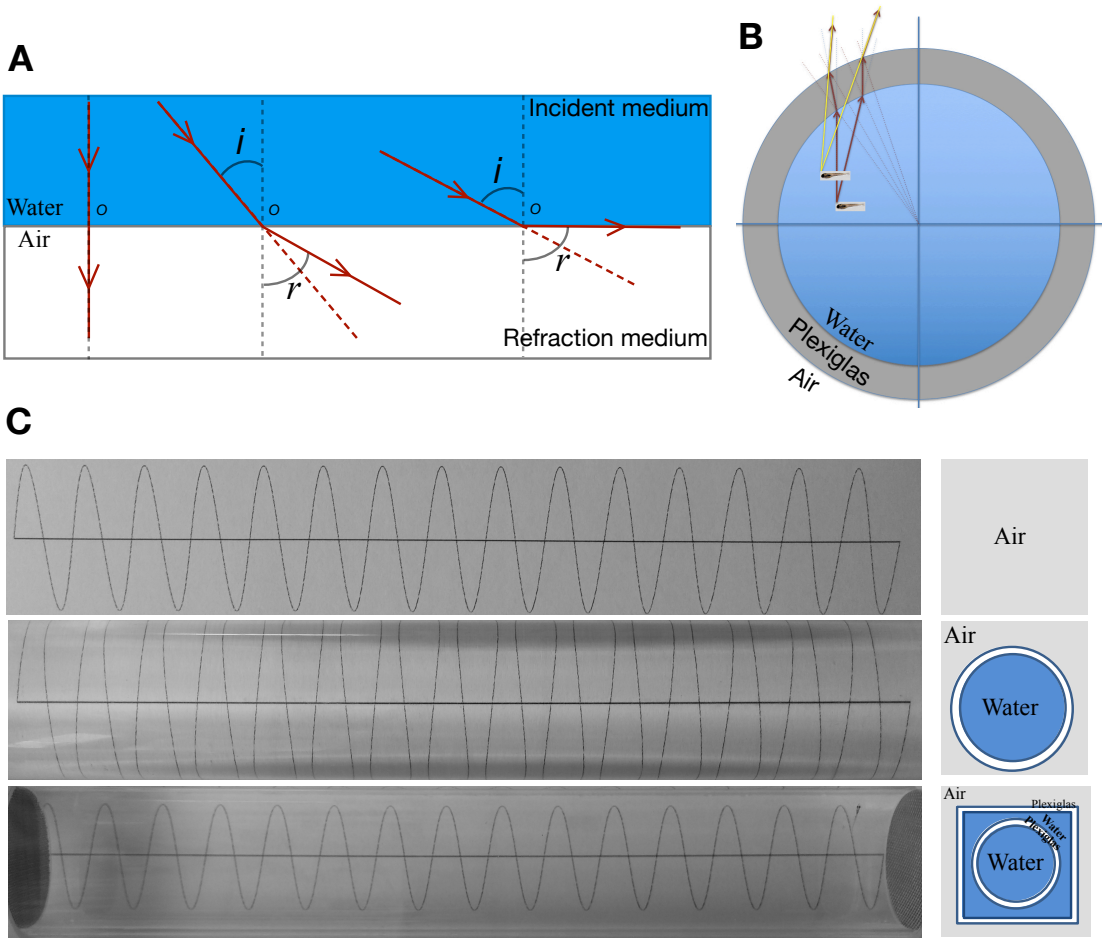

Figure 3.7: *A)When light passes through media with different refractive indices, refraction will happen according to the Snells law. B) Illustrates the lensing effect created by the curvature of the tube which is filled with water. Red lines indicate the light path to the camera and yellow lines show the imaginary position of the image of the fish seen by camera. C) Sinusoidal pattern as it is printed on a paper in shown in upper image and in the middle image the disturbed pattern of it when is shown through the Plexiglas tube filled with the water. The bottom image shows my approach of overcome this issue by putting the tube inside water.*

the lensing effect before correction. Then, I placed the tube inside the water and observed the sinusoidal curve (Figure 3.7 C lower panel). The tube with no correction shows a distorted sinusoidal wave due to the lensing effect, whereas the optical correction removes this distortion.

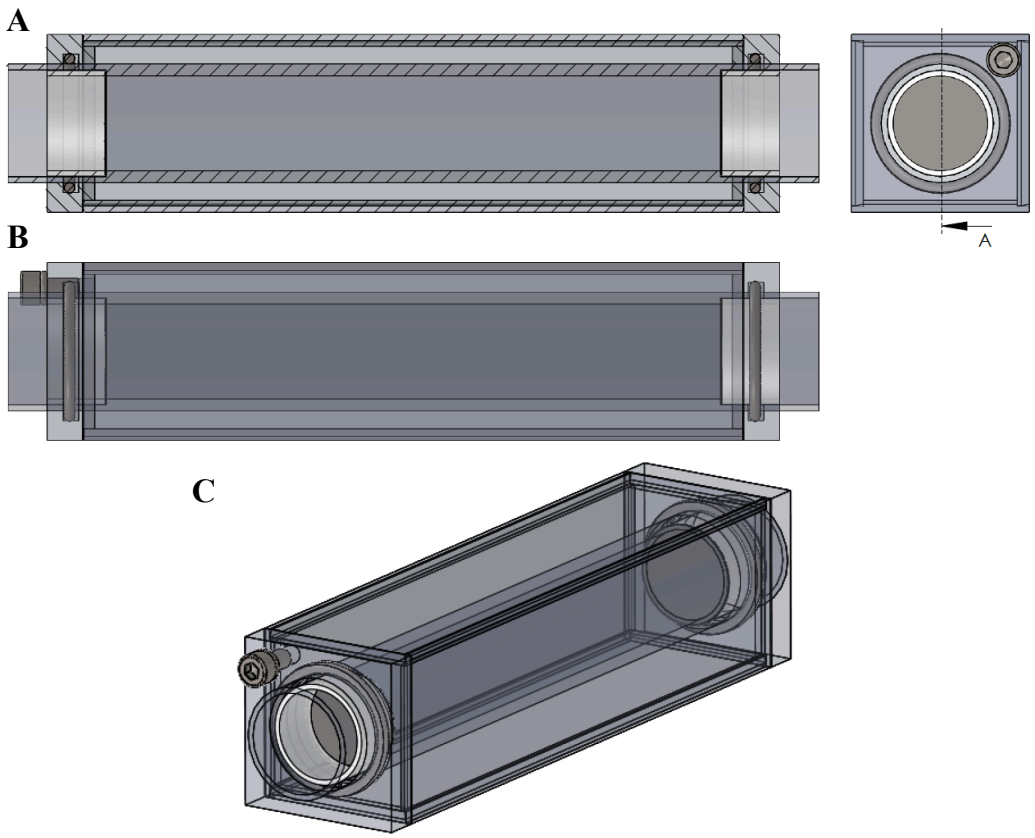

Figure 3.8: *Placing the imaging arena inside a cube, filled with water, removes the lensing effect. A and B show the technical drawing of the side view of imaging arena designed and built as described. C shows nicely the three dimensional view of the final design. These drawings are provided by the central workshop at the Helmholtz Zentrum München.*

To apply this solution for the behavior rig, I placed the tube inside a cube filled with water and made of flat Plexiglas, which corrects the lensing effect. The water is encapsulated in the cube to prevent optical distortions by vibrations (Figure 3.8). With this approach, I was able to create imaging arena free of lensing effect and vibration. In figure 3.9 an image of the optically corrected imaging arena with a 7 dpf larvae is shown. The larva despite being at the edge of the tube, is completely visible without showing optical distortions.

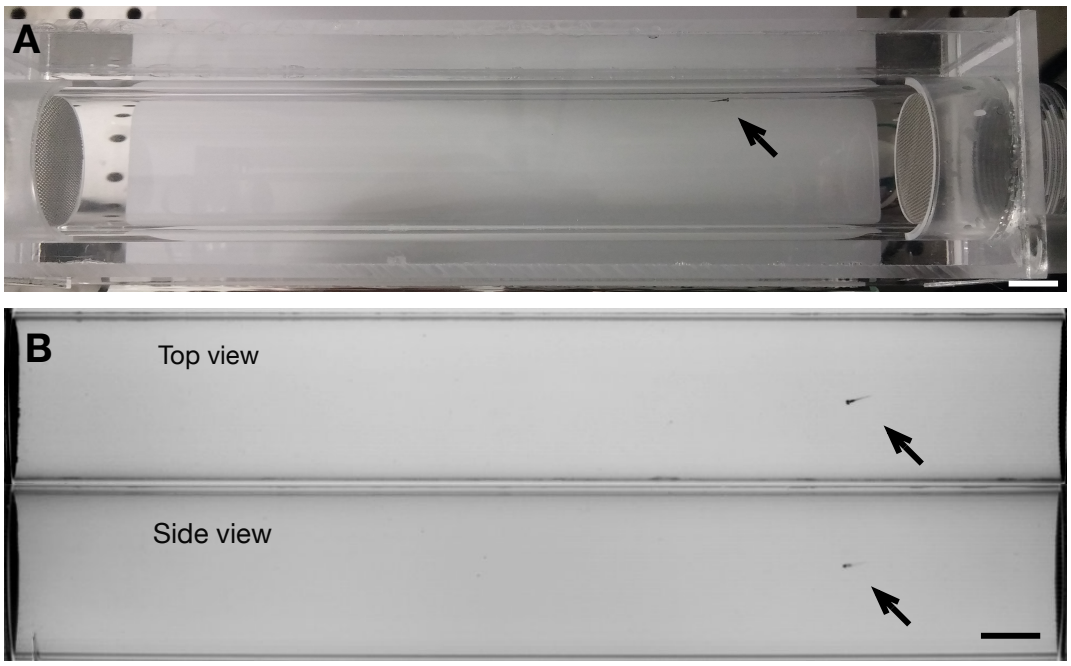

Figure 3.9: *A) An image of the optically corrected imaging arena with a 7 dpf larvae inside of it is illustrated. The larva is indicated by black arrows. The fish is completely visible without distortion even at the edge of the tube. B) The images which are captured by the acquisition camera from top and side views of fish with the optically corrected imaging arena. The larva is indicated by black arrows. Scale bars are 10 mm in panels A and B.*

3.3 Characterization of hydrodynamics inside the tube

During rheotaxis, fish may use one or multiple hydrodynamical features (velocity, velocity changes (acceleration), and pressure distributions) to detect the presence of the flow and determine flow direction. There are two fundamental source of forces in water currents, and their relative influence characterizes the flow. These are the inertial force and the viscous force. Inertial force is caused by water acceleration whereas the viscous force is the resistance of fluid to deformation. The relative magnitude of these two forces is defined as the Reynolds number. Low Reynolds numbers characterize a laminar (highly viscous) flow, whereas high numbers define a turbulent (highly inertial) flow. The hydrodynamics of a small fish depend on the angle of incidence of flow and the Reynolds number. At Reynolds numbers smaller than 103, the flow remains laminar because inertial forces are negligible. Otherwise, inertial forces become significant, leading to flow separation and the formation of vortices or curls on the flank of the fish opposite of that facing the flow (Vogel [1984]; Langlois and Deville [2014]).

The flow field velocity (V) is given by:

$$d^2V/d^2r + (1/r) \times (dV/dr) = -(1/n) \times (\Delta P/\Delta X) \tag{3.3}$$

in which

$$V = A + B \times r^2 \tag{3.4}$$

r is distance from the center of the pipe, A and B are constants to the boundary

conditions of the flow. $\Delta P/\Delta X$ is the pressure gradient. The velocity profile is three-dimensional however the transverse symmetry of the pipe allows to consider the flow in two dimensions. Laminarity results that at full development the flow remains constant, only varying in the radial direction. More ever, since there is no relative movement in the liquid-solid interface at the wall of the tube, the fluid velocity near the boundary approaches zero and it increases toward the center of the tube. Thus, the flow-velocity profile is defined:

$$V(r) = V_m \times [1 - (r^2/R^2)] \tag{3.5}$$

Where V_m is the maximum velocity defined as:

$$V_m = 1/4 \times \eta \times (\Delta P/\Delta X) \times R^2 \tag{3.6}$$

and η is the viscosity. In a continuously filled pipe with equivalent amount of liquid entering and leaving the pipe, the liquid is flowing at a steady rate. In other words, the flow is called steady if it does not change over time. For an incompressible viscous fluid (a fluid is incompressible if the density of its constituent element stays constant during motion) under non-slip conditions, the Navier-Stokes equations state that laminar flow has a quadratic distribution of velocity, being maximal in the center and zero at the boundary between water and the tube (Figure 3.10) (Vogel [1984]; Graebel [2007]). This property facilitates the determination of flow velocity in three-dimensions from two-dimensional flow profiles.

Of note, under such conditions the flow is a pseudovector field because flow velocity decreases outwards from the central axis (Figure 3.10). Thus, a local

rotational motion of the flow forms around any submerged solid object. This pseudovector field is called vorticity and is defined as the curl of the velocity of the flow vector V:

$$\vec{CurlV} = \nabla \times \vec{V} \tag{3.7}$$

The direction of the vector $\vec{CurlV}$ defines the axis of rotation and its magnitude depends on the strength of the rotation, which is zero at the center of the pipe and maximal near the boundary between the water and the pipe [Vogel [1984]; Graebel [2007]].

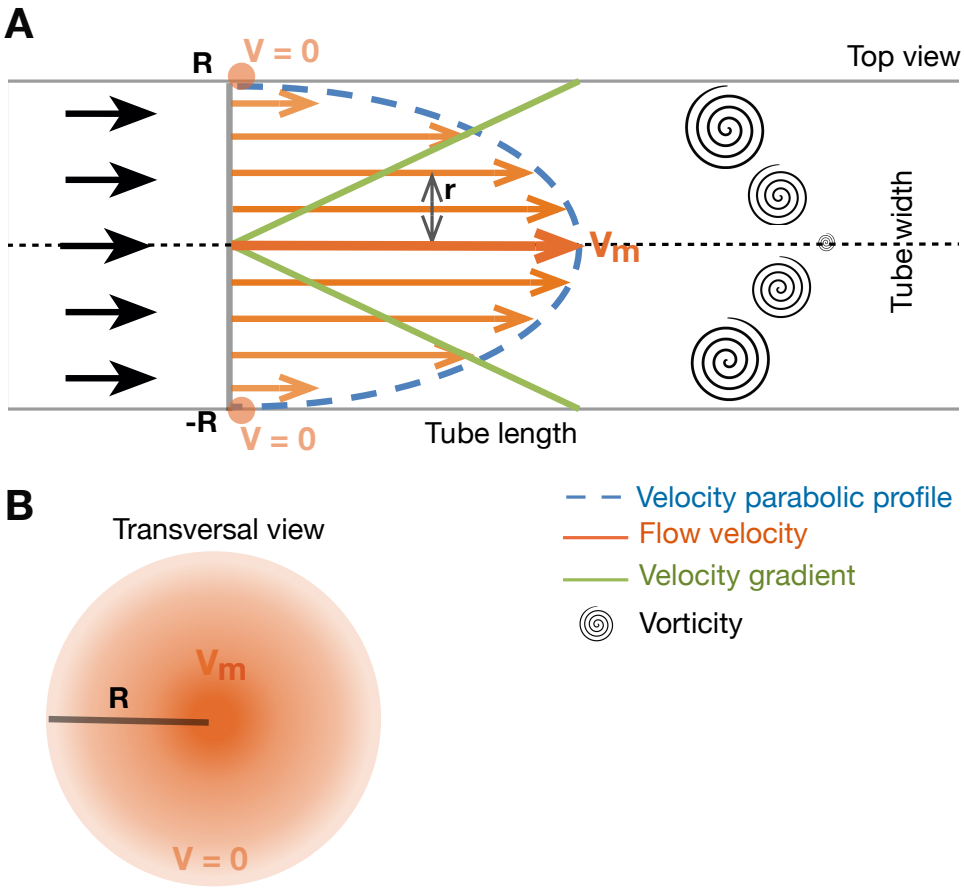

Figure 3.10: *Hydrodynamics of the water flow inside a pipe. A column of water moving at a constant velocity within the pipe will generate velocity gradient across its width. Water flows at higher velocity in the center of the pipe (darker colour) and lower toward the periphery (lighter colour), being zero within the boundary layer between the water and the pipes surface. The velocity gradient creates vorticity being maximal at the edge of the tube and minimal toward the center of the pipe. Panels A and B show the top and transversal view, respectively.*

One way to test whether flow is laminar in my rheotaxis rig is to quantify the trajectory of opaque particles suspended in the liquid. If the trajectory of the particles forms a straight line, the flow is laminar, otherwise the flow is considered turbulent as shown in figure 3.11 A and B.

I recorded the trace of a water-soluble dye delivered into the pipe through a small hole at the tip of a syringe needle placed in the middle of the water column at one end of the pipe. The data show that I can generate laminar flow in the rheotaxis rig (Figure 3.11 C-F).

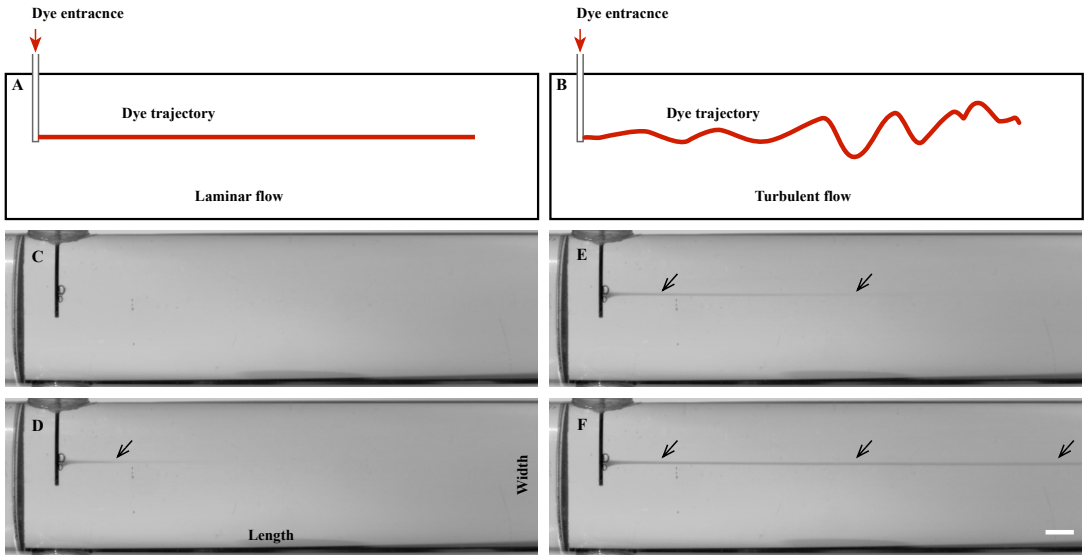

Figure 3.11: *Kymographs of the empirical test of water flow. A water-soluble dye was delivered into the water through a needle and it is videotaped. The straight line (A) shows the trajectory of dye and indicates a non-turbulent flow at the center of the pipe. Panel B shows the trajectory for turbulent flow. C-F) Four different time frames of trajectory of dye inside the tube, showing the progress of the flow and the trajectory. Trajectory stays in a straight line over the length of the pipe. Scale bar is 4 mm.*

Beside of having laminar flow, it is necessary to confirm that water flow inside the pipe can be captured by the formulae described above. Next, to determine the

flow velocity profile across the entire width of the pipe in three dimensions, I filled one end of the pipe with a dye and tracked its development over time. Empirical data show a parabolic profile of dye that is consistent with laminar flow across the entire water column (as shown in figure 3.12). Panel A of figure 3.12 gives the overall overview of the flow profile which at the beginning is flat (2d perspective) and over a specific period, develops into a parabola. While panels B-E shows the acquired images from the camera over time, representing the advances of the flow over time inside the tube.

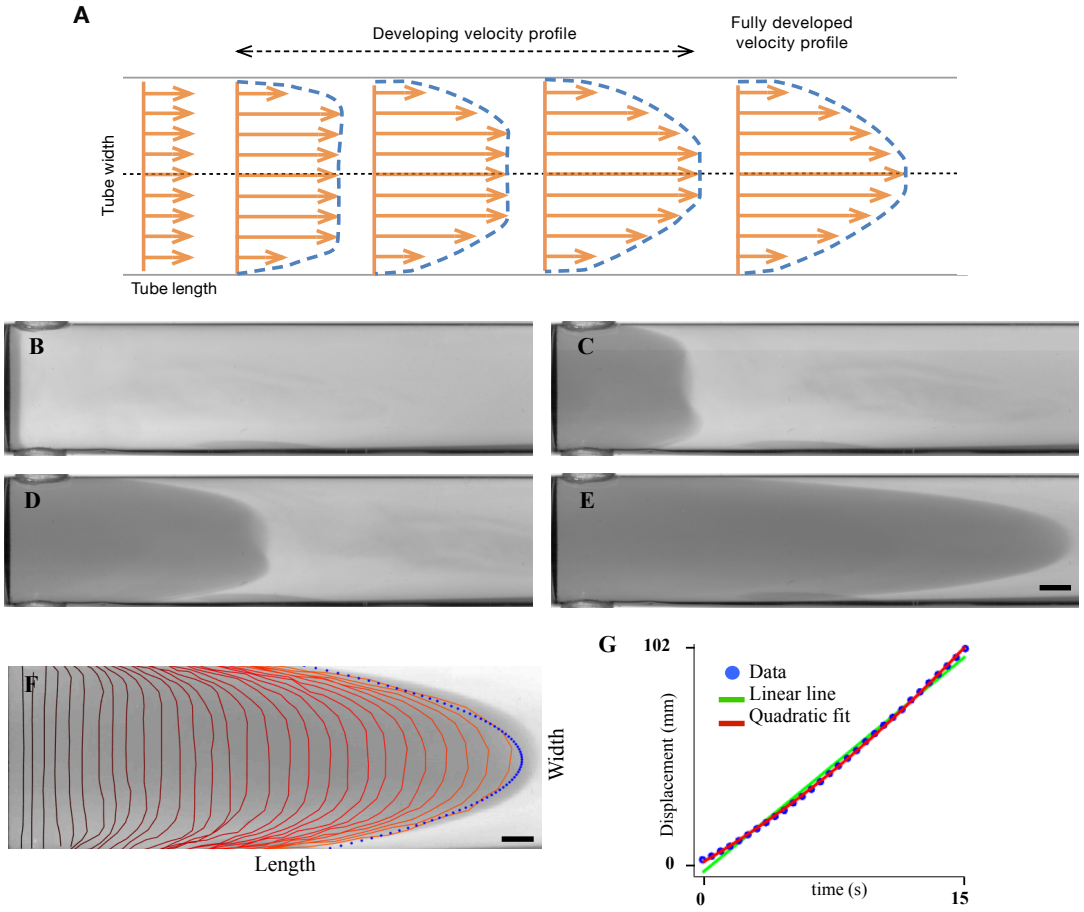

Figure 3.12: *A) Illustration of theoretical expectation of flow developments inside the pipe. At the beginning is flat and becomes parabolic at a fully developed stage. To test the profile in the pipe, the end of the pipe closest to the plunger was filled with water-soluble dye and the displacement of the dye-front was videotaped. The flow velocity profile across the pipe width develops over time (B-E) and forms a parabola at full development(E). F) Displacement of the dye-front is delineated in red at 0.25 seconds intervals. A blue dotted line was drawn to represents the theoretical profile of the fully developed flow. G) Plot of dye displacement at the center of the pipe (blue), fitting a quadratic (red) and linear increase (green). With the quadratic fitting, the first (quadratic) and second (linear) coefficients are 0.1 and 4.7. Scale bar is 4 mm.*

3.4 Limens for rheotaxis

I decided to determine rheotactic limen (liminal point) in larval zebrafish under infrared light (see Introduction - Optical sensitivity of zebrafish visual system). Limen is defined as a flow-velocity threshold above which zebrafish larvae orient to the direction of the flow. I used 7 dpf wild-type specimens, which already have a functional superficial lateral line, swim spontaneously, and express a rich behavioral repertoire that includes rheotaxis (Olszewski et al. [2012]; Suli et al. [2012]; Levi et al. [2015]; Olive et al. [2016]).

An example of a representative rheotactic behavior of a larva under flow is shown in panels A and B of figure 3.13. Animal performs a rhythmic swimming pattern illustrated with the swimming velocity and the orientation of the animal with respect to flow direction. Tail beating causes small fluctuation in body orientation which coincides with sharp peak increase in the swimming velocity.

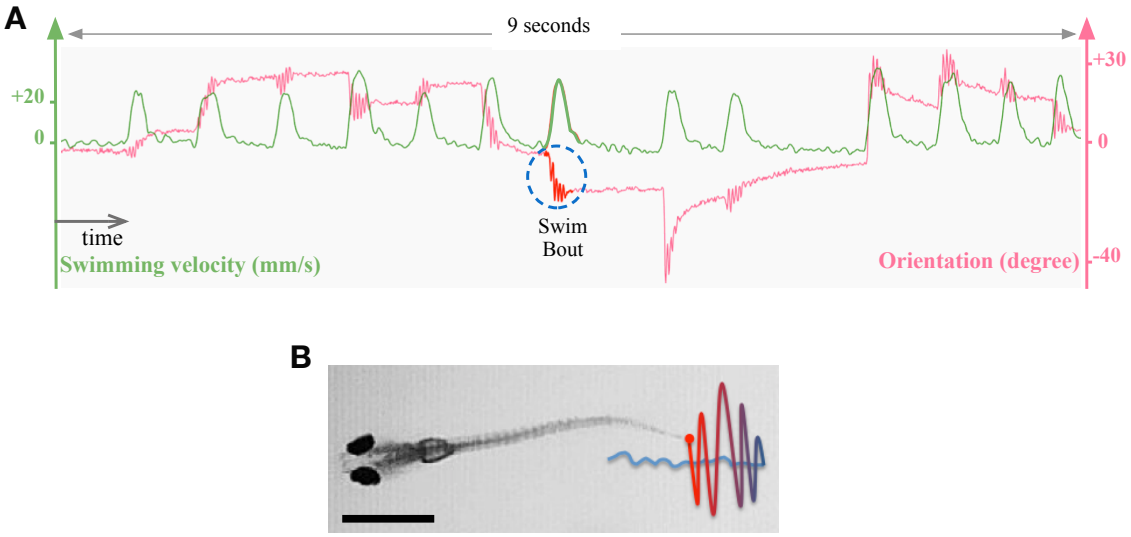

Figure 3.13: *A) An example of a representative rheotactic behavior of a 7 dpf larva under 6 mm/s flow for a duration of 9 seconds. The green trace represents swim velocity while the red trace represents the orientation of animal with respect to flow direction. Tail beating causes small fluctuation in body orientation as shown by the dashed blue line in A and in more details with higher resolution at B. Tail beating onset to offset is coloured with blue-to-red gradient, respectively. Scale bar is 1 mm.*

Fish body orientation is used to quantify rheotaxis. Orientation is measured at each recorded time point at a rate of 200 frames per second. Orientation of the larvae at each time point for the whole experiments (5000 - 6000 time points) is represented in figure 3.14 A to D for some selected experiments (each row represent one experiment). For better visualization and data quantification, the cosine of the orientation was plotted in panel E figure 3.14.

By measuring the orientation of the larva about the longitudinal axis of the pipe (which coincides with the direction of water flow), I found that in the absence of visual cues and under zero water flow, wild-type animals orient randomly (Figure 3.14 A and E). A bulk water flow of 3 mm/s biases larval orientation against the incoming flow, but still with a broad distribution (Figure 3.14 B and E). At 6 mm/s and 9 mm/s, fish consistently faces the current with a much narrower distribution (Figure 3.14 C, D and E).

This result is consistent with electrophysiological recordings from LANs in larval zebrafish performed by other groups and reported in the literature, which showed stronger responses to mechanical stimuli as water-flow velocity increases, reaching a plateau at 5 mm/s (McHenry and Lauder [2005]). Therefor based on these results I decided to conduct further behavioral analyses using water flowing at 6 mm/s.

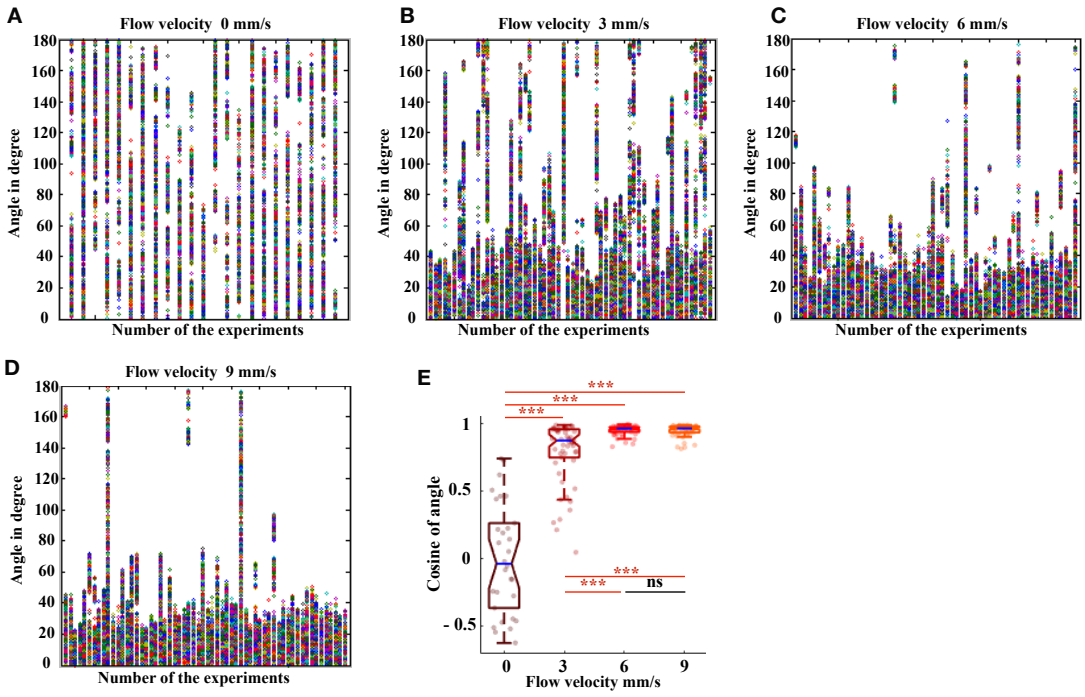

Figure 3.14: *Orientation of animal over the full length of time as a measure of the rheotaxis is shown in panels A to D. Each raw represents one experiment and each point on the raw represents the orientation of the animal in a time point. These raw data of orientation show the wide orientation for fish under no flow but narrower at higher flow velocities (3 mm/s panel B, 6 mm/s panel C and 9 mm/s panel D). E) Each point represents the cosine of the average orientation of individual larvae at 0, 3, 6 and 9 mm/s. The number of the animals with number of the trials are as follow, respectively for the mentioned conditions: n = 2 larvae with 30 trials in total, 6 larvae with 60 trials in total, 6 larvae with 60 trials in total, and 6 larvae with 60 trials in total. A perfect orientation against and toward flow has a cosine value of 1 and -1, respectively.*

3.5 Contribution of the lateral line to rheotactic performance

To reveal the contribution of individual components of the lateral line on rheotaxis, I used laser microsurgery (see materials and methods) to sever the peripheral and central axons of all LANs, effectively abolishing any communication between the lateral-line receptors and the brain. Cuts of central axons were performed in such a way to block the sensory input from the anterior lateral line only, posterior lateral line only or both.

Experimental conditions were 1) bilateral complete ablation (BCA), 2) unilateral complete ablation (UCA), 3) bilateral anterior ablation (BAA), and 4) bilateral posterior ablation (BPA). The control condition was a sham ablation, in which another part of the body was targeted by the laser and leaving the lateral line intact.

Panel A in figure 3.15 shows an example fluorescent image of the lateral-line sensory system. The fluorescent images of central projections of the posterior lateral line, anterior lateral line and both the anterior and posterior lateral line after severing are shown in the panels B-D, respectively. Laser mediated cuts of both the anterior and posterior lateral-line central axons causes complete degradation of the severed projections after 12 hrs (Figure 3.15 E), confirming the effectiveness of the manipulations.

The rheotaxis experiment was done 12 hours after severing and images of neurons were taken at the end of the experiment to certify the continuous absence of axons under each condition. My results show that BCA (effectively a complete loss the later-line system) strongly disrupted rheotaxis. BAA and BPA

affected rheotaxis partially. Remarkably, UCA strongly disrupted orientation to flow similarly to the loss of the entire lateral-line system. Sham-ablated animals responded to flow similarly to the non-ablated group (Figures 3.16 and 3.17).

In another experiment, I cut the peripheral axons of the posterior lateral line in 3 dpf larvae (Figure 3.15 F) and performed rheotaxis experiments when animals were 7 dpf. Peripheral axons, in contrast to central axons, are able to regenerate and quickly re-innervate peripheral receptors (Figure 3.15 G and H).

However, they normally re-innervated a different receptor than their original, modifying the spatial representation (somatotopy) of peripheral receptors in the brain. My interest with this experiment was to see whether animals after somatotopic rewiring are able to perform rheotaxis. Interestingly, my results show that indeed that is the case and these animals orient to water flow statistically similarly to intact animals (Figures 3.16 and 3.17).

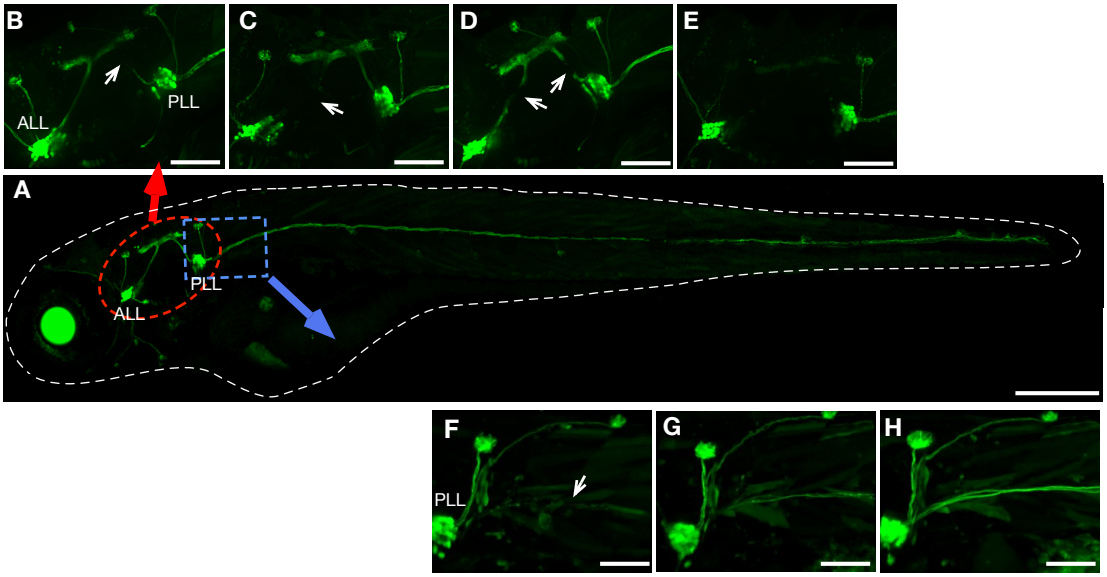

Figure 3.15: *A) Fluorescent images of a 7 dpf zebrafish larvae expressing GFP (green) in the entire LAN population. B-E) Images of the central LAN axons (region equivalent to the red box in A) captured after severing. Panels B, C and D are 2 hours after severing of PLL, ALL and entire lateral line, respectively. Panel E is 12 hours after severing the entire lateral line showing no axonal regeneration. F-H) Fluorescent images of laser-mediated severing of peripheral axons (region equivalent to the blue box in A, showing their progressive regeneration (from left to right). Images were captured 2 hours, 24 hours and 48 hours after severing.*

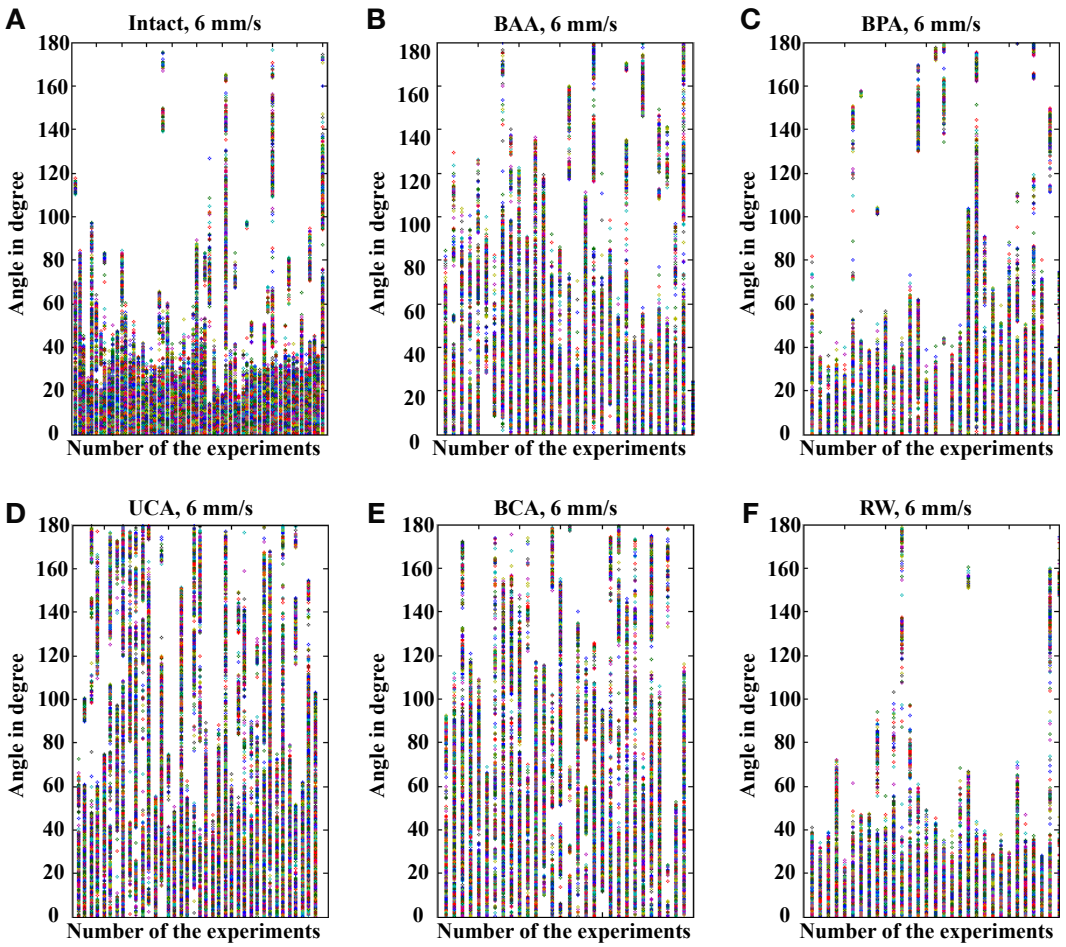

Figure 3.16: *Orientation of the animal over the full length of time as a measure of the rheotaxis is shown in panels A to F for intact (n = 6 larvae with 60 trials in total) and the following manipulated specimens at 7 dpf; bilateral anterior ablation (BAA, n = 8 larvae with 75 trials in total), bilateral posterior ablation (BPA, n = 5 larvae with 62 trials in total), unilateral complete ablation (UCA, n = 6 larvae with 54 trials in total), bilateral complete ablation (BCA, n = 6 larvae with 44 trials in total), somatotopic rewiring (RW, n = 10 larvae with 103 trials in total) at 6 mm/s flow. Each row represents one experiment and each point on the row represents the orientation of the animal in a time point. These raw data show wider orientation of UCA and BCA and slightly wider orientation of BAA in comparison to intact larvae under 6 mm/s flow.*

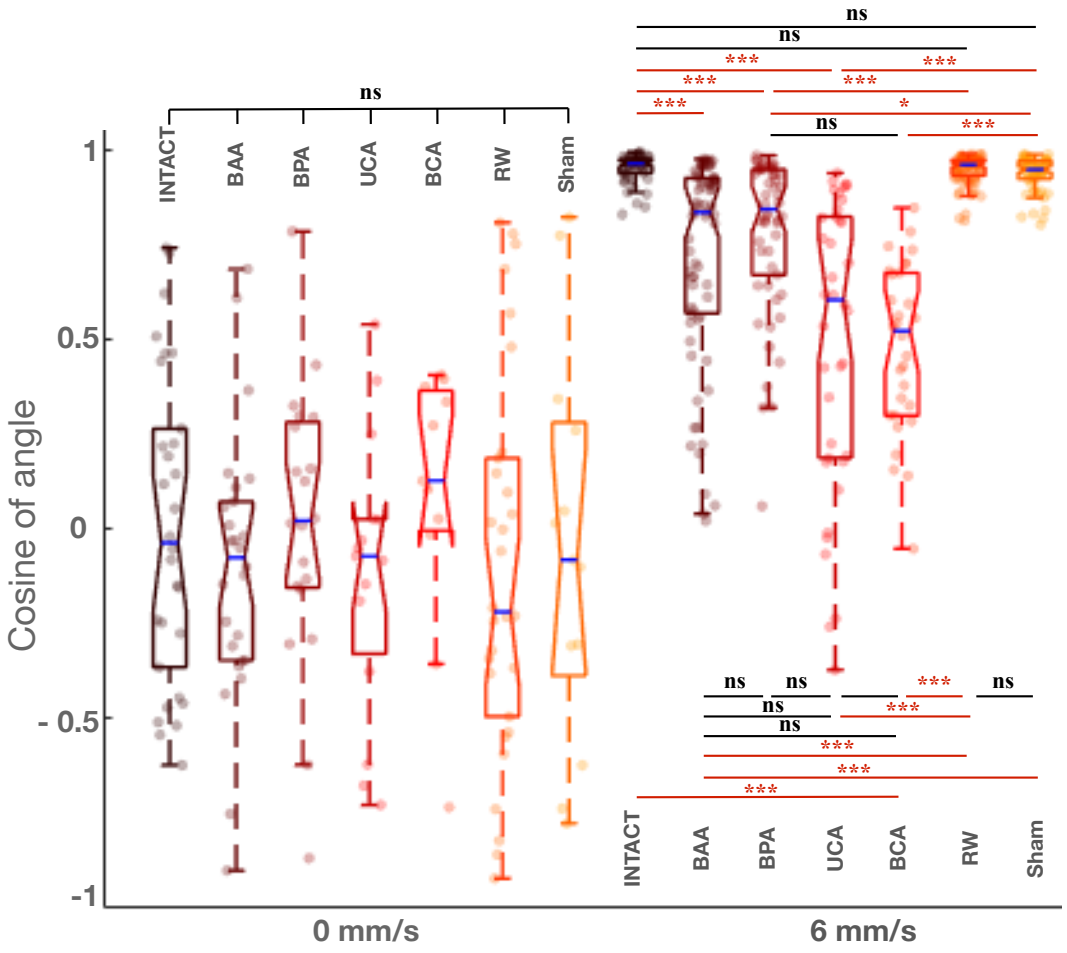

Figure 3.17: *Cosine of orientation of intact (n = 6 larvae with 60 trials in total) and the following manipulated specimens at 7 dpf; bilateral anterior ablation (BAA, n = 8 larvae with 75 trials in total), bilateral posterior ablation (BPA, n = 5 larvae with 62 trials in total), unilateral complete ablation (UCA, n = 6 larvae with 54 trials in total), bilateral complete ablation (BCA, n = 6 larvae with 44 trials in total), somatotopic rewiring (RW, n = 10 larvae with 103 trials in total) at 6 mm/s flow, and sham ablation (n = 6 larvae with 70 trials in total). For zero-flow conditions, I used intact (n = 2 larvae with 30 trials in total), BAA (n = 8 larvae with 26 trials in total), BPA (n = 5 larvae with 20 trials in total), UCA (n = 4 larvae with 11 trials in total), BCA (n = 3 larvae with 15 trials in total), RW (n = 10 larvae with 30 trials in total), sham (n = 5 larvae with 13 trials in total). Confidence levels for pairwise comparisons are ***p<0.001, **p<0.01, *p<0.05, ns p>0.05.*

3.6 Characterization of swim bouts

Swimming pattern of zebrafish larvae under flow (Figure 3.13 A and B) reveals that zebrafish perform a discrete collection of rhythmic tail beating (a bout). I employed a set of arbitrary rules to recognize and index swim bouts and to discriminate their sequence, amplitude and frequency during rheotaxis. Three actions were assigned: the onset (burst) and offset of the swim bout, frequency of the swim bout (number of the bouts animal performs in one second) and yaw angular changes within the swim bouts (Figure 3.19 A).

A semiautomatic Matlab code was written to load the orientation data of all trials and perform predefined calculations for each action. I extracted manually ~ 400 swim bouts and annotated the onset and offset as shown in figure 3.18 for the four condition of intact and BCA under zero and 6 mm/s flow velocity. In this figure all the swim bouts for each condition are overlaid and plotted from a common starting point at zero degrees. The amplitude and length of the bouts are the x and y axis of the figures. I counted the number of the swim bouts that larvae performed in a time course to calculate the swim bout frequency. The time length from onset to offset was calculated as the swim bout period. The yaw angular changes was calculated as the amplitude of the orientation changes in onset and offset.

These quantifications of swim bouts were done in four different groups of animals to reveal the influence of experimental conditions on swimming pattern. The conditions are different water currents (0 and 6 mm/s) and variations in access of animal to lateral-line sensory input (intact larvae and bi-lateral complete ablation).

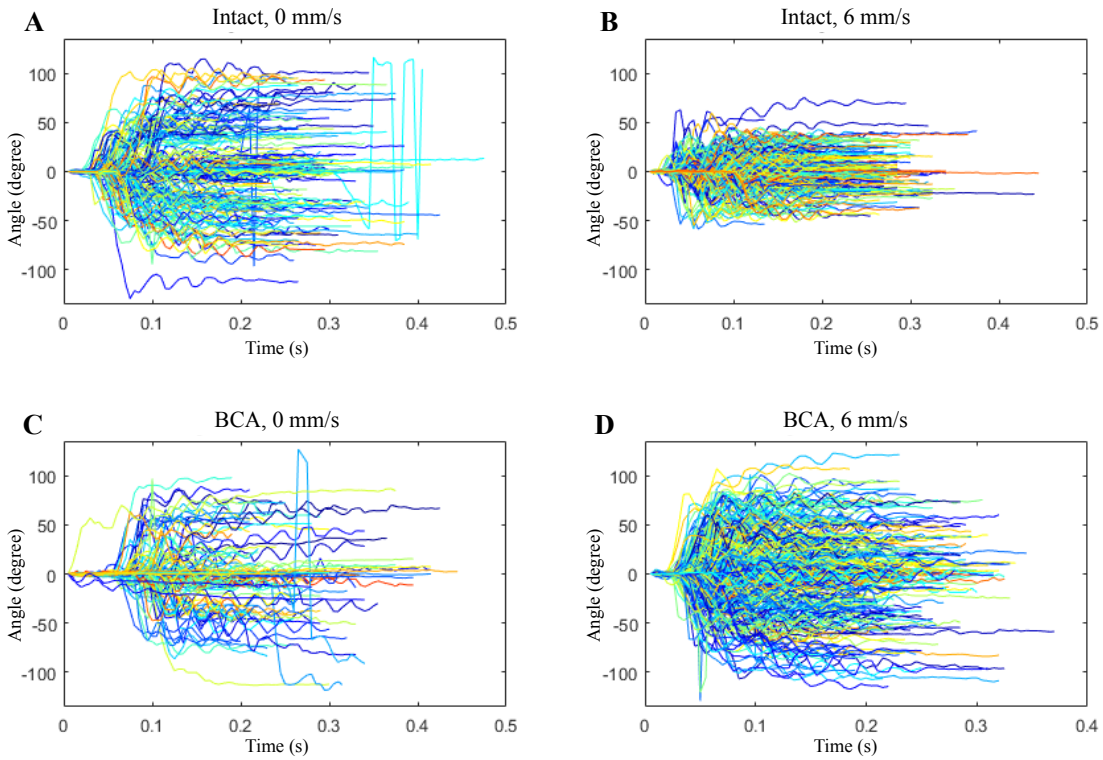

Figure 3.18: *Swim bouts of larvae under four condition of intact under zero flow (A) and 6 mm/s (B) and BCA larvae under zero flow (C) and 6 mm/s (D). Each colour represents one bout which are overlaid and plotted from common starting point at zero degrees for visualization. A bout may have different starting orientation though for visualization purpose, they are plotted from the same starting point while keeping the relative angular changes. The overall structure of the bouts for each condition is visible in each panel. Amplitude and length of the bouts are in z and x axis.*

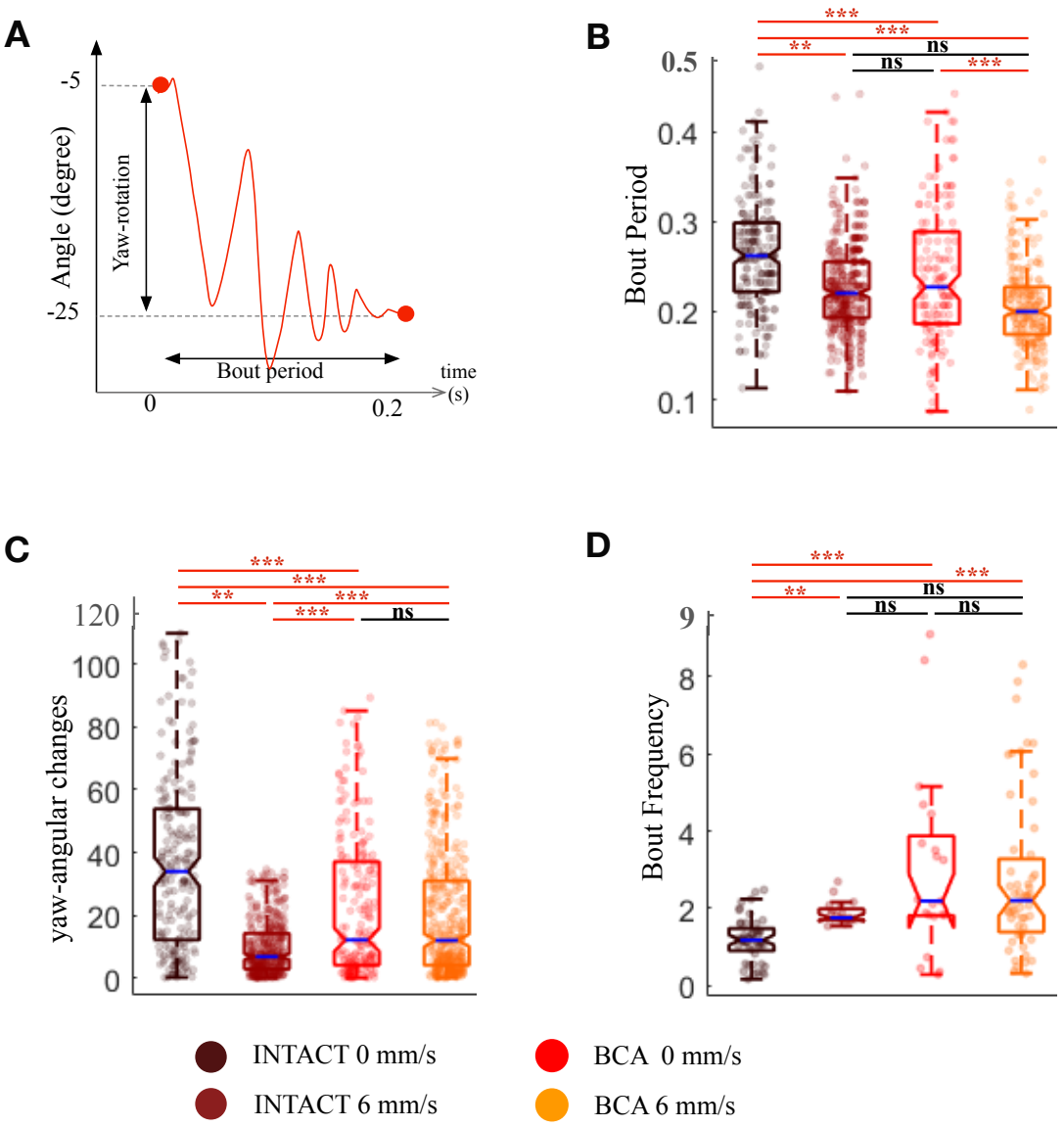

Figure 3.19: *Characterization of swim bout. A) A rhythmic tail beating of fish within 0.2 seconds. During this swim bout, the larva makes a yaw angular change of 20 degrees amplitude. B-D) Three rheotactic actions, the frequency (B) and the period (C) of swim bouts, and the amplitude of yaw rotations (D) from 400 bouts reveal fish reaction to four experimental conditions (colour coded). Swim bouts frequency of intact and BCA (bilateral complete ablation) larvae are measured at zero and 6 mm/s (B). Each dot represents the bout frequency extracted from a continued sequence of bouts. C) Swim bout period extracted from single bouts from all trials. Each dot represents the bout period. D) Amplitude of yaw rotations. Each dot represents the yaw angular changes calculated from single bouts from all trials.*

3.7 Field occupancy of swimming fish

To understand whether an animal locates itself in a specific position inside the tube under different conditions I determined the field occupancy, and how occupancy profiles change with the flow velocity. To do so, the swimming trajectory of animals was collected from time lapse recordings, and a Matlab code was written to measure field occupancy for all of trials, and to superimpose them as illustrated in figure 3.20. The main part of this script is an occupancy matrix defined with the size of the tube length and width. The matrix is defined by the following:

$$Occupation(x, y) = \sum_{trials} \sum_{t} A(x, y, t)$$

$$A(x, y, t) = \begin{cases} 1 & \text{if x,y belongs to trajectory} \\ 0 & \text{if x,y does not belong to trajectory} \end{cases}$$

By loading the trajectory of each trial, the elements of the occupancy matrix were matched with the tracking coordinates to assign a value of 1 for the position. Values of occupancy matrix elements are summed-up each time a fish is found in the same position. At the end of loading all the trials, values of the matrix are normalized to a range of 0 and 1 and are visualized as a heat map (Figures 3.20 and 3.21).

Intact animals under no flow display random localization in the transversal and longitudinal axes of the pipe (Figure 3.20 A), whereas in the presence of flow (6 mm/s), animals are mostly found in the center of the tube (Figures 3.20 B and 3.21 B). To understand whether different occupancy patterns necessitate lateral-line activity, I measured the occupation profile of animals with manipu-

lation identical to those mentioned above. At 6 mm/s flow, BAA and BPA fish have occupancy profiles similar to intact fish (Figure 3.20 C and D), while UCA and BCA fish display aberrant occupancy patterns (Figure 3.20 E and F). Interestingly, fish with rewired somatotopy have a similar occupancy pattern to intact controls.

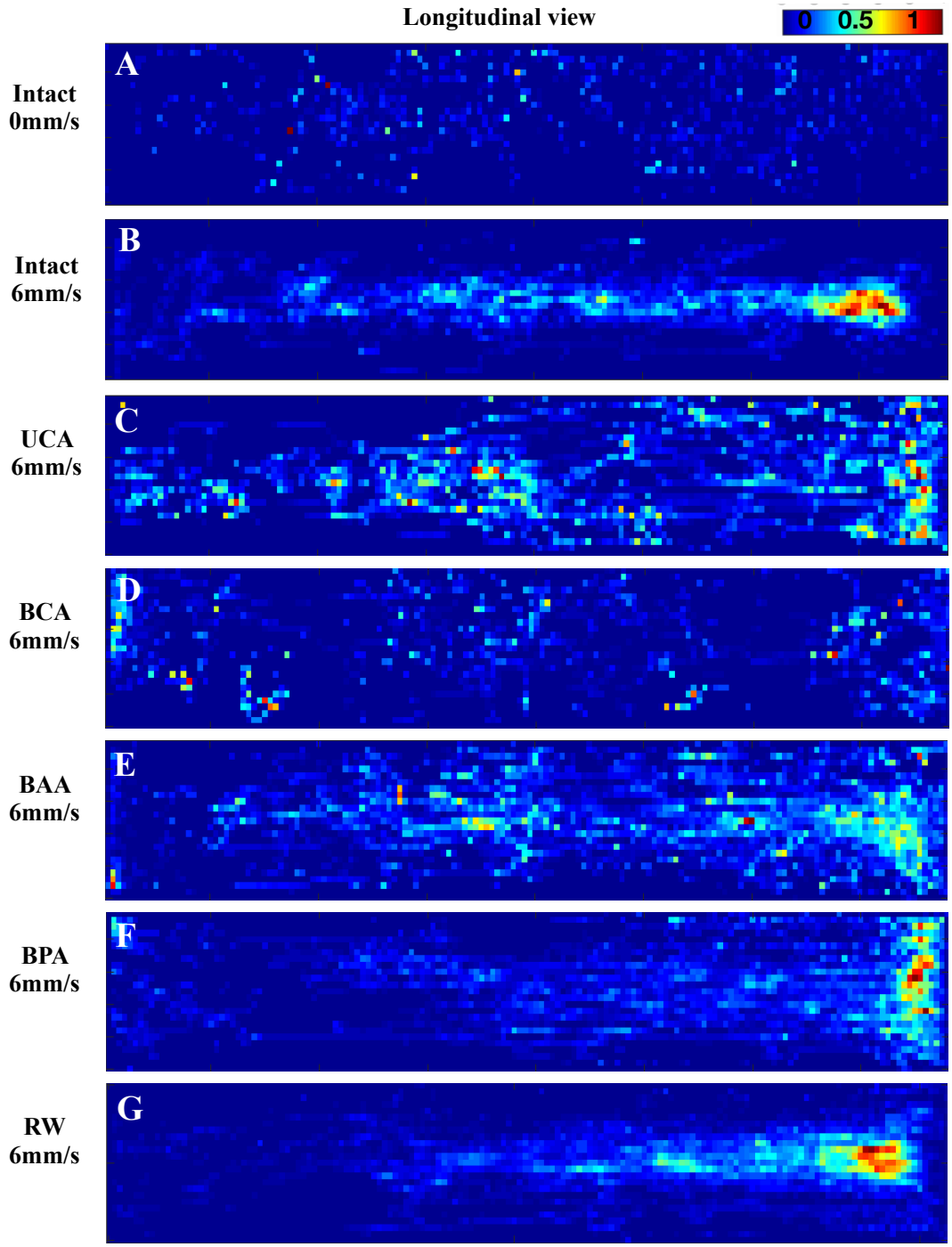

Figure 3.20: *Longitudinal view of the field occupancy. Level of the occupation is colour coded from blue (lower) to red (higher). Panel A represents the occupancy*

pattern of intact larvae at zero flow (n = 2 larvae with 30 trials in total). Panels B to G represent the occupation pattern of intact larvae (n = 6 larvae with 60 trials in total), UCA larvae (n = 6 larvae with 54 trials in total), BCA larvae (n = 6 larvae with 44 trials in total), BAA larvae (n = 8 larvae with 75 trials in total), BPA larvae (n = 5 larvae with 62 trials in total), re-wired somatotopy larvae (RW) (n = 10 larvae with 103 trials in total) under 6 mm/s flow, respectively.

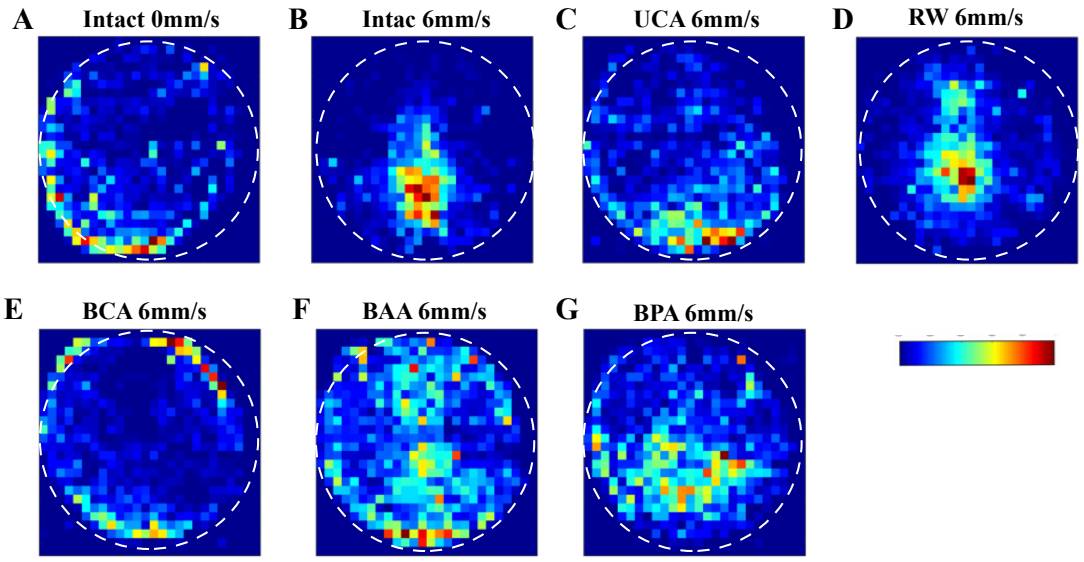

Figure 3.21: *Transversal view of field occupancy. Level of the occupation is colour-coded from blue (lower) to red (higher). Panel A represents the occupancy pattern of intact larvae at zero flow (n = 2 larvae with 30 trials in total). Panels B to G represent the occupation pattern of intact larvae (n = 6 larvae with 60 trials in total), UCA larvae (n = 6 larvae with 54 trials in total), BCA larvae (n = 6 larvae with 44 trials in total), BAA larvae (n = 8 larvae with 75 trials in total), BPA larvae (n = 5 larvae with 62 trials in total), and re-wired somatotopy larvae (RW) (n = 10 larvae with 103 trials in total) under 6 mm/s flow, respectively.*

To compare these occupancy profiles in more details, the marginal distributions were considered. Marginal distributions are calculated by summing-up all

the values across the longitudinal axis (Figure 3.22 A).

For each experimental condition (flow velocities and lateral line manipulations) mean, median, mode, standard deviation (std), skewness and kurtosis (Table 3.1) together with the symmetric comparison (Figure 3.22) were done. Mean and median of the distributions were very similar to each other suggesting that they follow the normal distribution. The std is high for all conditions except for the intact and somatotopy-rewired larvae at 6 mm/s flow. Skewness was not high and varied marginally between conditions (Table 3.1).

For this symmetric comparison marginal distributions are divided into halves as are shown with thin and thick lines in right panels of figure 3.22 panel B. Kolmogorov-Smirnov test has been applied to compare the two halves of the marginal distributions. The p-values are shown as a number beside each condition in figure 3.22 panel B. The statistical results suggest that only intact larvae under no flow condition have asymmetrical occupation profile while other experimental conditions have symmetric profile. Intact larvae under no flow experience no stimulus and therefore position themselves randomly inside the tube. Despite these results, the prediction is that if the number of observations were increased, this occupation pattern will become symmetric.

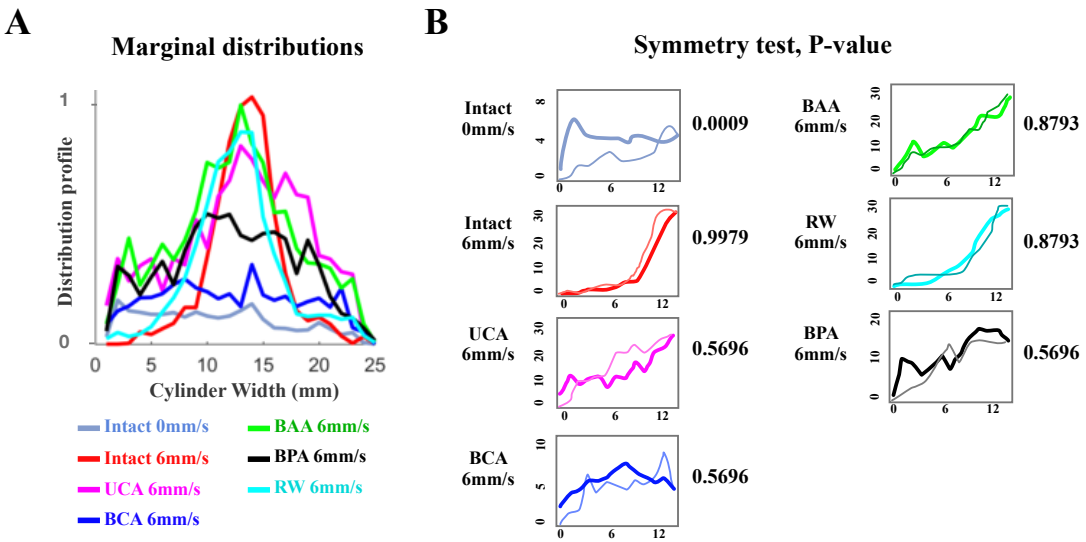

Figure 3.22: *A) Marginal distribution of occupancy across the width of the tube. Experimental conditions are colour-coded. B) Marginal distribution across tube width is divided in two halves (thin and thick lines) and compared to each other to test whether the distribution is symmetric. Kolmogorov-Smirnov test has been applied and the result p-value are shown.*

	Intact 0mm/s	Intac 6mm/s	UCA 6mm/s	BCA 6mm/s	BAA 6mm/s	BPA 6mm/s	RW 6mm/s
Mean	[9.9353]	[13.3159]	[13.0332]	[12.1617]	[12.6157]	[12.1879]	[12.7901]
Median	[9]	[13]	[13]	[12]	[13]	[12]	[13]
Mode	[2]	[14]	[13]	[5]	[13]	[10]	[13]
Std	[6.1185]	[3.4440]	[5.6707]	[6.5875]	[5.4684]	[5.6051]	[3.9925]
Skewness	[0.4045]	[-0.2200]	[-0.2811]	[0.0015]	[-0.0684]	[-0.0355]	[0.2624]
Kurtosis	[2.1055]	[4.3306]	[2.2930]	[1.7461]	[2.3696]	[2.1888]	[3.6966]

Table 3.1: *Six parameters for the marginal distribution of the occupancy are compared between various conditions. These comparisons help to understand the profile of the occupancy. Mean and median values are very similar to each other suggesting that they follow the normal distribution. Standard divination is high for all conditions except for the intact and rewired larvae at 6 mm/s.*

Marginal distributions are pairwise compared within the experimental conditions to test whether two profiles are drawn from the same distribution. Kolmogorov-Smirnov test is used and the outcome p-values are presented. These results suggest that all the manipulations have an influence on occupation profile at 6 mm/s flow.

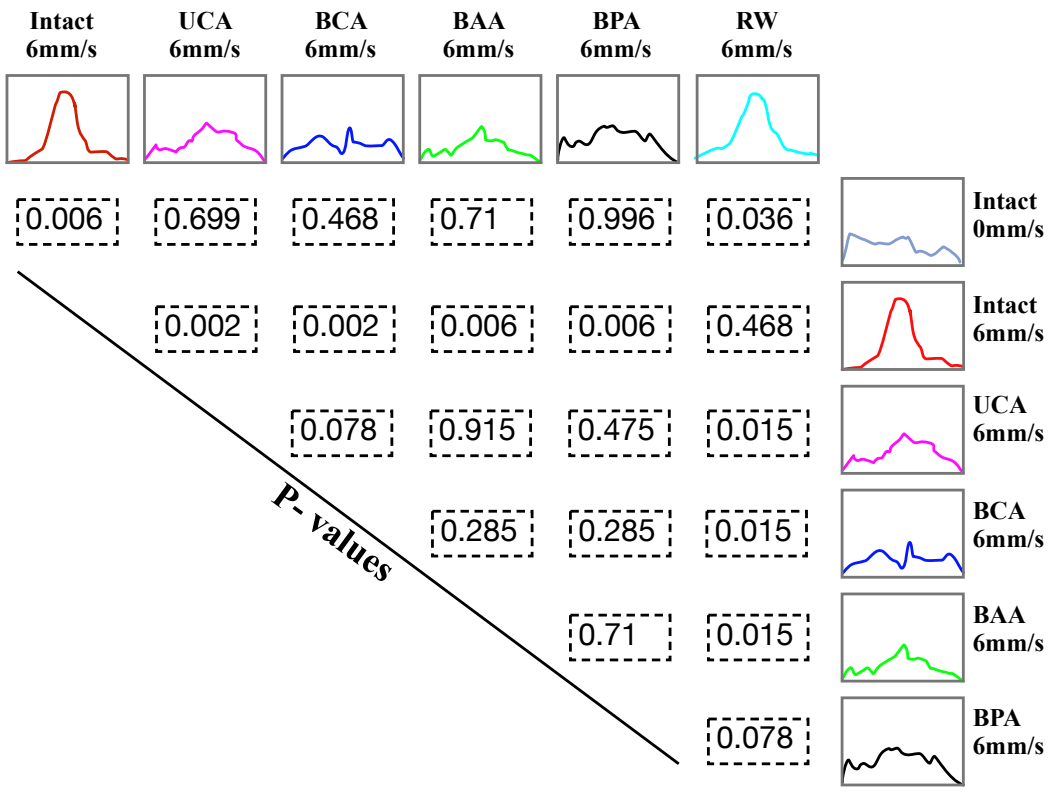

Table 3.2: *Marginal distribution of occupancy across the width of the tube colour-coded for each experimental condition. Pairwise Kolmogorov-Smirnov test was performed to test whether two samples are drawn from the same distribution to compare the occupation profile of larvae under different conditions.*

3.8 Field occupancy with respect to rheotactic performance

Field occupancy measurement provides information on where the animal locates itself inside the tube and how this profile changes with experimental conditions. Yet it is not clear from this measurement alone whether the animal is actively choosing specific areas of the water column during rheotaxis.

Therefore, a scoring system was created to address this issue by describing where inside the tube, larvae perform better rheotaxis. To do so, the swimming trajectory together with the orientation of the animal at each time point were collected from time-lapse recordings and a Matlab code was written to measure field occupancy with animal orientation for all trials.

A matrix was defined with the size of the tube length and width and each element of this matrix defines the position inside the tube. The value of each element of the matrix defines the overall orientation of all the superimposed trials. If the orientation of the animal is between 0-30 degrees, the element of the matrix which corresponds to the spatial location of the fish gets the value of +1. The values decrease gradually at steps of 1/3 as the angle of orientation increases (Figure 3.23 A). At the end the matrix is normalized to a range of values between 0 and 1 and for visualization, the values from the matrices are represented as a heat map and plotted (Figure 3.23 B-F).

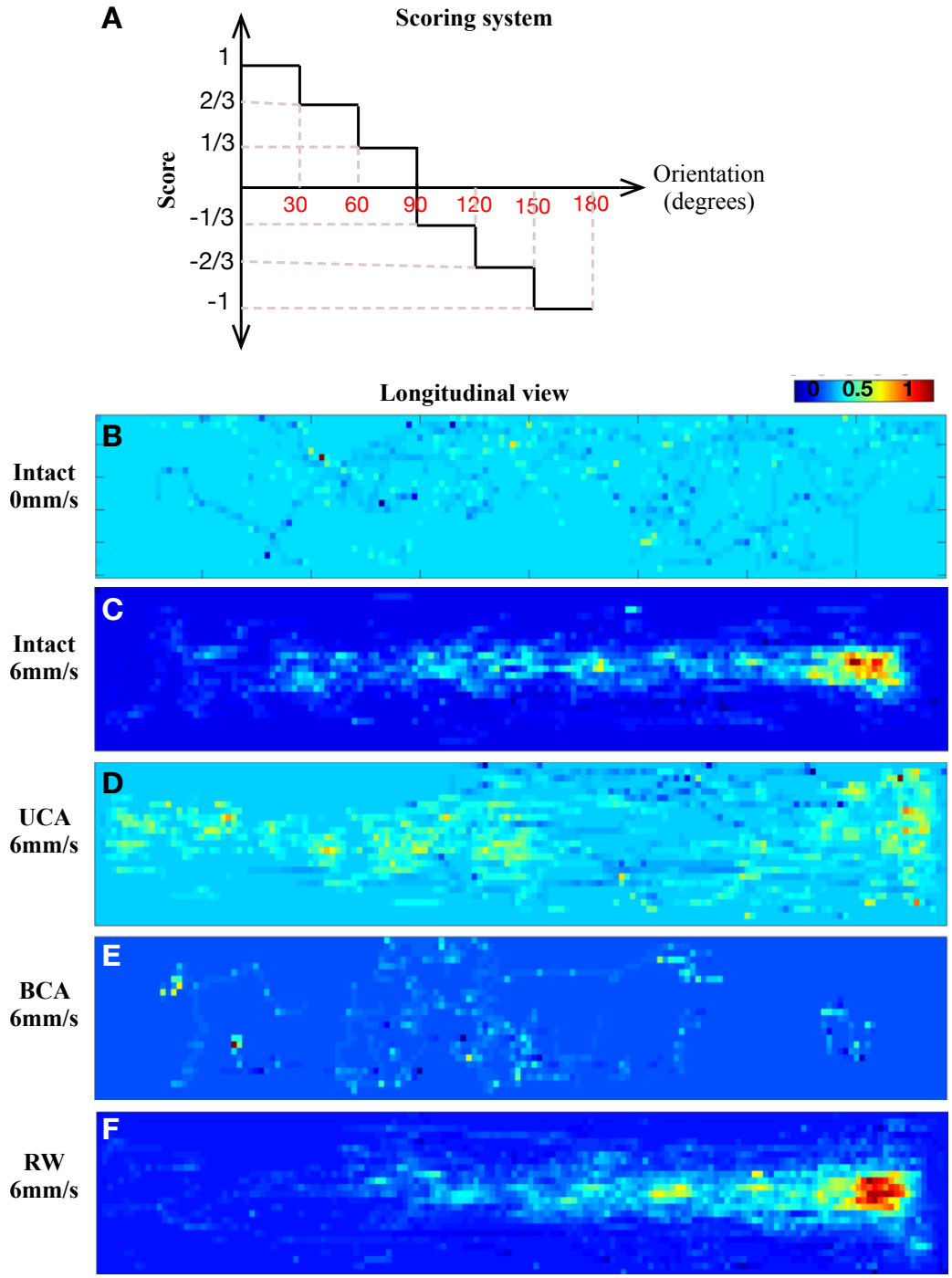

Figure 3.23: *Quantification of orientation of larvae relative to occupancy based on the scoring assay (panel A). Scores +1 for orientation at 0-30 degrees and the values decrease gradually at steps of 1/3 as the angle of orientation increases. B-F) Heat-map plots of the results from the scoring for different experimental conditions.*

These results reveal that intact larvae under no flow have random orientation and random occupancy (Figure 3.23 B), whereas at 6 mm/s flow the score is higher (meaning better orientation) when animals occupy the center of the pipe (Figure 3.23 C). This pattern disappears for UCA and BCA animals (Figure 3.23 D and E). Rewired animals display a pattern similar to that of intact larvae at 6 mm/s flow (Figure 3.23 F).

3.9 Impact of the vestibular system on rheotaxis

To assess the influence of the vestibular system on rheotaxis, I have designed an experiment in which I placed the rig, camera and illumination device on top of a small breadboard connected to the actuators shaft that moves only in horizontal plane with the same characteristic as used for rheotaxis experiment. A ruler (with centimeter resolution) was pinned to the ground to show the relative movement of the rig, which was moved at the same velocity of 6 mm/s used for the rheotaxis experiments figure 3.24. Rig displacement in this way does not generate water flow inside the pipe but there is a relative movement with respect to the ground.

I quantified data as mentioned in previous sections for the swimming trajectory and orientation over time (Figure 3.25). The trajectory plot shows that animals actively swim in either directions regardless of the direction of rig movement (Figure 3.25 A). Moreover, orientation is not correlated to the movement of the rig (Figure 3.25 B). My results reveal that zebrafish larvae do not react to whole-rig movement. Therefore, the vestibular system does not influence the rheotactic behavior of zebrafish larvae in my experimental setup.

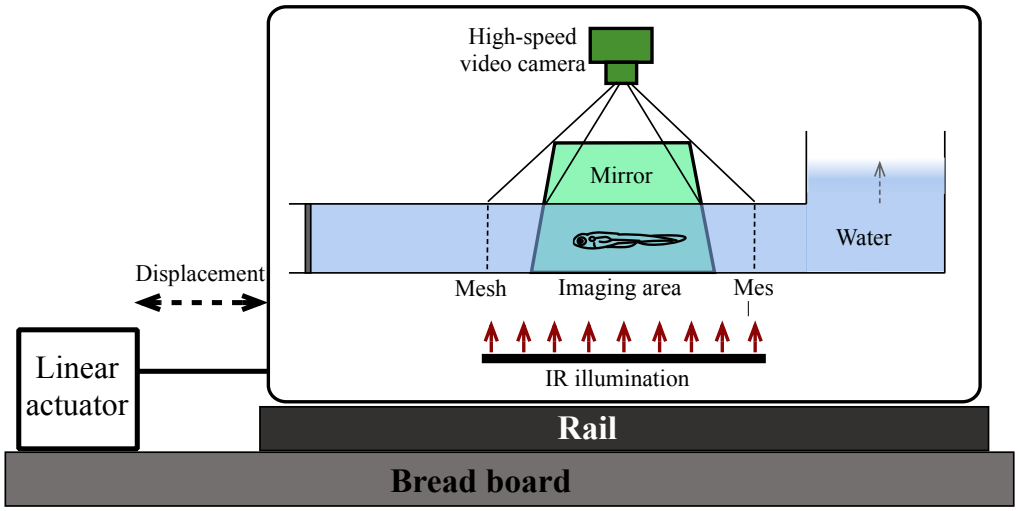

Figure 3.24: *The rig was accelerated in the same way as the water inside the tube. In this way, the whole rig was placed on top of the breadboard and all have moved together, including fish inside the tube.*

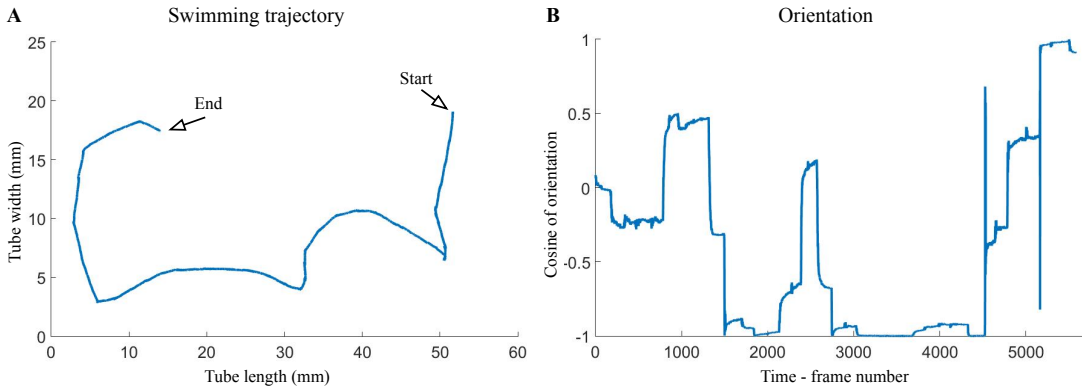

Figure 3.25: *Quantification of a single experiment on larvae swimming under the condition of accelerated rig as described in figure 3.24. A) Swimming trajectory and B) orientation of the larvae over time.*

3.10 Temporal dynamics of larval zebrafish orientation in the presence of water flow

Fish behavior was recorded at high temporal resolution (200 fps) to analyze the dynamics of orientation during rheotaxis. A unit vector was assigned to the orientation of the animal at each recorded time point (every 5 ms), and colour-coded over the course of the experiment (starts with the blue and ends with the red). There for the direction of these vectors show the orientation of the animal (panel A in figures 3.26, 3.27 and 3.28 for intact larvae at 0 mm/s, intact larvae at 6 mm/s and BCA larvae at 6 mm/s, respectively). The vector in the middle of the circle represents the initial orientation of the larvae. The colour changes of the vectors from blue to red reveal the time revolution of animal orientation. This approach can be extended for many trials by assigning circles with different radii to the trials as illustrated in panel B in figures 3.26, 3.27 and 3.28 for intact larvae at 0 mm/s, intact larvae at 6 mm/s and BCA larvae at 6 mm/s, respectively. In these plots 30 trials are represented in circles with different randomly assigned radius and the length of the unit vectors at each time point is scaled down to fit the page. The black spots in these plots mark the initial orientation of the animal.

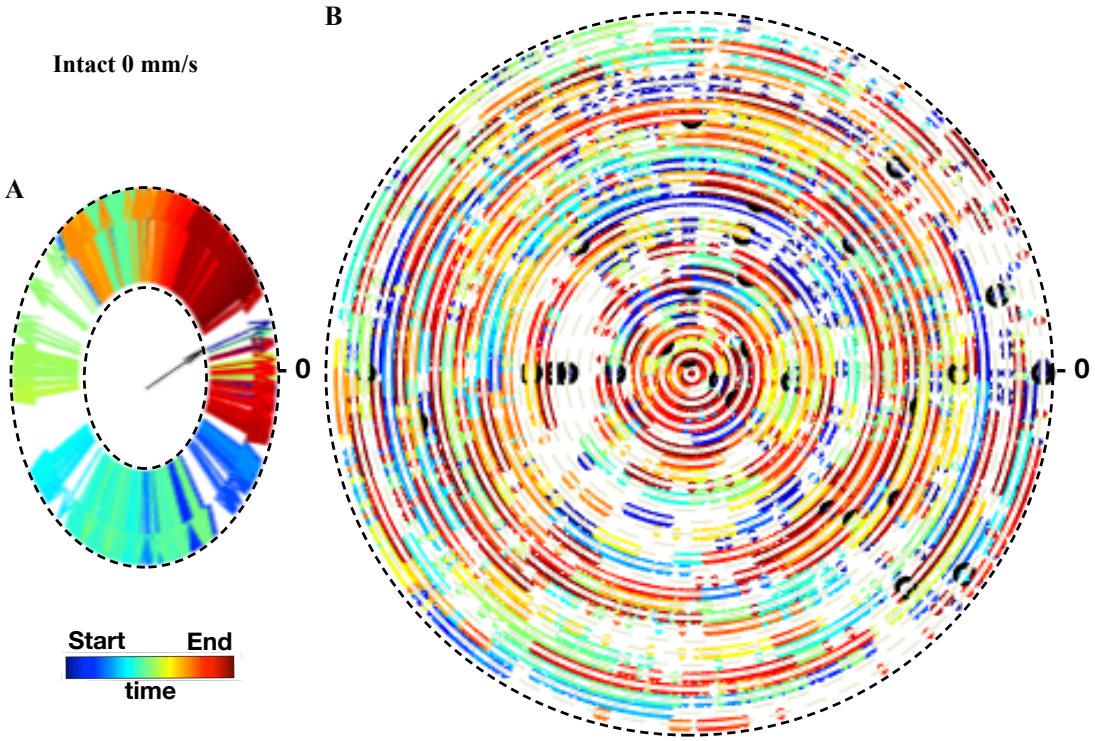

Figure 3.26: *Temporal dynamics of intact larvae orientation under zero flow. A) 360-degrees circular representation of one trial of intact larvae under zero flow which is used to generate panel B. This panel is aimed for better visualization of the temporal progression of orientation. The black spot within circle indicates the initial orientation of the specimen relative to flow direction at the onset of flow. B) Superimposed 360-degrees circular representation of orientation from 30 trials. Each circle (with increased radial values) represents a trial. Time progression is colour-coded from start (blue) to end (red) within each trial. A black dot in each circle marks the initial orientation of the larva at the beginning of the trial. Initial orientation of the larvae is random. Flow direction is indicated by a black arrow and coincides with an angular value of 0 (zero).*

Fish under no flow show no particular orientation preference (Figure 3.13 C). Time-resolved evolution of orientation showed that fish under no flow do not display iterative sequence of yaw angular changes (i.e. the arrows that indicate animal orientation over time are scattered and intermingled as shown in figure 3.26). However, when subjected to water flow at 6 mm/s, animals orient against the flow as shown in figure 3.27 A and C .

For instance, fish was at the orientation of 90 degrees (black arrow at the center of the circle in figure 3.27 A and C) and over the time starts to turn toward the zero degrees (following the colours from dark blue to light blue) which then starts rhythmic orientation centered at zero degrees (red coloured area). This pattern is repeated in all of the trials which is opposite of intact larvae under 0 mm/s flow (Figure 3.26) where colours are uniformly distributed over the circles. In other hand, at 6 mm/s most of the orientations (coloured vectors) are centered around zero (red overshadows the other colours).

At 6 mm/s flow, yaw rotations become non-stereotypic but predictable (Figure 3.27): when fish are not facing upstream, they consistently move in one direction along the horizontal plane, to eventually face flow. When they face the upstream direction, yawing becomes strongly symmetric and iterative about the longitudinal axis of the tube (coincident with the direction of water flow).

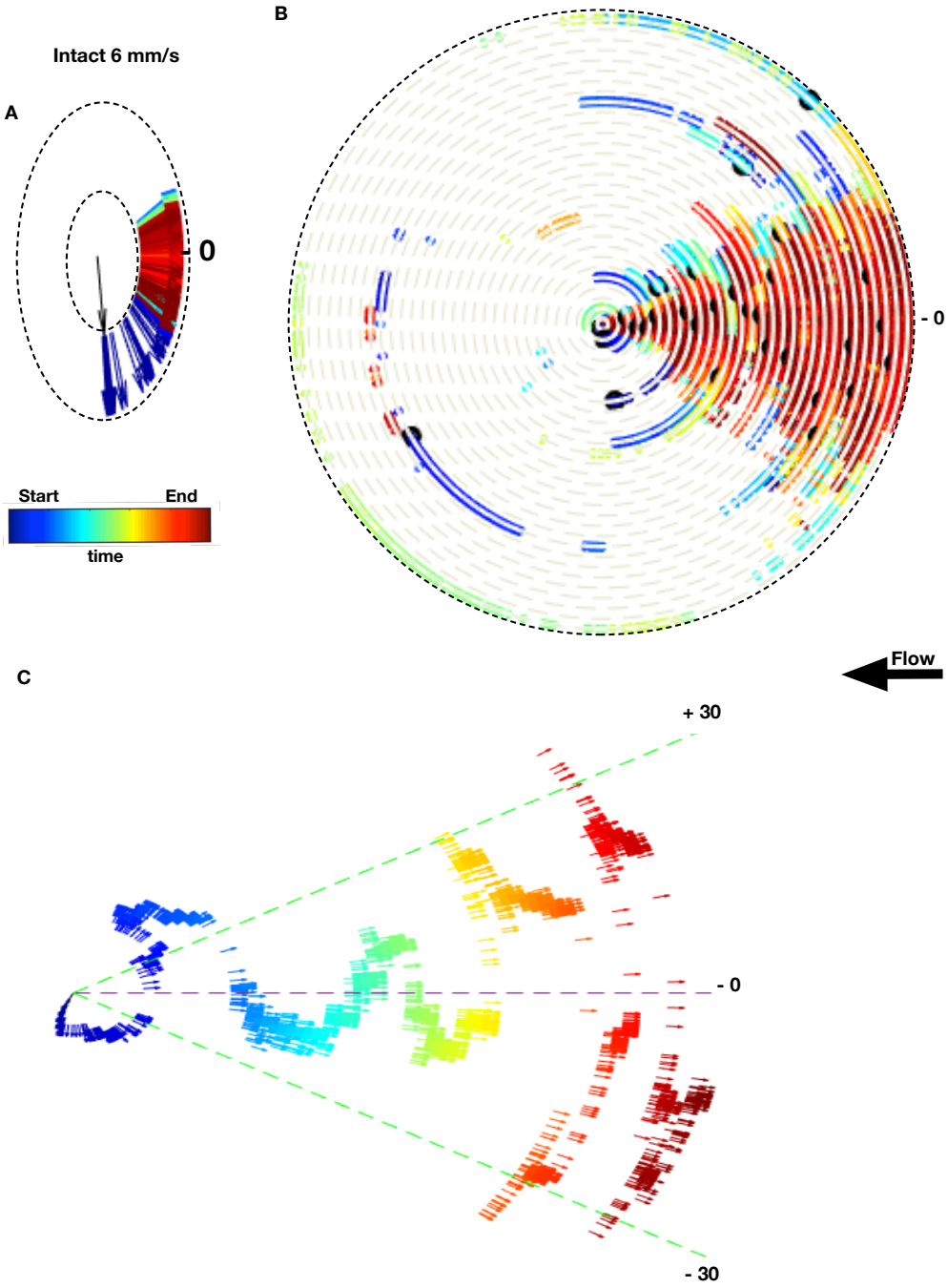

Figure 3.27: *Temporal dynamics of intact larval orientation under 6 mm/s flow. Panels A and B are same as described in caption of figure 3.26. C) Shows the temporal dynamics of orientation over time same as panel A but here the circle is expanded to avoid overlapping of vectors so the dynamics will be more visible.*

BCA animals do not orient as well as intact animals against the water-flow direction (Figure 3.17). Analyzing the dynamics of orientation suggests that the animal do not perform the same dynamic seen in intact larvae that being the rhythmic orientation around zero degrees. Figure 3.28 shows that the dynamics is more similar to the intact larvae under 0 mm/s flow where colours are mixed and there is no preference of orientation neither overshadowing of red colour around the zero degrees.

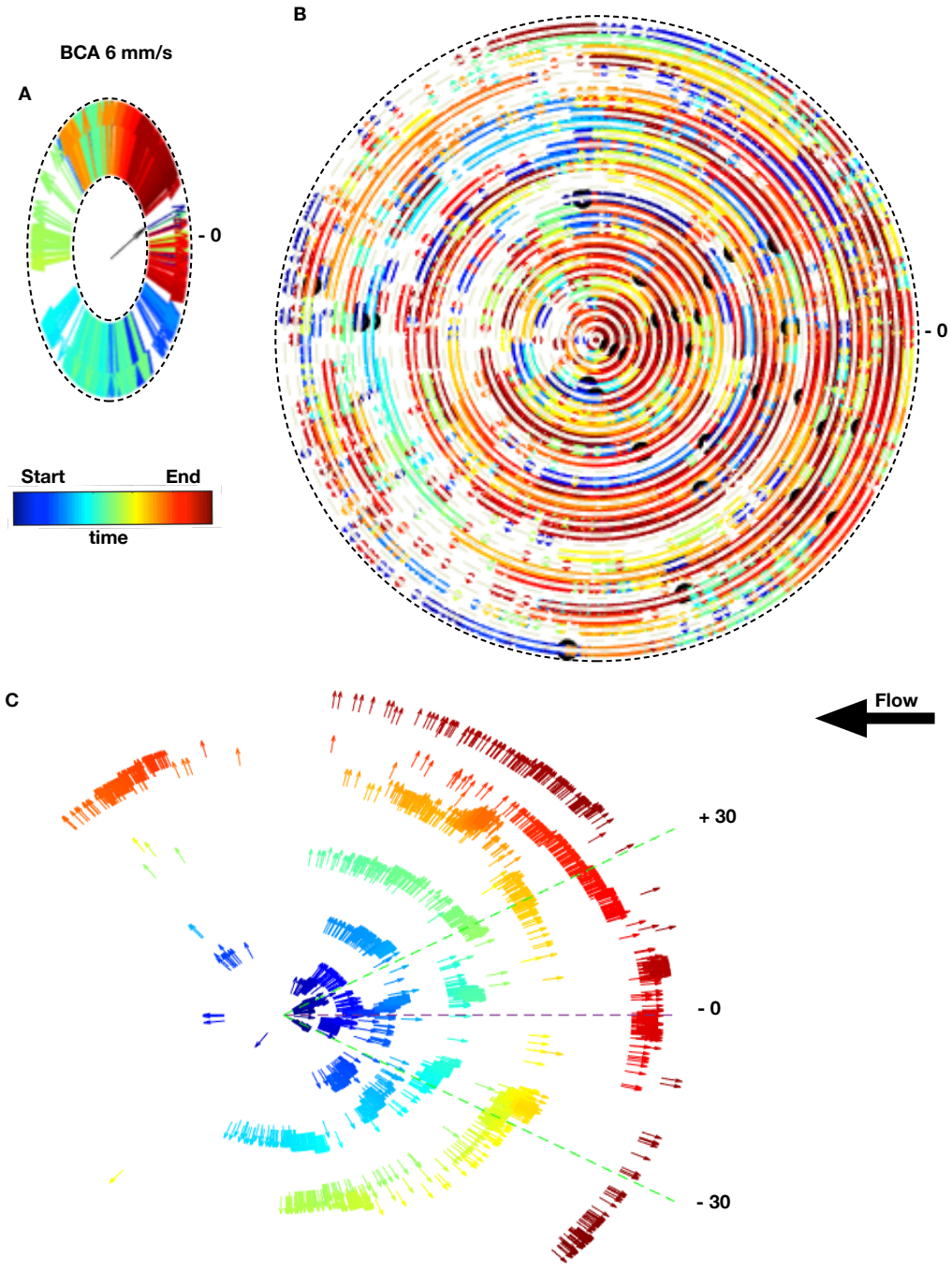

Figure 3.28: *Temporal dynamics of BCA larval orientation at 6 mm/s flow. Panels are same as described in caption of figure 3.27.*

Chapter 4

Discussion

4.1 Rheotaxis is a multisensory behavior

Rheotaxis refers to the ability of an animal to orient relative to the direction of water flow. In principle, aquatic animals may use visual or mechanical cues to detect the presence of flow and determine its direction. Because water currents can displace animals, the visual, vestibular and somatosensory systems could be used for rheotaxis, either together or independently. In fishes, vision and mechanosensation by the lateral line play the most important roles in rheotaxis, and animals normally use both simultaneously (Montgomery et al. [1997]; Coombs and Montgomery [2014]; Chagnaud and Coombs [2014]). Many studies have demonstrated that vision dominates the integrated information. Therefore fish normally determine water flow indirectly, by assessing their own displacement against an external reference frame via whole visual-field motion. Yet, the lateral line becomes essential for rheotaxis in the absence of visual cues (Figure 3.17). When both the lateral line and the vision are absent fish are not able to perform

rheotaxis as effectively.

In my thesis I aimed at investigating the mechanisms by which zebrafish can detract the presence of water currents and determined their direction using a single sensory modality, that enabled by the mechanosensory lateral line. To this aim, I designed an experimental paradigm that included a behavioral rig consisting of transparent cylindrical pipe made of Plexiglas and a linear actuator to create the water flow. This rig simultaneously enables control of water currents and high-resolution three-dimensional videography of unrestrained larval zebrafish.

I also showed that zebrafish does not use touch or the vestibular system for the perception of flow during rheotaxis. In conclusion, I could show that zebrafish larvae can perform rheotaxis in a laminar water current using exclusively its lateral-line system.

4.2 Exploiting hydromechanical inhomogeneities

The neuromasts of the superficial lateral line are bidirectionally sensitive to shear force, and their excitation pattern is largely proportional to the velocity of flowing water (Chagnaud et al. [2008]; Windsor and McHenry [2009]; McHenry and Liao [2014]). Accordingly, neuromasts are ideally suited to process changes of direction and magnitude in water flow. The directional tuning and linear arrangement of the majority of the neuromasts along the trunk and tail of the fish suggest that the lateral-line system filters the three-dimensional hydrodynamic field to render it two-dimensional (Figure 4.1 C). In my behavioral rig, as well as in some natural

conditions, flowing water generates a radial velocity gradient from the boundary between water tan the cylinder wall, towards the center of the water column.

Notably, two-dimensional (radial) velocity gradients provide insufficient information for larval zebrafish to identify flow direction because, as mentioned above, its lateral line is a linear sensor-array that is bilateral-symmetric and whose axis of sensitivity is bidirectional. Thus, the lateral line provides intrinsically ambiguous information. This is because, in principle, it cannot determine left and right and, consequently, cannot discriminate flow in anterior-posterior from the posterior- anterior direction.

One wonders, therefore, how can the zebrafish solve this ambiguity. Notably, a laminar current is rotational around submerged objects, including fishes, due to boundary conditions. This rotation results in water flowing in opposite directions around the animal. It follows that a laminar current contains sufficient information to solve the front-rear ambiguity, provided that the animal can extract this information from the flow. I hypothesized that the lateral-line system may be able to obtain such information if fish can perform recurrent comparisons of rotational flow over time. Below, I discuss in more detail the evidence supporting this mechanism.

Larval fish experience high viscous drag due to its small Reynolds number, which reduces slippage between swim-bouts and in turn maximizes the hair-cells sensitivity to mechanical stimuli. It has been shown that the hair cells are poor sensors of direct currents, suggesting that a stationary fish will be unable to persistently detect flow unless it uses a fixed external reference frame. Moreover, the efferent system generally uncouples external sensory information from stimuli generated by self-motion. Thus, the efferent system of the lateral line is likely to decrease mechanoreception during swimming. It transpires that active movement

is necessary for continuous detection of flow, but that hair-cell stimulation must optimally occur at discrete periods during inter-bouts.

One must highlight that for a steady flow, the Bernoulli's principle relates flow velocity with differential pressure, such that higher velocity is accompanied by a decrease in pressure and vice versa (Graebel [2007]). Thus, the sensation of pressure differences across the pipe could also explain flow-induced variations in rheotaxis. However, I do not favor this explanation since pressure gradients are normally sensed by the canal lateral-line sensory system (Suli et al. [2012]), which in zebrafish does not develop until the animal is at least 30 days old (Graebel [2007]).

During an active swimming, zebrafish larvae perform discrete and rhythmic tail beating. Results from this study shows that zebrafish larvae perform rheotaxis via discrete swim bouts (Figure 3.19 A) which generate recurrent snapshots of mechanical signals. These swim bouts are characterized by horizontal (yaw), vertical (pitch) and forward movements (McHenry and Lauder [2005]) (Figure 3.13 A). Iterative yaw movements enable the fish to perform temporal comparisons of rotational flow magnitude and direction after each swim bout (Figure 4.1 C). Time-resolved evolution of fish orientation showed differences at different water flow velocities. Under no flow there is no iterative sequence of yaw angular changes at any time point while at 6 mm/s, fish iteratively moves so that eventually faces the flow.

All together, my findings reveal that during rheotaxis zebrafish larvae use iterative patterns of small-amplitude yaw movements and discrete swim bouts where they capture rotational mechanical cues across the horizontal plane. This may explain the typical behavior of the fish during rheotaxis: if it does not face the direction of flow, it executes sequential yaw movements of high amplitude

in the same direction until it aligns itself against flow. If it faces flow, high-amplitude angular changes across the horizontal plane decrease in frequency, and become smaller and symmetrical about the direction of the flow (Figure 3.22).

I also explored a possible alternative explanation for lateral-line mediated rheotaxis, that the topographic map of the lateral line enables rheotaxis. Generally, the topographic representation of receptors in the brain forms a neuroanatomical code of the external sensory field. For example different time-of-arrival of mechanical waves along the tarsal receptors in Notonecta underlies the insects ability to detect flow direction (Wiese [1974]). The lateralis neural circuit in zebrafish is somatotopically organized. Because displacement of the neuromast cupula occurs with the wavefront of the hydromechanical stimulus (Windsor and McHenry [2009]), a current that sequentially stimulates neuromasts may enable fish to detect flow and potentially determine its direction using temporal integration of signals from neuromasts along its rostrocaudal axis. Therefore, a temporal sequence of excitation of the neuromasts along the lateral line may be represented in a low-dimensional map in the brain, from which water-flow direction can be derived (Alexandre and Ghysen [1999]; Liao [2010]).

To test this possibility, I took advantage of the regenerative ability of the peripheral axons of laterals afferent neurons, and the fact that regenerating peripheral axons almost always reinnervate neuromasts different that their original, resulting in extensive disruption of the lateral-line topographic map (Pujol-Martí et al. [2014]). After severing the entire axonal population of the posterior lateral line on both sides of the fish, the specimens were subjected to the rheotactic assay after axons had regenerated. These fish were able to orient to the direction of flow identically to intact controls, indicating that the topographic map of the lateral line does no govern rheotaxis. This experiment yielded an inroad to the discussed

mechanosensory-based mechanism in this study because regenerating axons always re-establish synapses with hair cells of the original orientation regardless of neuromast position. These results suggest pressure to preserve directional tuning, as opposed to fine-grained topographic representation. Collectively, these findings reveal that ipsilateral somatotopy is dispensable for the ability of larval zebrafish to orient to flow, and that simultaneous bilateral mechanosensation is essential for rheotaxis.

I found that orientation to flow was strongly affected by bilateral ablation of the lateral line (Figure 3.17). One possible explanation for this result is that the loss of bilateral reception decreases the precision or the accuracy of orienting behavior. I therefore devised a way to disambiguate these possibilities by considering that loss of accuracy (accumulation of systematic errors) should results in a skew of orientation, whereas the loss of precision (equating to the introduction of random errors) should affect orientation in a symmetric manner. I found that unilateral elimination of the lateral line does not produce a lateral bias of swimming along the horizontal plane (Figures 3.20 and 3.22 and Table 3.2), which suggests that rheotactic decline after unilateral ablation of the lateral line is a consequence of loss of orienting precision and, therefore, impaired determination of flow direction.

4.3 Mechanosensory-based mechanism for rheotaxis in larval zebrafish

From my data and previous results reported in the literature, our mechanosensory-based mechanism for rheotaxis states that:

1 - The neuromast epithelium can detect the axis but not direction of water flow due to the dual planar polarization of its constituent hair cells. All the hair cells in a neuromast are physical coupled by an overlying gelatinous cupula (Figures 1.2 and 1.3) (Flock and Wersall [1962]; McHenry and Liao [2014]).

2 - The cupula bends at low frequencies where viscous drag dominates (Chagnaud et al. [2008]; McHenry and Liao [2014]). Furthermore, stereocilia deflection equates in magnitude the displacement of the cupula (Curcic-Blake and Netten [2005]; Windsor and McHenry [2009]). Therefore, neuromast excitation is largely proportional to the velocity of the flow.

3 - The lateral line system is maximally sensitive to stimulation along the longitudinal axis of the fish due to the directional tuning of the majority of the neuromasts in their linear arrangement (Figures 1.2 and 1.3) (López-Schier et al. [2004]; Pujol-Martí et al. [2014]).

4 - The information acquired by the neuromast epithelium is preserved in downstream elements because the response of the LANs are linearly related to the stimulus (direction and magnitude of cupular displacement, equating to vectors) (Haehnel-Taguchi et al. [2014]; Levi et al. [2015]).

5 - Each LAN exclusively synapses with equal numbers of hair cells of identical orientation in individual neuromasts, thus decomposing the three-dimensional sensory scene, and transmitting to the brain a unique direction of mechanical stimulation by separate channels, independently from each neuromast (Figure 1.3 C) (Faucherre et al. [2009]; Trapani and Nicolson [2011]; Pujol-Martí et al. [2014]). Some piscine species present lateral-line canals (involved in detection of

flow acceleration) (Webb [2014]). However, lateral-line canals present in larval zebrafish (Pujol-Martí et al. [2014]; Hildebrand et al. [2017]).

6 - The LAN population forms a somatotopic map, so that each neuromast is topographically represented as LAN projections along a dorsoventral column in the hindbrain (Figure 1.2 A) (Alexandre and Ghysen [1999]; Liao [2010]; Pujol-Martí et al. [2014]).

7 - The first output of the LANs in the hindbrain is strictly ipsilateral (Alexandre and Ghysen [1999]; Liao [2010]; Pujol-Martí et al. [2014]; Hildebrand et al. [2017]).

8 - Accordingly, bilateral integration of signal must occur beyond the first relay station in the hindbrain.

Practically, the conditions listed above predict the outcome of several manipulations. First, the randomization of hair-cell orientation should generate neuromasts that simultaneously respond to many directions of mechanical stimulation, rendering them unable to perform vectorial filtering. Second, alteration of the topographic map will prevent comparison of the temporal sequence of neuromast stimulation along the lateral line system. Third, removal of mechanosensory inputs from one side of the fish will disable bilateral integration.

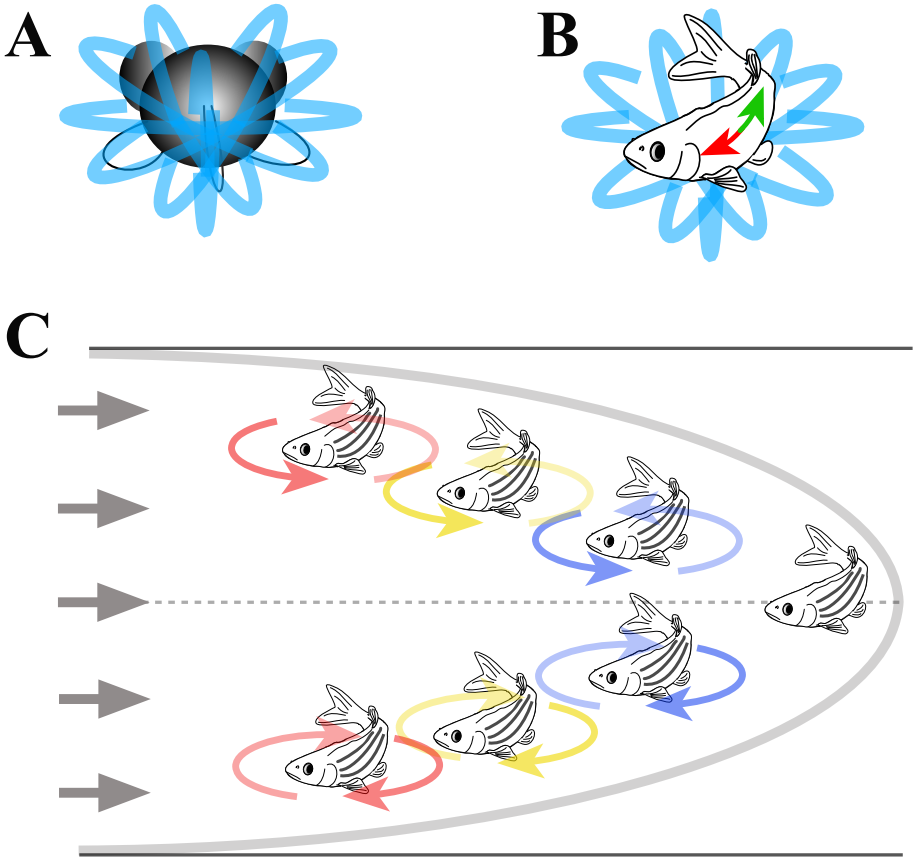

Figure 4.1: *A) A solid submerged object, including larval zebrafish, will experience a isosymmetric rotational motion of water around its periphery (blue circles). B) The posterior lateral line system is mostly sensitive to currents in the rostrocaudal direction (red and green arrows). Consequently, the lateral-line system is maximally sensitive to stimulation along the rostrocaudal axis of the fish. C) Depicts the general strategy used by the zebrafish to determine water-flow direction when executing horizontal movements. The magnitude of the local rotational flow will change radially (colour coded) (blue = low, red = high), and its direction (shown by arrowheads) across the midline.*

4.4 Conclusion

My PhD thesis work has revealed that when visual cues are not available, hydromechanical information is sufficient for fish to engage in counter-flow swimming (Olszewski et al. [2012]; Olive et al. [2016]). A mechanistic explanation for mechanosensation-mediated rheotaxis posits that the lateral line captures vectorial mechanical information along the horizontal plane (Figure 4.1 C). The neuronal circuit uses bilateral signals to detect the presence of a current and to determine its direction, and this is enabled by the animals iterative swimming behavior, which allows the brain to compare changes in the magnitude and direction of the rotational flow around its body. As to the relevance of this study to conditions in the wild, a small fish in their natural habitat will very likely be exposed to flow conditions such as those that this study has used in the rheotactic assay. This, for example, will occur along a shore, large submerged boulders or tree trunks in slow moving streams. Although this study highlights bilateral integration of local flow-field rotation as the basis of rheotaxis under laminar flow, fish may nonetheless employ ipsilateral somatotopy and flow-velocity gradients in more complex current regimes that characterize natural environments. Addressing this issue in future studies and possibly in other species will be important because it will help to reveal the fundamental computations that allow organisms to orient to currents in the absence of an external reference frame.

References

M. B. Ahrens, J. M. Li, M. B. Orger, D. N. Robson, A. F. Schier, F. Engert, and R. Portugues. Brain-wide neuronal dynamics during motor adaptation in zebrafish. *Nature*, 485:471–477, 2012. 3

M. B. Ahrens, M. B. Orger, D. N. Robson, J. M Li, and P. J. Keller. Whole-brain functional imaging at cellular resolution using light-sheet microscopy. *Nat. Meth.*, 10:413–420, 2013. 3

D. Alexandre and A. Ghysen. Somatotopy of the lateral line projection in larval zebrafish. *Proc. Natl. Acad. Sci. U.S.A.*, 96:7558–7562, 1999. 87, 90

P. Andermann, J. Ungos, and D.W. Raible. Neurogenin1 defines zebrafish cranial sensory ganglia precursors. *Dev. Biol.*, 251, 4558, 2002. 16

G. P. Arnold. Rheotropism in fishes. *Biol. Rev. Camb. Philos. Soc.*, 49:515–576, 1974. 5, 12

H. Bleckmann. *Role of the Lateral Line in Fish Behaviour*, pages 177–202. Springer, Boston, MA, Boston, MA, 1986. 5

H. Bleckmann and T. H. Bullock. *Central nervous physiology of the lateral line, with special reference to cartilaginous fishes*, pages 387–408. Springer, New York, NY, 1989. 5

H. Bleckmann and R. Zelick. Lateral line system of fish. *Integr. Zool.*, 4:13–25, 2009. 5

G. Bradski. Opencv. *Dr. Dobb's Journal of Software Tools*, 2000. 22

M. Broxton, L. Grosenick, S. Yang, N. Cohen, A. Andalman, K. Deisseroth, and M. Levoy. Wave optics theory and 3-D deconvolution for the light field microscope. *Opt. Express*, 21:25418–25439, 2013. 3

B. P. Chagnaud, H. Bleckmann, and M. H. Hofmann. Lateral line nerve fibers do not code bulk water flow direction in turbulent flow. *Zoology*, 111:204 – 217, 2008. 84, 89

Boris Philippe Chagnaud and Sheryl Coombs. *Information Encoding and Processing by the Peripheral Lateral Line System*, pages 151–194. Springer New York, New York, NY, 2014. 83

S. Coombs and J. Montgomery. *The Role of Flow and the Lateral Line in the Multisensory Guidance of Orienting Behaviors*, pages 65–101. Springer, Berlin, Heidelberg, 2014. 10, 83

B. Curcic-Blake and S. M. Netten. Rapid responses of the cupula in the lateral line of ruffe (Gymnocephalus cernuus). *J. Comp. Physiol. A Neuroethol. Sens. Neural. Behav. Physiol.*, 191:393–401, 2005. 89

W. Denk, J. H. Strickler, and W. W. Webb. Two-photon laser scanning fluorescence microscopy. *Science*, 248, 1990. 3

S. Dijkgraaf. A short personal review of the history of lateral line research. *Springer, New York*, pages 3–14, 1989. 5

A. Edelstein, N. Amodaj, K. Hoover, R. Vale, and N. Stuurman. Computer control of microscopes using Manager. *Curr. Protoc. Mol. Biol.*, Chapter 14: Unit14.20, 2010. 35

R. E. Engeszer, L. B. Patterson, A. A. Rao, and D. M. Parichy. Zebrafish in the wild: a review of natural history and new notes from the field. *Zebrafish*, 4: 21–40, 2007. 2

A. Faucherre, J. Pujol-Martí, K. Kawakami, and H. López-Schier. Afferent neurons of the zebrafish lateral line are strict selectors of hair-cell orientation. *PLOS ONE*, 4:e4477, 2009. 10, 15, 89

A. Flock and J. Wersall. A study of the orientation of the sensory hairs of the receptor cells in the lateral line organ of fish, with special reference to the function of the receptors. *J. Cell Biol.*, 15:19–27, 1962. 8, 89

G. S. Fraenkel and D. L. Gunn. *The orientation of animals*. Dover Publications, Inc., New York, 1961. 10

R. W. Friedrich, G. A. Jacobson, and P. Zhu. Circuit neuroscience in zebrafish. *Current Biology*, 20:R371–R381, 2010. 3, 4

A. Ghysen and C. Dambly-Chaudiere. The lateral line microcosmos. *Genes Dev.*, 21:2118–2130, 2007. 6

W. P. Graebel. *Advanced Fluid Mechanics*. Academic Press, 2007. 47, 48, 86

M. Haehnel-Taguchi, O. Akanyeti, and J. C. Liao. Afferent and motoneuron activity in response to single neuromast stimulation in the posterior lateral line of larval zebrafish. *Journal of Neurophysiology*, 112:1329–1339, 2014. 89

S. Hartmann, R. Vogt, J. Kunze, A. Rauschert, K. D. Kuhnert, J. Wanzenbock, D. K. Lamatsch, and K. Witte. Zebrafish larvae show negative phototaxis to near-infrared light. *PLOS ONE*, 13:e0207264, 2018. 4, 17

D. G. C. Hildebrand, M. Cicconet, R. M. Torres, W. Choi, T. M. Quan, J. Moon, A. W. Wetzel, A. Scott Champion, B. J. Graham, O. Randlett, G. S. Plummer, R. Portugues, I. H. Bianco, S. Saalfeld, A. D. Baden, K. Lillaney, R. Burns, J. T. Vogelstein, A. F. Schier, W. A. Lee, W. K. Jeong, J. W. Lichtman, and F. Engert. Whole-brain serial-section electron microscopy in larval zebrafish. *Nature*, 545:345–349, 2017. 2, 6, 10, 90

B. Hofer. Studien ber die Hautsinnesorgane der Fische. I. Die Funktion der Seitenorgane bei den Fischen. *Ber Kgl Bayer Biol Versuchsstation München*, 1:115–164, 1908. 5

N. G. Holtzman, M. K. Iovine, J. O. Liang, and J. Morris. Learning to Fish with Genetics: A Primer on the Vertebrate Model Danio rerio. *Genetics*, 203: 1069–1089, 2016. 2

A. J. Hudspeth. Sensory Transduction in the Ear. *In Principles of neural science*, pages 614–624, 2000. 8

A. J. Hudspeth and D. P. Corey. Sensitivity, polarity, and conductance change in the response of vertebrate hair cells to controlled mechanical stimuli. *Proc. Natl. Acad. Sci. U.S.A.*, 74:2407–2411, 1977. 8

W. Y. Hwang, Y. Fu, D. Reyon, M. L. Maeder, S. Q. Tsai, J. D. Sander, R. T. Peterson, J. R. Yeh, and J. K. Joung. Efficient genome editing in zebrafish using a CRISPR-Cas system. *Nat. Biotechnol.*, 31:227–229, 2013. 2

R. Jander. Ecological aspects of spatial orientation. *Annual Review of Ecology and Systematics*, 6:171–188, 1975. 10

J. Janssen, V. Sideleva, and H. Biga. Use of the lateral line for feeding in two Lake Baikal sculpins. *J. Fish Biol.*, pages 404–416, 1999. 5

C. B. Kimmel, K. Hatta, and W. K. Metcalfe. Early axonal contacts during development of an identified dendrite in the brain of the zebrafish. *Neuron*, 4: 535–545, 1990. 10

K. S. Kindt, G. Finch, and T. Nicolson. Kinocilia mediate mechanosensitivity in developing zebrafish hair cells. *Dev. Cell*, 23:329–341, 2012. 15

A. B. Kroese and N. A. Schellart. Velocity- and acceleration-sensitive units in the trunk lateral line of the trout. *J. Neurophysiol.*, 68:2212–2221, 1992. 6

W. E. Langlois and M. O. Deville. *Slow Viscous Flow*. Switzerland: Springer International Publishing, New York, 2014. 46

R. Levi, O. Akanyeti, A. Ballo, and J. C. Liao. Frequency response properties of primary afferent neurons in the posterior lateral line system of larval zebrafish. *J. Neurophysiol.*, 113:657–668, 2015. 53, 89

E. D. Levin and D. T. Cerutti. *Behavioral Neuroscience of Zebrafish*. CRC Press/Taylor, Francis, 2009. 1

J. C. Liao. Organization and physiology of posterior lateral line afferent neurons in larval zebrafish. *Biol. Lett.*, 6:402–405, 2010. 10, 87, 90

G. Lopes, N. Bonacchi, J. Frazao, J. P. Neto, B. V. Atallah, S. Soares, L. Moreira, S. Matias, P. M. Itskov, P. A. Correia, R. E. Medina, L. Calcaterra, E. Dreosti,

J. J. Paton, and A. R. Kampff. Bonsai: an event-based framework for processing and controlling data streams. *Front. Neuroinform.*, 9:7, 2015. 20

H. López-Schier and A. J. Hudspeth. Supernumerary neuromasts in the posterior lateral line of zebrafish lacking peripheral glia. *Proc. Natl. Acad. Sci. U.S.A.*, 102:1496–1501, 2005. 16

H. López-Schier, C. J. Starr, J. A. Kappler, R. Kollmar, and A. J. Hudspeth. Directional cell migration establishes the axes of planar polarity in the posterior lateral-line organ of the zebrafish. *Dev. Cell*, 7:401–412, 2004. 8, 89

E. P. Lyon. On rheotropism. i. — rheotropism in fishes. *American Journal of Physiology – Legacy Content*, 12:149–161, 1904. 12

M. J. McHenry and G. V. Lauder. The mechanical scaling of coasting in zebrafish (Danio rerio). *J. Exp. Biol.*, 208:2289–2301, 2005. 55, 86

M. J. McHenry and J. C. Liao. *The Hydrodynamics of Flow Stimuli*, pages 73–98. Springer, New York, 2014. 84, 89

M. J. McHenry, K. E. Feitl, J. A. Strother, and W. J. Van Trump. Larval zebrafish rapidly sense the water flow of a predator's strike. *Biology Letters*, 5:477–479, 2009. 5, 16

A. Meier, R. Nelson, and V. P. Connaughton. Color Processing in Zebrafish Retina. *Front Cell Neurosci*, 12:327, 2018. 4, 17

W. K. Metcalfe. Sensory neuron growth cones comigrate with posterior lateral line primordial cells in zebrafish. *J. Comp. Neurol.*, 238:218–224, 1985. 10

J. Mogdans and H. Bleckmann. Coping with flow: behavior, neurophysiology and modeling of the fish lateral line system. *Biol. Cybern.*, 106:627–642, 2012. 5

J. Montgomery and J.A. Macdonald. Sensory tuning of lateral line receptors in antarctic fish to the movements of planktonic prey. *Science*, pages 195–196., 1987. 5

J. Montgomery, C. F. B, and A. G. Carton. The lateral line can mediate rheotaxis in fish. *Nature*, pages 960–963, 1997. 5, 83

A. Muto, M. Ohkura, G. Abe, J. Nakai, and K. Kawakami. Real-time visualization of neuronal activity during perception. *Curr. Biol.*, 23:307–311, 2013. 16

R. Olive, S. Wolf, A. Dubreuil, V. Bormuth, G. Debrgeas, and R. Candelier. Rheotaxis of larval zebrafish: Behavioral study of a multi-sensory process. *Frontiers in Systems Neuroscience*, 10:14, 2016. 53, 92

J. Olszewski, M. Haehnel, M. Taguchi, and J. C. Liao. Zebrafish larvae exhibit rheotaxis and can escape a continuous suction source using their lateral line. *PLOS ONE*, 7:e36661, 2012. 53, 92

P. Oteiza, I. Odstrcil, G. Lauder, R. Portugues, and F. Engert. A novel mechanism for mechanosensory-based rheotaxis in larval zebrafish. *Nature*, 547:445–448, 2017. 12, 16, 39

DM Parichy. Advancing biology through a deeper understanding of zebrafish ecology and evolution. *Elife*, 4:e05635, 2015. 2

G. H. Parker. *The function of the lateral-line organs in fishes.* US Government Printing Office, 1904. 5

T. J. Pitcher, B. L. Partridge, and C. S. Wardle. A blind fish can school. *Science*, 194:963–965, 1976. 5

R. Portugues, C. E. Feierstein, F. Engert, and M. B. Orger. Whole-brain activity maps reveal stereotyped, distributed networks for visuomotor behavior. *Neuron*, 81:1328–1343, 2014. 3

J. Pujol-Martí and H. López-Schier. Developmental and architectural principles of the lateral-line neural map. *Front Neural Circuits*, 7:47, 2013. 6, 10

J. Pujol-Martí, A. Zecca, J. P. Baudoin, A. Faucherre, K. Asakawa, K. Kawakami, and H. López-Schier. Neuronal birth order identifies a dimorphic sensorineural map. *J. Neurosci.*, 32:2976–2987, 2012. 15

J. Pujol-Martí, A. Faucherre, R. Aziz-Bose, A. Asgharsharghi, J. Colombelli, J. G. Trapani, and H. López-Schier. Converging Axons Collectively Initiate and Maintain Synaptic Selectivity in a Constantly Remodeling Sensory Organ. *Current Biology*, 24:2968–2974, 2014. 6, 10, 87, 89, 90

S. Quirin, D. S. Peterka, and R. Yuste. Instantaneous three-dimensional sensing using spatial light modulator illumination with extended depth of field imaging. *Opt. Express*, 21:16007–16021, 2013. 3

R Core Team. *R: A Language and Environment for Statistical Computing*. R Foundation for Statistical Computing, Vienna, Austria, 2013. 27

S. L. Renninger and M. B. Orger. Two-photon imaging of neural population activity in zebrafish. *Methods*, 62:255–267, 2013. 3

M. Satou, H.A. Takeuchi, J. Nishii, M. Tanabe, S. Kitamura, N. Okumoto, and M. Iwata. Behavioral and electrophysiological evidences that the lateral line

is involved in the inter-sexual vibrational communication of the salmon (land-locked red salmon, Oncorhynchus nerka). *Journal of Comparative Physiology*, 5:539–549, 1994. 5

J. Schindelin, C. T. Rueden, M. C. Hiner, and K. W. Eliceiri. The imagej ecosystem: An open platform for biomedical image analysis. *Molecular Reproduction and Development*, 82:518–529, 2015. 28

P. Soille. *Morphological Image Analysis: principles and Applications*. IMPRINT Springer, Berlin, Heidelberg, 1999. 22

A. Suli, G. M. Watson, E. W. Rubel, and D. W. Raible. Rheotaxis in larval zebrafish is mediated by lateral line mechanosensory hair cells. *PLOS ONE*, 7: e29727, 2012. 53, 86

J. G. Trapani and T. Nicolson. Physiological recordings from zebrafish lateral-line hair cells and afferent neurons. *Methods in Cell Biology*, 100:219–231, 2010. 35

J. G. Trapani and T. Nicolson. Mechanism of spontaneous activity in afferent neurons of the zebrafish lateral-line organ. *J. Neurosci.*, 31:1614–1623, 2011. 89

J. C. Tuthill and R. I. Wilson. Parallel Transformation of Tactile Signals in Central Circuits of Drosophila. *Cell*, 164:1046–1059, 2016. 5

W. J. Van Trump and M. J. McHenry. The morphology and mechanical sensitivity of lateral line receptors in zebrafish larvae (Danio rerio). *J. Exp. Biol.*, 211: 2105–2115, 2008. 5

S. Vogel. *Life in Moving Fluids: The Physical Biology of Flow*. Princeton University Press, 1984. 46, 47, 48

C. M. Walsh, D. M. Bautista, and E. A. Lumpkin. Mammalian touch catches up. *Curr. Opin. Neurobiol.*, 34:133–139, 2015. 5

J. F. Webb. *Morphological Diversity, Development, and Evolution of the Mechanosensory Lateral Line System*, pages 17–72. Springer, New York, 2014. 90

K. Wiese. The mechanoreceptive system of prey localization innotonecta. *Journal of comparative physiology*, 92:317–325, 1974. 87

S. P. Windsor and M. J. McHenry. The influence of viscous hydrodynamics on the fish lateral-line system. *Integr. Comp. Biol.*, 49, 2009. 84, 87, 89

T. Xiao, T. Roeser, W. Staub, and H. Baier. A GFP-based genetic screen reveals mutations that disrupt the architecture of the zebrafish retinotectal projection. *Development*, 132:2955–2967, 2005. 15, 16

S. J. Zottoli and C. Van Horne. Posterior lateral line afferent and efferent pathways within the central nervous system of the goldfish with special reference to the Mauthner cell. *J. Comp. Neurol.*, 219:100–111, 1983. 10

Nomenclature

ANOVA Analysis of variance

BAA Bilateral anterior ablation

BCA Bilateral complete ablation

BPA Bilateral posterior ablation

CAN Controller area network

cLANs caudorostral lateralis afferent neurons

CMOS Complementary metal-oxide semiconductor

CNS Central nervous system

CRISPR Clustered regularly interspaced short palindromic repeats

DiASP 4-(4-diethylaminostyryl)-N-methylpyridinium iodide

dLANs dorsoventral lateralis afferent neurons

DNA Desoxyribonucleic acid

dpf Days post-fertilization

EGFP Enhanced green fluorescent protein

fps Frames per second

Gal4 Yeast transcriptional activator

GCaMP Genetically encoded calcium indicator

Hz Hertz

IR Infrared

LANs Lateralis afferent neurons

LED Light-emitting diode

mM Millimolar

mm/s Millimeter per second

nl Nanoliter

nm Nanometer

occupation Spatial position of the fish within the pipe

OpenCV Open source computer vision

PCI Peripheral component interconnect

rLANs rostrocaudal lateralis afferent neurons

ROI Region of interest

std Standard deviation

tg Transgenic line

UCA Unilateral complete ablation

UV Ultraviolet

vLANs ventrodorsal lateralis afferent neurons

Appendix A

Appendix A: Matlab Code

Empirical fully developed velocity profile of water flow inside the tube:

```
% Half of the tube width in mm
TWH = 12;
% Pixel to length (mm) scale
PtoL = 0.07;
% Tube width
re = -TWH/PtoL : 3 : TWH/PtoL;
% Calculate the fully developed velcity profile
VelocityProfile = (6.77/PtoL)*(1 - re.^2/((TWH/PtoL).^2));
% Radial distance inside the tube
r = sqrt((SideY_on - TW/2).^2 + (TopY_on - TW/2).^2);
% Velocity that fish is experiencing - parabolic modeling in mm/s
Vr = 2 * velo * (1 - (r/(TW/2)).^2);
% Plot the profile
plot(VelocityProfile,re,'b.','markersize',8)
```

Cosine of the animal orientation:

```
OrCos(fn,1) =  nanmean(cosd(TopO_on));
```

Script to run for each experiment:

```
% Clear the memory and history and close open windows in Matlab
clear all
close all
clc
% for loop on N which is the total number of experiments, to be loaded
for fn = 1 : N;
folder_name = [path,num2str(fn)];
% Calling the LoadDirectoryJ.m and ImportdataJ.m scripts which
% perform the initial preparation for data quantifications. Read in
% the next pages for these functions
LoadDirectoryJ;
ImportdataJ;
% Create name structure to save the output results with their
% Corresponding data name automatically
asas = name{1,3};
Name = {'orienration',asas(1:4),asas(end-2:end)};
Name = strjoin(Name,'_');
% Delete old ones and save new data in case the programs runs
% Multiple time to avoide possible overwriting issues
cd(folder_name);
delete([Name,'.mat']);
% Save data
S.(newName) = orientation;
save(fullfile(folder_name,newName), '-struct', 'S');
```

```
end
```

Loaddirectory.m which is called in the main script above:

```
% Add path to the current directory
addpath(genpath(fullfile(pwd)))
addpath(genpath(folder_name));
% Recoding frame rate
hz = 200;
% Pixel to length (mm) scale for top view
PtoL_Top = 0.155;
% Pixel to length (mm) scale for side view
PtoL_Side = 0.163;
% Tube width in mm
TW = 24;
% Import side-view data
SideDir = {folder_name,'Side.csv'};
Sideload = strjoin(SideDir,'/');
[S,delimiterOutt] = importdata(Sideload);
% Fish position along the tube length in mm
Side_x = PtoL_Side * S(:,1);
% Fish position along the tube depth in mm
Side_y = PtoL_Side * S(:,2);
% Fish orientation in degree
Side_o = convang(S(:,3),'rad','deg');
% Import top-view data
TopDir = {folder_name,'Top.csv'};
Topload = strjoin(TopDir,'/');
[T,delimiterOut] = importdata(Topload);
% Fish position along the tube length in mm
```

```
Top_x = PtoL_Top * T(:,1);
% Fish position along the tube width in mm
Top_y = PtoL_Top * T(:,2);
% Fish orientation in degrees
Top_o = convang(T(:,3),'rad','deg');
% Load the info.txt file
Info_name = {folder_name,'info.txt'};
InfoDir = strjoin(Info_name,'/');
str = fileread(InfoDir);
Info = strtrim(regexp( str, '(\r|\n)+', 'split'));
% Condition on minimum flow duration in second
% Minimum flow duration of rheotaxis in second
FlowDurlim = 18;
% Flow duration in second
FlowDur = (size(Top_x,1) - Onn)./hz;
if FlowDur < FlowDurlim
 h = msgbox('Flow duration is low');
 % display folder in which data are loaded
 folder_name
end
fstr = FlowDur*hz - FlowDurlim*hz;
% Fame where movies will analyse for Flow on
FlowOn = Onn + fstr;
% Last frame of recording where flow turned off
FlowOff = size(Top_x,1);
velofind =
 strsplit(folder_name,'\s*mms\s*','DelimiterType','RegularExpression');
veloabs = velofind{1,2};
% Flow direction
Flowdir = Info{1,1};
velojoin = {Flowdir(1,1),veloabs(1,4)};
```

```
% Velocity in mm/s
velo = str2num(strjoin(velojoin));
C = strsplit(folder_name,'/');
name = C(size(C,2)-2:size(C,2));
```

Importdata.m, which is called in the main script above:

```
% Angles outputs from Bonsai are in the range of 0 to 360 degrees.
% Zero angle means toward right side of the monitor and 180 degrees
% means toward left side of the monitor. The down side angles are
% between 0 and 180 degrees (clockwise). I convert it to 0:-90:180
% + 0:90:180 and consider always 0 (based on water flow direction) in
% opposite direction of water flow. Then if fish does positive rheotaxis,
% its angle will be 0, turning to left side will have negative angle
% and to right side will have positive angle.
% Top view
if Flowdir == '-x'
 for i=1:size(Top_o,1)
  if Top_o(i,1) > 180
   Top_o(i,1) = Top_o(i,1) - 360;
  end
 end
end
if Flowdir == '+x'
 for i=1:size(Top_o,1)
  Top_o(i,1) = Top_o(i,1) - 180;
 end
end
% Side view
if Flowdir == '-x'
```

```
 for i=1:size(Side_o,1)
  if Side_o(i,1) > 180
   Side_o(i,1) = Side_o(i,1) - 360;
  end
 end
end
if Flowdir == '+x'
 for i=1:size(Side_o,1)
  Side_o(i,1) = Side_o(i,1) - 180;
 end
end
% Seperate data in two parts of flow-on and flow-off
% Top view
TopX_on = Top_x(FlowOn:FlowOff);
TopX_off = Top_x(1:FlowOn);
TopY_on = Top_y(FlowOn:FlowOff);
TopY_off = Top_y(1:FlowOn);
TopO_on = Top_o(FlowOn:FlowOff);
TopO_off = Top_o(1:FlowOn);
% Side-view
SideX_on = Side_x(FlowOn:FlowOff);
SideX_off = Side_x(1:FlowOn);
SideY_on = Side_y(FlowOn:FlowOff);
SideY_off = Side_y(1:FlowOn);
SideO_on = Side_o(FlowOn:FlowOff);
SideO_off = Side_o(1:FlowOn);
% Time vector in second
time = 0:1/hz:size(Side_x,1)/hz;
% Flow is on
time_on = time(FlowOn:FlowOff);
% Flow is off
```

```
time_off = time(1:FlowOn);
```

Occupation function to calculate occupancy profile:

```
function [occupancy] = Occupation_fun(TopX_on,TopY_on,SideY_on)
% TopX_on, TopY_on, SideY_on are fish orientation in top and side view.
for i = 1:size(TopY_on,1)
     xx = ceil(TopX_on(i,1));
     yy = ceil(TopY_on(i,1));
     if xx>0 && yy>0
             occupancy(xx,yy) = occupancy(xx,yy) +1;
     end
end
end
```

Example of using occupation function for N number of data to calculate and overlay occupation profile all together:

```
% Clear the memory and command history and close the open windows
clear all
close all
clc
% Add path to the current directory
addpath(genpath(fullfile(pwd)))
for fn = 1:N
 folder_name = [path,num2str(fn)];
 % Calling back the LoadDirectoryJ.m script
 LoadDirectoryJ
 % Calling back the ImportdataJ.m script
```

```
 ImportdataJ
 % To flip data vertically
 if Flowdir == '-x' ;TopX_on = 156 - TopX_on; end
  % Calling the function Occupation_fun to calculate the occupation
  occupancy = Occupation_fun(TopX_on,TopY_on,SideY_on);
  % Clear variables in each run
  clearvars -except o*
 end
end
% Normalize the occupancy
occupancy17dNF = mat2gray(occupancy7dNF);
% Plot the occupancy
set(figure(1),'position',[10 50 1200 1070])
imagesc(occupancy17dNF')
colormap jet
h = colorbar;
set(get(h,'title'),'string','Occup %','fontsize',11);
title('7dNf','fontsize',13)
set(gca,'XTickLabel',' ')
set(gca,'YTickLabel',' ')
% Save
F = getframe(gcf);
imwrite(F.cdata,path,'png');
```

Marginal distribution of occupancy:

```
% Marginal distribution along width of the tube
Md_width = sum((occupancy17dNF),1);
% Marginal distribution along length of the tube
Md_length = sum((occupancy17dNF),1);
```

```
% Plot
set(figure,'position',[10 50 250 250])
h1 = plot(Md_width);
set(h1,'linewidth',2,'color','r')
h2 = plot(Md_width);
set(h2,'linewidth',2,'color','b')
```

scoring system:

```
% Clear the memory and command history and close the open windows
clear all
close all
% add path to the current directory
addpath(genpath(fullfile(pwd)))
for fn = 1:N
 folder_name = [path,num2str(fn)];
 % Calling the LoadDirectoryJ.m script
 LoadDirectoryJ
 % Calling the ImportdataJ.m script
 ImportdataJ
 delta=30; % range of the angle in the scoring system.
 % Scores based on my scoring system
 values = [1 2/3 1/3 -1/3 -2/3 -1 -1 -2/3 -1/3 1/3 2/3 1];
 % Make angles from 0:360
 for i = 1 : size(TopO_on,1)
 if TopO_on(i,1) < 0
  TopO_on(i,1) = TopO_on(i,1) + 360;
 end
 end
 % Scooring
```

```
 for i = 1 : size(TopO_on,1)
  xx = ceil(TopX_on(i,1));
  yy = ceil(TopY_on(i,1));
  if xx == 0
   xx=1;
  end
  if yy == 0
   yy=1;
  end
  for j = 1:13
   if TopO_on(i,1) >=(j-1)*delta && TopO_on(i,1)<j*delta
   a = values(j);
  end
  end
  OrSc(fn,1) = OrSc(fn,1) + a;
  OrSc(xx,yy) = OrSc(xx,yy) + a;
  end
 OrSc = mat2gray(OrSc);
end
```

Appendix B

Appendix B: ImageJ / Fiji Macro

In the rheotaxis rig, the camera records top and side view of the behaving animal in high frame rate of 200 fps for the long duration of 24 seconds. At the end of the experiment, images are saved as .avi in two files, which consist of top view and side view. The following macro, concatenates them and creates one single .avi file.

```
open("/I.00.avi");
open("/I.01.avi");
run("Concatenate", "title=[Concatenated Stacks] image1=I.00.avi
image2=I.01.avi image3=[-- None --]");
run("AVI", "compression=JPEG frame=100 save=[/name_001.avi]");
File.delete("/_config.xsv")
File.delete("/I.avi.extra.bin")
File.delete("/I.00.avi")
File.delete("/I.01.avi")
close();
```

Appendix C

Appendix C: Publications and Presentations

This study has contributed to the following publications:

1 **Amir Asgharsharghi**, Weili Tian, Melanie Haehnel-Taguchi, Hernán López-Schier. Sarm1 is dispensable for mechanosensory-motor transformations in zebrafish. microPublication Biology, 2021, 10.17912/micropub.biology.000369

2 Gema Valera, Daniil A. Markov, Kayvan Bijari, Owen Randlett, **Amir Asgharsharghi**, Jean-Pierre Baudoin, Giorgio A. Ascoli, Ruben Portugues, Hernán López-Schier. A neuronal blueprint for directional mechanosensation in larval zebrafish. Current Biology, 2021, ISSN 0960-9822

3 Jesús Pujol Marti, Adle Faucherre, Razina Aziz-Bose, **Amir Asgharsharghi**, Julien Colombelli, Josef G. Trapani, and Hernán López-Schier. Converging axons

collectively initiate and maintain synaptic selectivity in a constantly remodeling sensory organ. Current Biology, 24(24):29682974, 2014b. ISSN 09609822

Achievements of this study are presented to the following conferences and meetings:

1 Amir Asgharsharghi and Hernán López-Schier. Mechanosensory control of rheotaxis. Federation of European Neuroscience Societies (FENS) Forum of Neuroscience, Berlin, 7-11 July 2018 (with peer-reviewed abstract)

2 Amir Asgharsharghi and Hernán López-Schier. Spatiotemporal navigation of zebrafish larvae under flow. 11th international conference on methods and techniques in behavioral research, Measuring behavior, Manchester Metropolitan University, 6-8 June 2018 (with peer-reviewed abstract)

3 Amir Asgharsharghi, Gema Valera, Jean-Pierre Baudoin, Hernán López-Schier. Rheotaxis behavior in larval zebrafish. LMU-Harvard Young Scientists Forum (YSF), From Molecules to Organisms IX, Munich, 23-27 July 2017

4 Amir Asgharsharghi and Hernán López-Schier. Neuronal bases and motor dynamics of zebrafish swimming against water currents. Imaging Structure and Function in the Zebrafish Brain conference, Max-Planck Institute of Neurobiology, Munich, 8-9 December 2016

Appendix D

Appendix D: Eidesstattliche Erklärung

Hiermit erkläre ich an Eides statt, dass ich die vorliegende Dissertation gemäß der Prüfungsordnung der Technische Universität München selbstständig, ohne unzulässige fremde Hilfe und unerlaubte Hilfsmittel angefertigt habe.

München, den 07.07.2021

_____

Amir Asgharsharghi Bonab